PRECLINICAL STUDIES ON ATM KINASE INHIBITORS AS ANTI-CANCER AGENTS

by

Serah Choi

B.A. Human Biology, Stanford University, 1999

Submitted to the Graduate Faculty of

Pharmacology and Chemical Biology in partial fulfillment

of the requirements for the degree of

Doctor of Philosophy

University of Pittsburgh

2011

UNIVERSITY OF PITTSBURGH

School of Medicine

This dissertation was presented

by

Serah Choi

It was defended on

July 25, 2011

and approved by

Chairperson: Richard A. Steinman, MD, PhD, Associate Professor of Medicine, Department of Pharmacology and Chemical Biology

Thomas Conrads, PhD, Adjunct Associate Professor, Department of Pharmacology and Chemical Biology

Bennett Van Houten, PhD, Professor, Department of Pharmacology and Chemical Biology

Jian Yu, PhD, Associate Professor, Department of Pathology

Dissertation Advisor: Christopher J. Bakkenist, PhD, Assistant Professor of Radiation Oncology, Department of Pharmacology and Chemical Biology.

PRECLINICAL STUDIES ON ATM KINASE INHIBITORS AS ANTI-CANCER AGENTS

Serah Choi, PhD

University of Pittsburgh, 2011

Ataxia telangiectasia-mutated (ATM) is a serine/threonine protein kinase that has critical functions in the cellular responses to DNA damage, including cell cycle checkpoint activation and DNA repair. Since ataxia telangiectasia individuals, who have homozygous mutations in ATM, are exquisitely radiosensitive there is considerable interest in inhibiting the kinase activity of ATM to increase the efficacy of targeted radiotherapy. In this dissertation work, I sought to understand the cellular responses to radiation when ATM kinase activity is transiently inhibited using the small molecule ATM kinase inhibitor KU55933. During my PhD, our laboratory has shown that transient ATM kinase inhibition one hour post-irradiation results in radiosensitization, increased chromosome aberrations and abrogation of sister chromatid exchange. I contributed to these findings by showing that the cellular radiosensitization seen in H460 cells with kinase-inhibited ATM was identical to that seen when ATM protein was disrupted using siRNA prior to the insult. In addition, I demonstrated that 15 minutes of ATM kinase activity post-irradiation is sufficient to trigger the G_2/M cell cycle checkpoint, and that subsequent transient inhibition of ATM with KU55933 does not affect recovery from this checkpoint. To gain a more global view of the functional consequences of kinase-inhibited ATM following irradiation, I utilized a SILAC-based tandem mass spectrometry approach, combined with a subcellular fractionation protocol, to determine ATM kinase-dependent spatial proteome dynamics in response to radiation-induced DNA damage. Analysis of the chromatin-associated

proteome revealed that the retention of 53BP1 at chromatin is decreased when the kinase activity of ATM is inhibited following ionizing radiation (IR). Using fluorescence recovery after photobleaching in live cells, I determined that the stability of IR-induced GFP-53BP1 foci is decreased when the kinase activity of ATM is inhibited following IR. These results provide a roadmap for understanding ATM kinase-dependent spatial protein dynamics in response to DNA damage.

TABLE OF CONTENTS

LIST OF FIGURES

PREFACE

To my advisor, Chris, I would like to express my deepest gratitude for your mentorship and dedication to my scientific training. I will be forever grateful for the education and experience that I gained in your laboratory.

To my thesis committee, Richard Steinman, Thomas Conrads, Bennett Van Houten and Jian Yu, thank you for serving on my committee and for your sharing your wisdom.

To my career advisor, Tim Oury, thank you for your guidance.

To past scientific mentors, Rick Wood, Jim Pipas, Clodagh O'Shea and Frank McCormick, thank you for helping me in my scientific training.

To my labmates-- Jay White, Armin Gamper and Katherine Fu-- and my colleagues-- Greg Gan, Stacey Lin, Wei Qian, Olga Momcilovic, David Svilar, Xixi Wong and Mel Price -- thank you for the engaging scientific discussions and camaraderie. To the members of the DNA repair group at the Hillman Cancer Center, the Department of Pharmacology and Chemical Biology and the University of Pittsburgh MSTP, thank you for challenging me to develop scientifically and for cultivating a wonderful training environment. To Patricia Smith, thank you for all of your kindness and support throughout graduate school.

To my family, thank you for your constant love. Mom, thank you for being an amazing role model, for giving me strength and for teaching me to seek knowledge and truth. Dad, thank you for teaching me compassion and for motivating me to become a physician scientist. To my

siblings, Segene and Selyn, thank you for all of your support and humor. To my dog, Chloe, thank you for reminding me to appreciate the grass and the trees. And finally, to my partner Trey, thank you for your love and friendship….over thousands of frequent flyer miles and Skype calls…for believing in me and for inspiring me.

Chapters 2 and 3 contain figures from the following manuscripts:

> White JS, Choi S, Bakkenist CJ. Irreversible chromosome damage accumulates rapidly in the absence of ATM kinase activity. Cell Cycle. 2008 May 1;7(9):1277-84.
>
> White JS, Choi S, Bakkenist CJ. Transient ATM kinase inhibition disrupts DNA damage-induced sister chromatid exchange. Sci Signal. 2010 Jun 1;3(124):ra44.

The experiments described in Figures 4 and 5 were executed by Christopher J. Bakkenist. The experiments described in Figures 7A, 8, 10 and 11 were executed by Jason S. White.

I would also like to acknowledge and thank my collaborators on the project described in Chapter 4: Rohith Srivas, Brian L. Hood, Banu Dost, Bennett Van Houten, Nuno Bandeira, Thomas P. Conrads and Trey Ideker.

1.0 INTRODUCTION

1.1 ATAXIA TELANGIECTASIA (A-T)

Ataxia telangiectasia (A-T) is an autosomal recessive disorder characterized by progressive neurodegeneration, oculocutaneous telangiectasia, defects in B and T cell–mediated immunity, increased susceptibility to malignancies (mainly lymphoid neoplasms) and radiosensitivity.[1,2] A-T is a rare disease, with an incidence of 1 to 2.5 in 100,000.[3,4] A-T is caused by biallelic mutations in the *ATM* gene, which is located at 11q22.3 and covers 160 kb of genomic DNA.[5] The ATM protein is produced from a 13 kb transcript that encodes for a protein that is predicted to be 315 kDa, but migrates at approximately 370 kDa on SDS-PAGE.[5] ATM is a protein kinase, and cells derived from patients with the classical A-T phenotype lack ATM kinase activity as a result of either compound heterozygosity or, less frequently, homozygosity for truncating mutations (frameshift or nonsense mutations). In both cases, the mutations result in an absence of stable ATM protein.[6,7] Radiosensitivity (increased cell death following ionizing radiation exposure) was first documented when an A-T patient with cancer had a toxic reaction to radiation therapy, and is now considered a salient feature of A-T.[8] Cells derived from A-T patients exhibit defective cell cycle checkpoint responses to ionizing radiation (IR), profound

radiosensitivity, and high levels of chromosome aberrations, indicating the importance of ATM for the maintenance of chromosome stability and radioprotection.[2]

1.2 THE PIKK FAMILY

ATM is a member of phosphoinositide 3-kinase-related protein kinase (PIKK) family, which also includes ATR (ATM and rad3 related protein kinase), DNA-PK_{cs} (DNA-dependent protein kinase catalytic subunit), mTOR (mammalian target of rapamycin), and hSMG1.[5,9] The PIKK family of proteins are large proteins (2547 to 4128 amino acids) and serine/threonine protein kinases that share a C-terminal protein kinase domain, flanked by an N-terminal FAT (FRAP, ATM, TRRAP) domain composed of HEAT (Huntingtin, Elongation factor 3, A subunit of protein phosphatase 2A and TOR1) repeats, and a C-terminal FATC (FAT C-terminus) domain (Figure 1).[9] The FATC domain is a small domain comprised of 32 amino acids that is required for PIKK kinase activity [9]. Since the FAT and FATC domains flank the PIKK kinase domain it has been suggested that they interact and function in kinase regulation [10]. There is little sequence similarity between the kinases outside of these common domains; the remainder of each protein consists of more HEAT repeats that may serve as protein–protein interaction surfaces [9,11]. ATM, ATR and DNA-PK_{cs} have roles in DNA repair and are activated by DNA lesions: DNA double-strand breaks (DSBs) activate ATM and DNA-PK_{cs}, and single-stranded DNA (ssDNA) gaps activate ATR [9].

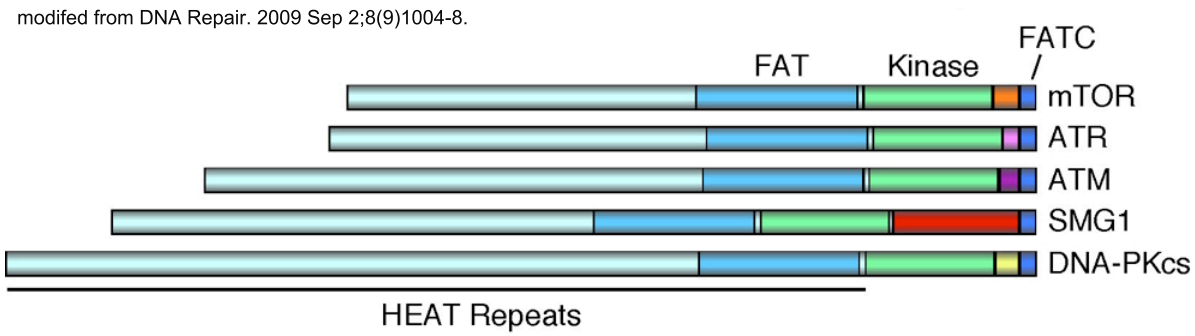

Figure 1. The phosphoinositide 3-kinase-related protein kinase (PIKK) family

Although ATM, DNA-PK_{cs} and ATR all have affinity for nucleic acids, they required proteins or protein complexes that directly bind DNA for DNA lesion recognition. The Mre11-Rad50-Nbs1 (MRN) complex recruits ATM to DSBs, the Ku70-Ku80 protein complex recruits DNA-PK_{cs} to DSBs and ATRIP recruits ATR to ssDNA via its interaction with the ssDNA binding protein RPA [12-14]. The N-terminal HEAT repeat region of each PIKK serves as the binding site for the recruitment complexes, and is mediated through a common motif near the C-terminus of Nbs1, Ku70, and ATRIP [9,15].

1.3 ATM KINASE ACTIVITY

ATM is a serine/threonine protein kinase with a consensus phosphorylation motif of hydrophobic-X-hydrophobic-[S/T]-Q. ATM kinase activity is rapidly stimulated in cells exposed to ionizing radiation (IR). [16-18] ATM kinase activation is associated with autophosphorylation on serine-1981, which is an exceptionally sensitive marker for ATM kinase activity in cells.[16] ATM

kinase activity is increased in cells exposed to as little as 0.05 Gy IR and following the introduction of just two DSBs per cell.[16,19] Following 0.4 Gy IR, ATM kinase activity is maximal within 15 minutes, at which point over 50% of ATM is phosphorylated in cells.[16]

A considerable body of literature documents the ATM kinase-dependent mobilization, modification and upregulation of proteins critical for the induction of cell cycle checkpoints and apoptosis following IR. Over 1,000 ATM and ATR kinase-dependent phosphorylations have been identified in cells exposed to IR.[20-22] ATM kinase-dependent phosphorylations have been found to modify proteins involved in DNA replication, DNA repair, cell cycle progression, and numerous signaling pathways.[20-22] Despite these efforts, the indispensable ATM kinase-dependent mechanisms that ensure genome stability and cell survival are not well understood. Isolating changes in protein function that are causally related to A-T or its cellular phenotypes may be particularly challenging since stress-activated kinases such as ATM have little selective pressure to restrict functionally insignificant phosphorylations.

1.4 ATM KINASE ACTIVITY IN CELL CYCLE CHECKPOINTS

ATM kinase activity is essential for the induction of cell cycle checkpoints during S-phase and at the G_1/S and G_2/M boundaries following IR. Cell cycle checkpoints prevent cell cycle progression in the presence of chromosome damage and allow sufficient time for chromosome repair.[23] One of earliest cellular phenotypes described in A-T cells was a defect in the intra-S-phase checkpoint.[24] A-T cells lack the ability to inhibit DNA synthesis following irradiation, a phenomena described as "radioresistant DNA synthesis."[24] ATM kinase-dependent phosphorylations on BRCA1, FANCD2 and NBS1 have been implicated in the intra-S-phase

checkpoint.[25-27] Activation of the G_1/S checkpoint following IR requires ATM kinase-dependent induction of FBXO31-mediated cyclin D1 degradation, and maintenance of the G_1/S checkpoint requires the ATM kinase-dependent induction of p53-dependent p21 transcription.[28-30]

The G_2/M checkpoint following IR relies on the ATM kinase-dependent phosphorylations on BRCA1 and hRAD17.[31-33] Cell cycle checkpoint abrogation in G_2/M impairs the repair of chromosomal breaks in A-T cells.[34] Notably, the G_2/M checkpoint attracted considerable attention as a cancer therapeutic target since many cancer cells, like A-T cells, harbor defective G_1/S checkpoints and cancer cells depend on the G_2/M checkpoint far more than normal cells.[35,36] Presumably, disruption of the G_2/M cell cycle checkpoint by an ATM kinase inhibitor could increase the efficacy of radiotherapy and chemotherapies by allowing cancer cells containing damaged chromosomes to proceed directly into mitosis, thereby promoting chromosome instability, imbalanced cell division and ultimately cell death.[37] However, several lines of evidence convey that the cellular radiosensitivity seen in A-T cells is not entirely attributed to defective cell cycle checkpoint activation.[38-41] For example, irradiated A-T cells held in G_0 for up to 18 hours, far longer than needed for maximum repair of radiation-induced DNA lesions, do not exhibit a reduction in the number of chromosome aberrations or cell death.[38] Similarly, when aphidicolin is used to block the G_1/S-phase transition in irradiated A-T cells, there is no evidence for a reduction in cell death.[39] Furthermore, the use of premature chromosome condensation (PCC) has shown that irradiated A-T cells can be held continuously post-irradiation in G_0 for up to 48 hours without evidence for a reduction in the number of chromosome aberrations.[40] Finally, sublethal irradiation results in increased yields of chromosome aberrations in unstimulated A-T lymphocytes, but not normal lymphocytes.[41]

1.5 ATM KINASE ACTIVITY IN DNA REPAIR

There is accumulating evidence that ATM kinase activity is required to phosphorylate substrates that function in the repair of DSBs. DSBs are repaired by two principal mechanisms: non-homologous end-joining (NHEJ) and homologous recombination (HR).[42] HR is the most accurate DSB repair mechanism but is generally restricted to the S- and G_2-phases of the cell cycle when DNA has been replicated and a sister chromatid is available as a repair template.[43] NHEJ operates throughout the cell cycle but assumes most importance in G_1.[44] The core NHEJ machinery includes DNA-PK_{cs}, XRCC4, Ligase IV and Artemis.[44] ATM kinase-dependent Artemis activity is implicated for the resolution of approximately 10% of DSBs that are repaired several hours following IR.[45,46] While an ATM kinase-dependent phosphorylation on Artemis serine 645 has been identified, the phosphorylation site has not been found to have a function in DNA repair or cellular radioprotection.[47]

Generally, HR repair of a DSB involves the processing of a DSB to give single-stranded DNA (ssDNA), formation of a filament on the ssDNA ends, strand invasion into a homologous sequence to form a D-loop and DNA polymerase extension.[43] In mammalian cells, ATM kinase activity has been implicated in HR repair through numerous substrates. Disruption of ATM substrates DCK, EHMT1, FBXC11 and NUMA1 reduced the HR repair of an I-Sce-1-induced DSB.[21] In addition, ATM kinase-dependent phosphorylations on MRE11, RAD50 and NBS1 (MRN complex) have been identified.[21,27] Finally, ATM kinase activity has also been implicated in DSB end resection via CtIP, which is also involved in the HR repair functions of the MRN complex.[48-50]

1.6 ATM KINASE ACTIVITY AND CANCER

Following exposure to ionizing radiation (IR), A-T cells display defective cell cycle checkpoints, residual chromosomal breaks, slower DNA double-strand break (DSB) rejoining than wild-type cells, and a failure to repair all DSBs, all of which could contribute to the radiosensitivity of A-T cells.[40,51-53] Therefore, it has been proposed that inhibition of ATM may give rise to radiosensitization.[37] Studies performed thus far indicate that selective ATM kinase inhibitors do in fact radiosensitize cells and therefore, may be effective agents in the treatment of cancers that are resistant to radiation therapy.[54-56]

Recently, inhibition of ATM kinase activity has been shown to be toxic to cancer cells with somatic mutations in genes that are synthetic lethal with ATM kinase activity. Two genes are synthetic lethal if mutation of either gene alone is compatible with viability but mutation of both genes leads to death.[57-59] The term "synthetic lethality" has been redefined to include synthetic lethal interactions between a mutated gene and a pharmacologically targeted gene. A synthetic lethal approach is advantageous for cancer therapy because pharmacologically targeting a gene that is synthetic lethal with a cancer-relevant mutation selectively kills cancer cells while sparing normal cells, thereby enhancing the therapeutic index (ratio of the toxic dose to the effective dose of a drug) between the tumor and normal tissue.[57-59] A synthetic lethal approach also enables targeting tumors driven by loss-of-function mutations in tumor suppressor genes, which historically have been difficult to target by other strategies.[60-63] Genotype-specific agents based on synthetic lethality can also be used as monotherapies, or to enhance the efficacy of cytotoxic therapies used at lower doses, thereby decreasing off-target side effects.[60,64,65]

The paradigm for synthetic lethal approach for cancer is poly(ADP-Ribose) polymerase (PARP) inhibition in BRCA1-/- and BRCA2-/- tumors. PARP functions in the base excision

repair of DNA single-strand breaks (SSBs) and PARP inhibitors cause an accumulation of unrepaired SSBs that induce toxic DSBs via collapsed DNA replication forks.[66] PARP inhibitors selectively kill BRCA-/- cancer cells, while sparing BRCA+/+ and BRCA+/- normal cells and show promise in the clinic for the treatment of patients with cancers associated with BRCA1 or BRCA2 mutations.[67,68]

Several studies have reported synthetic lethal interactions with inhibition of ATM kinase activity. The ATM kinase inhibitor KU55933 has been shown to kill pancreatic tumor cell lines deficient in the Fanconi anemia (FA) pathway.[69] The FA pathway, which functions in the repair of DNA interstrand crosslinks, is mutated in >10% of pancreatic cancers and >15% of lung cancers have inactivated FANCF.[70,71] In addition, KU55933 has been shown to kill p53-deficient lung cancer cell lines when treated with doxorubicin, demonstrating a synthetic lethal interaction between ATM kinase signaling and p53 when cells are challenged with a DNA damaging agent.[72,73] Future studies are needed to further elucidate the mechanisms underlying these synthetic lethal interactions. Given the high frequency of p53 or/and FA pathway mutations in cancers, these exciting findings highlight the potential therapeutic value of ATM kinase inhibitors.[70,71,74]

In these studies, I sought to understand the cellular responses to radiation when ATM kinase activity is transiently inhibited using the small molecule ATM kinase inhibitor KU55933.

2.0 ATM KINASE INHIBITORS

2.1 INTRODUCTION

To date, three selective inhibitors of ATM kinase activity have been identified: KU55933, CP46672217 and KU60019.[54-56] Prior to the discovery of these compounds, studies to test the consequences of ATM kinase inhibition in cells have utilized the nonspecific small molecules caffeine and wortmannin.[75,76] However, caffeine and wortmannin inhibit related kinases including ATR, DNA-PK and PI3K at the concentrations required to inhibit ATM.[76-81] Moreover, the broad nonspecific effects of caffeine and wortmannin and the high effective concentration of caffeine (1 mmol/L) prohibit their use in the clinic.[37] The advent of the selective ATM kinase inhibitors KU55933, CP46672217 and KU60019 enables preclinical studies to test the efficacy of ATM kinase inhibitors as anti-cancer agents.[54] Furthermore, selective ATM kinase inhibitors are powerful tools for studying the role of ATM kinase signaling in the DNA damage response.[54] The primary focus of my PhD has been to undertake preclinical studies using the ATM kinase inhibitor KU55933. Here, we test the effectiveness and reversibility of KU55933 and KU60019 in cells. In addition, we test the effectiveness of a controversial dual ATM/ATR kinase inhibitor, CGK733.[82-84]

2.2 BACKGROUND

The first selective small molecule ATM kinase inhibitor KU55933 (2-morpholin-4-yl-6-thianthren-1-yl-pyran-4-one) was identified by KuDOS Pharmaceuticals through screening a combinatorial library based around the nonspecific PI3K inhibitor LY294002 (Figure 2).[54,77] The IC_{50} of KU55933 (i.e. the concentration of KU55933 that achieved 50% inhibition of ATM kinase activity) is 12.9 +/-0.1 nmol/L *in vitro*; the K_i is 2.2 nmol/L.[54] Moreover, KU55933 exhibits a 100-fold differential in selectivity for ATM over other members of the PIKK family *in vitro*.[54] The ATM protein used in those *in vitro* assays were obtained from HeLa nuclear extracts by immunoprecipitation with rabbit polyclonal antiserum raised to the COOH-terminal 400 amino acids of ATM.[54]

KU55933 is a competitive ATP inhibitor.[54] The morpholine oxygen in KU55933 is critical for ATM kinase inhibition; KU-58050, which replaces the morpholine moiety in KU55933 with a piperidine, had a calculated IC_{50} against ATM of 2.96 ± 0.44 μmol/L.[54] Based on the crystal structure of the porcine PI3K p110γ subunit in complex with LY294002, it is conjectured that the morpholine acts through hydrogen bonding within the hinge region of the ATP-binding site of ATM.[85] However, the crystal structure of ATM bound with KU55933 has not yet been reported.[54] KU60019, the second-generation KuDOS Pharmaceuticals ATM kinase inhibitor, was developed in an effort to improve the bioavailability and pharmacokinetics of KU55933 while preserving its selectivity for ATM (Figure 2).[56] KU60019 has an IC_{50} of 6.3 nmol/L, 50% lower than that of KU55933, and an almost identical target spectrum as

KU55933.[56] Importantly, off-target effects of KU55933 or KU60019 in cells at doses that inhibit ATM are yet to be demonstrated.

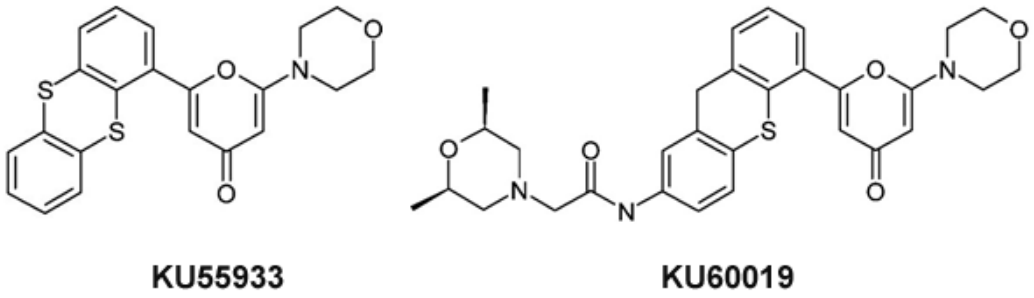

Figure 2. Chemical structures of the ATM kinase inhibitors KU55933 and KU60019

The Pfizer compound CP466722 [2-(6,7-dimethoxyquinazolin-4-yl)-5-(pyridin-2-yl)-2H-1,2,4-triazol-3-amine] was identified by screening a library of 1,500 compounds using an *in vitro* ELISA approach which detects a decreased ability of purified ATM kinase to phosphorylate GST-p53 substrate.[55] Like KU55933 and KU60019, CP466722 is a potent inhibitor of ATM and does not inhibit PI3K or PIKKs in cells at concentrations used to inhibit ATM.[55]

A fourth compound, CGK733 was reported to inhibit both ATM and ATR kinase activities and block their checkpoint signaling with great selectivity (Figure 3).[82] CGK733 was described as a small molecule capable of reversing replicative senescence.[82] Senescence, which was induced in human primary BJ fibroblasts by overexpression of the dominant negative form of the telomeric t-loop formation protein Trf-2 ($TRF1^{\Delta B \Delta M}$), was monitored by automated fluorescence microscopy after adding compounds from a library of ~20,000 synthetic organic

molecules.[82,86,87] CGK733 induced cell growth in the senescent cells and senescence markers such as the senescence-associated β-galactosidase activity disappeared in cells treated with CGK733. In addition, the removal of CGK733 reverted cells back to a senescent phenotype. In order to identify the molecular target of CGK733, the magnetism-based interaction capture (MAGIC) method was used and ATM was identified as the target of CGK733.[82,88] CGK733 was reported to have an inhibitory effect on the kinase activity of ATM and ATR *in vitro*, and negligible effects on DNA-PK or any other kinases that are known to phosphorylate p53.[82] Thus, CGK733 was discovered as a new small molecule inhibitor selective for ATM and ATR.[82]

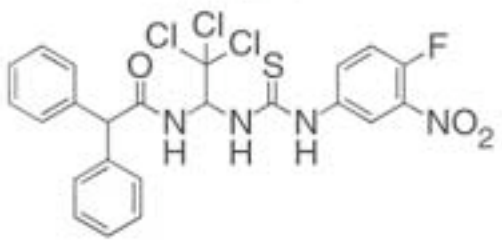

CGK733

Figure 3. Chemical structure of the ATM and ATR kinase inhibitor CGK733

Two years after publication, the paper reporting the identification of CGK733 and its molecular targets was retracted.[83,84] An investigation by the Korean Advanced Institute of Science and Technology could find no evidence that the MAGIC screen to identify CGK733 as an anti-senescence agent was carried out and revealed that the subsequent experiments exploring the cellular effects of CGK733 utilized chemical compounds similar but not identical to CGK733.[84] Yet, the retraction letter did not specifically address whether CGK733 is a *bona fide* ATM and/or ATR inhibitor and confusion ensued regarding the inhibitory effects of CGK733.[84] CGK733 continues to be commercially marketed by Sigma-Aldrich and Tocris Bioscience as an

ATM and ATR inhibitor. Indeed, several manuscripts employing CGK733 as an inhibitor of the kinase activities of ATM and/or ATR have been published in respected journals, in which no controls were presented to demonstrate that CGK733 inhibits the kinase activity of either ATM or ATR.[89,90]

2.3 MATERIAL AND METHODS

2.3.1 Cell lines, irradiation and inhibitor treatment

The normal diploid fetal human lung fibroblast cell line IMR90 and the transformed lung cell line NCI-H460, which is wild-type for p53, were purchased from the American Type Culture Collection (ATCC, Manassas, VA). IMR90 were cultured in DMEM and H460 were cultured in RPMI, both supplemented with 10% FBS (Atlanta Biologicals). KU55933 and KU60019 (KuDOS Pharmaceuticals) were reconstituted in DMSO and used at a 10 μM and 1μM, respectively. CGK733 (Tocris Bioscience and Sigma) was reconstituted in DMSO and used at 10 μM. ETP-46464 at 10 μM in DMSO was a kind gift of Dr. Oscar Fernandez-Capetillo (Genomic Instability Group, Spanish National Cancer Centre, Madrid, Spain). Cells were γ-irradiated in a Shepherd Mark I Model 68 [^{137}Cs] irradiator (J.L. Shepherd & Associates, San Fernando, CA).

2.3.2 Antibodies

Rabbit monoclonal anti-ATM 1981S-P antisera (EP1890Y, Epitomics, Burlingame, CA), anti-ATM antisera (MAT3-4G10/8, Sigma-Aldrich, St. Louis, MO), anti-p53 (sc6243-G, Santa Cruz Biotechnology, Santa Cruz, CA), anti-P53 15S-P (9284, Cell Signaling Technology, Danvers, MA), anti-CHK2 (Ab5/DCS270, Neomarkers, Fremont, CA), anti-CHK2 68T-P (2661, Cell Signaling), anti-CHK2 (1C12, Cell Signaling), anti-CHK1 317S-P (2344, Cell Signaling), anti-CHK1 (2G1D5, Cell Signaling) and generic anti-HSC70 (sc-1059, Santa Cruz Biotechnology) were used in immunoblotting. Whole cell extracts were prepared in lysis buffer: 50 mM Tris-HCl pH 7.5, 150 mM NaCl, 50 mM NaF, 50 mM NEM, 1% Tween-20, 0.5% NP40 and 1 x protease inhibitor mixture (Roche Applied Science, Indianapolis, IN). Lysates were resolved in 3-8% Tris-Acetate gels (Invitrogen, Carlsbad, CA).

2.4 RESULTS

2.4.1 KU55933

In order to determine the concentration of KU55933 that is required to inhibit ATM kinase activity in IMR90 cells, ATM serine 1981 phosphorylation, p53 protein levels and p53 serine 15 phosphorylation were immunoblotted one hour following exposure to 5 Gy γ-rays. We used KU55933 at 10 μM since this concentration has been used previously to inhibit ATM kinase activity in a variety of cell types.[54] Next, we determined the minimal amount of time prior to irradiation that cells needed to be incubated with 10 μM KU55933 to inhibit ATM kinase

activity in cells. ATM kinase activity was inhibited when 10 μM KU55933 was added to cells 5 minutes prior to irradiation (Figure 4).[19] We also determined the minimal amount of time for the removal of KU55933 prior to irradiation in order to recover ATM kinase activity in cells following incubation with 10μM KU55933 for one hour. ATM kinase activity was not inhibited when 10 μM KU55933 was removed from cells five minutes prior to irradiation (Figure 4).[19] Thus, the effective intracellular half-life of the ATM kinase inhibition by KU55933 in IMR90 cells is less than one hour.[19]

In order to more precisely determine the effective half-life of ATM kinase inhibition by KU55933 in IMR90 cells, ATM serine 1981 phosphorylation and CHK2 threonine 68 phosphorylation were immunoblotted 15 minutes following exposure to 5 Gy γ-rays. Again, ATM kinase activity was inhibited when 10 μM KU55933 was added to cells five minutes prior to irradiation (Figure 4)[19] Likewise, ATM kinase activity was not inhibited when 10 μM KU55933 was removed from cells five minutes prior to irradiation (Figure 4).[19] The effective intracellular half-life of the ATM kinase inhibition by KU55933 in IMR90 cells is therefore less than or equal to 15 minutes.

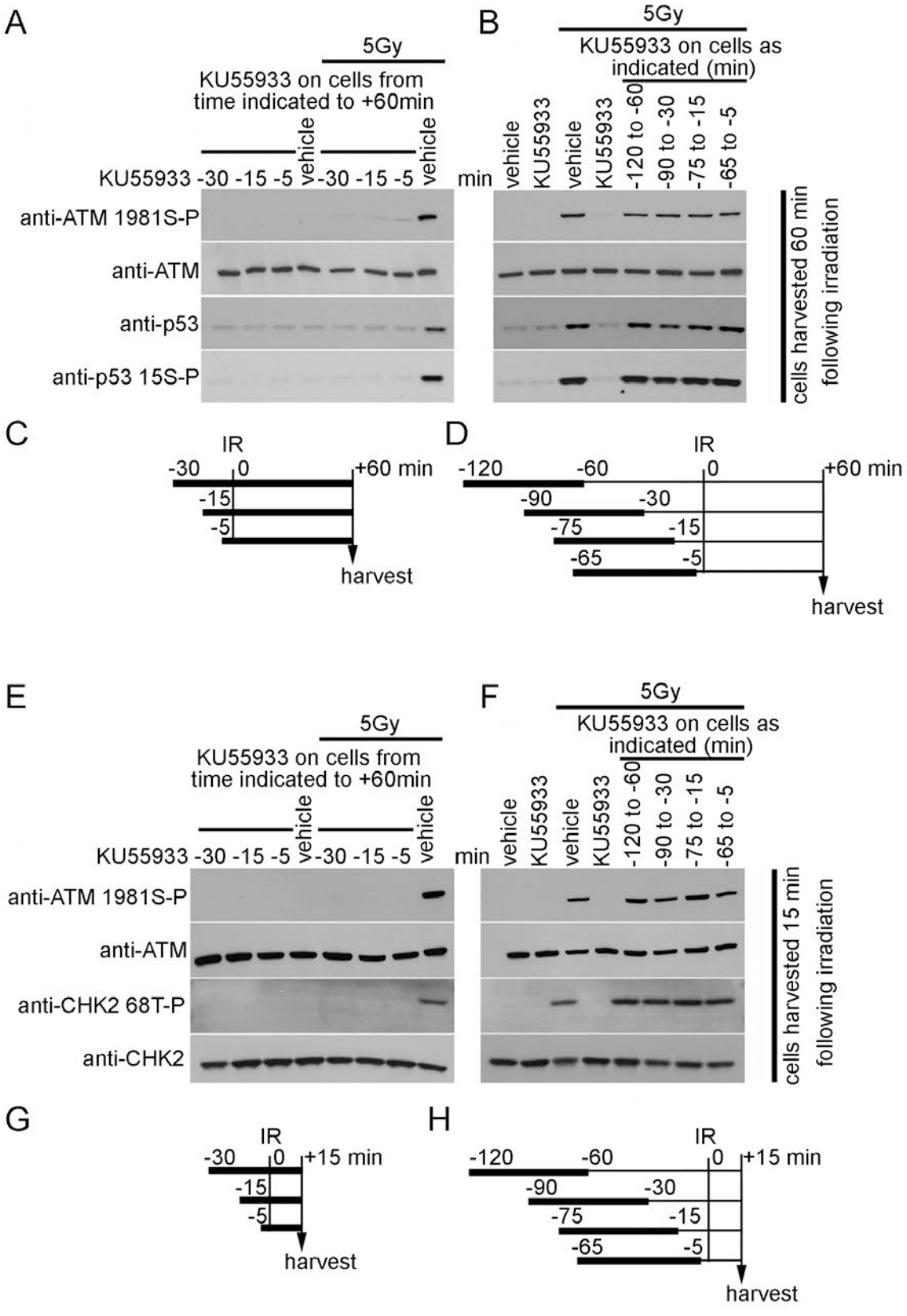
A
5Gy
KU55933 on cells from time indicated to +60min
vehicle
vehicle
KU55933 -30 -15 -5 -30 -15 -5
anti-ATM 1981S-P
anti-ATM
anti-p53
anti-p53 15S-P
B
5Gy
KU55933 on cells as indicated (min)
min
vehicle
KU55933
vehicle
KU55933
-120 to -60
-90 to -30
-75 to -15
-65 to -5
cells harvested 60 min following irradiation
C
IR
-30
0
+60 min
-15
-5
harvest
D
IR
-120
-60
0
+60 min
-90
-30
-75
-15
-65
-5
harvest
E
5Gy
KU55933 on cells from time indicated to +60min
vehicle
vehicle
KU55933 -30 -15 -5 -30 -15 -5
anti-ATM 1981S-P
anti-ATM
anti-CHK2 68T-P
anti-CHK2
F
5Gy
KU55933 on cells as indicated (min)
min
vehicle
KU55933
vehicle
KU55933
-120 to -60
-90 to -30
-75 to -15
-65 to -5
cells harvested 15 min following irradiation
G
IR
-30
0
+15 min
-15
-5
harvest
H
IR
-120
-60
0
+15 min
-90
-30
-75
-15
-65
-5
harvest

Figure 4. KU55933 functions as a "molecular switch" in cells.

A. ATM kinase activity is inhibited in IMR90 cells one hour following irradiation when 10 μM KU55933 is added to the cells five minutes prior to the irradiation. 10 μM KU55933 was added at the time indicated before the irradiation and left on the cells until lysis. **B.** ATM kinase activity is undiminished in IMR90 cells one hour following exposure to 5 Gy γ-rays when 10 μM KU55933 is removed from the cells five minutes prior to the irradiation. Cells were exposed to 10 μM KU55933 for one hour culminating at the time indicated prior to the irradiation (-120 min -60 min, -90 min to -30 min, -75 min to 15 min and -65 min to -5 min). Media containing KU55933 was then removed and replaced with pre-conditioned media. KU55933 was added to the control samples at -30 minutes and left on the cells. **C/D.** Black bars indicate when KU55933 was on the cells in A and B, respectively. **E.** ATM kinase activity is inhibited in IMR90 cells 15 minutes following exposure to 5 Gy γ-rays when 10 μM KU55933 is added to the cells five minutes prior to the irradiation. 10 μM KU55933 was added at the times indicated before the irradiation and left on the cells until lysis. **F.** ATM kinase activity is undiminished in IMR90 cells 15 minutes following exposure to 5 Gy γ-rays when 10 μM KU55933 is removed from the cells five minutes prior to the irradiation. Cells were exposed to 10 μM KU55933 for one hour culminating at the time indicated prior to the irradiation (-120 min -60 min, -90 min to -30 min, -75 min to 15 min and -65 min to -5 min). Media containing KU55933 was then removed and replaced with pre-conditioned media. KU55933 was added to the control samples at -30 minutes and left on the cells. G/H. Black bars indicate when KU55933 was on the cells in **E** and **F,** respectively.

2.4.2 KU60019

Studies were performed to determine the effective intracellular half-life of KU60019 indicate that KU60019 also functions as a molecule switch to inhibit ATM kinase activity in cells.[91] When 1 μM KU60019 was added to IMR90 cells five minutes prior to the irradiation, ATM kinase activity was inhibited 15 minutes following irradiation (Figure 5).[91] ATM kinase activity was restored in IMR90 fibroblasts 15 minutes following exposure to 5 Gy IR when 1 μM KU60019 was removed from fibroblasts five minutes prior to the irradiation (Figure 5).[91]

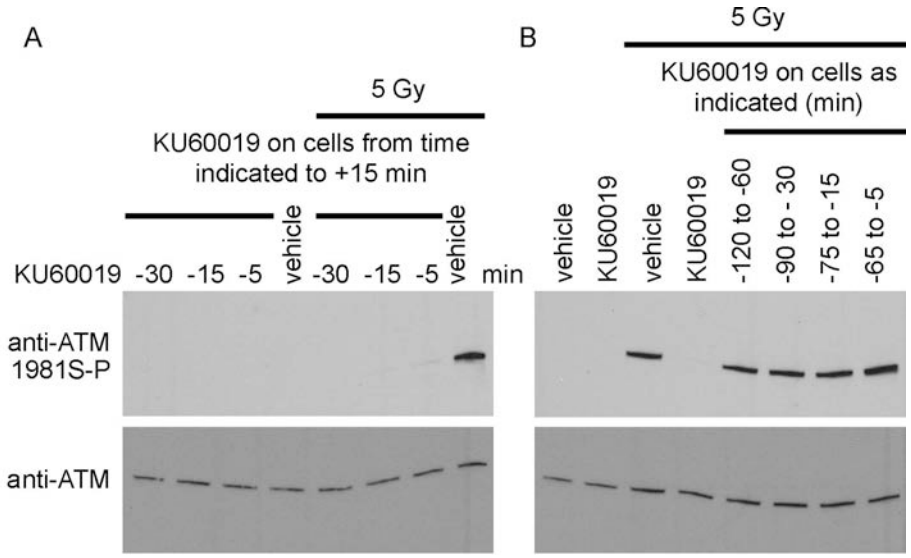

Figure 5. KU60019 functions as a "molecular switch" in cells.

A. ATM kinase activity is inhibited in IMR90 fibroblasts 15 min following irradiation when 1 μM KU60019 is added to fibroblasts 5 min prior to the irradiation. 1 μM KU60019 was added at the time indicated before the irradiation and left on the cells until lysis. **B.** ATM kinase activity is undiminished in IMR90 fibroblasts 15 min following exposure to 5 Gy IR when 1 μM KU60019 is removed from fibroblasts 5 min prior to the irradiation. Cells were exposed to 1 μM KU60019 for a 1 h period culminating at the time indicated prior to the irradiation (-120 min to -60 min, -90 min to -30 min, -75 min to -15 min and -65 min to -5 min). Media containing 1 μM KU60019 was then removed and replaced with preconditioned media. 1 μM KU60019 was added to the control samples at -30 min and left on the cells.

2.4.3 CGK733

To test whether CGK733 inhibits ATM or ATR kinase activity in cells, we determined the effects of CGK733 on cells exposed to either ionizing radiation (IR) or ultraviolet radiation (UV). We examined the well-characterized IR-inducible ATM kinase-dependent phosphorylations on ATM serine 1981 and CHK2 threonine 68 to determine whether CGK733 inhibits the kinase activity of ATM.[16,92] H460 human lung cancer cells were treated with 10 μM CGK733, 10 μM KU55933 or 1 μM KU60019 and exposed to 5 Gy γ-rays. H460 were used because we have previously documented the ATM-dependent effects of both KU55933 and KU60019 in these cells and we selected a concentration of 10 μM CGK733 because this is the higher dose reported to inhibit the kinase activities of ATM and ATR in human cells.[19,82,89-91] We observed that 10 μM CGK733 did not inhibit the IR-induced phosphorylation of either ATM serine 1981 or CHK2 threonine 68 one hour following irradiation whereas both 10 μM KU55933 and 1 μM KU60019, which served as positive controls for the experiment, abrogated both the IR-induced phosphorylation of ATM serine 1981 and CHK2 threonine 68 (Figure 6). Similar results were obtained using CGK733 purchased from Sigma-Aldrich (data not shown). We conclude that, contrary to previous reports, 10 μM CGK733 does not inhibit the kinase activity of ATM under these conditions.

In order to determine whether CGK733 inhibits the kinase activity of ATR we examined the phosphorylation of ATM on serine 1981 and the well-characterized UV-induced phosphorylation on CHK1 serine 317.[93] To date, three selective inhibitors of ATR kinase activity have been identified: 45, VE-821 and ETP-46464.[94-96] We treated H460 cells with 10 μM

CGK733 (Tocris Biosciences) or 10 μM ETP-46464 and exposed cells to 10 J/m^2 UV radiation. We observed that 10 μM CGK733 did not inhibit the UV-induced phosphorylation of CHK1 serine 317 six hours following irradiation whereas 10 μM ETP-46464, which served as a positive control for the experiment, abrogated the UV-induced phosphorylation of CHK1 serine 317 (Figure 6). Furthermore, the phosphorylation of ATM serine 1981 was increased in cells incubated in 10 μM ETP-46464 that were exposed to 10 J/m^2 UV radiation. This observation has been reported previously and is consistent with a model in which inhibition of the kinase activity of ATR results in an accumulation of double-strand DNA breaks, perhaps due to the disruption of protein complexes that protect stalled replication forks from endonucleases.[95] We conclude that, contrary to previous reports, 10 μM CGK733 does not inhibit the kinase activity of ATR under these conditions. We have been unable to demonstrate any inhibition of either the kinase activity of ATM or ATR by CGK733.

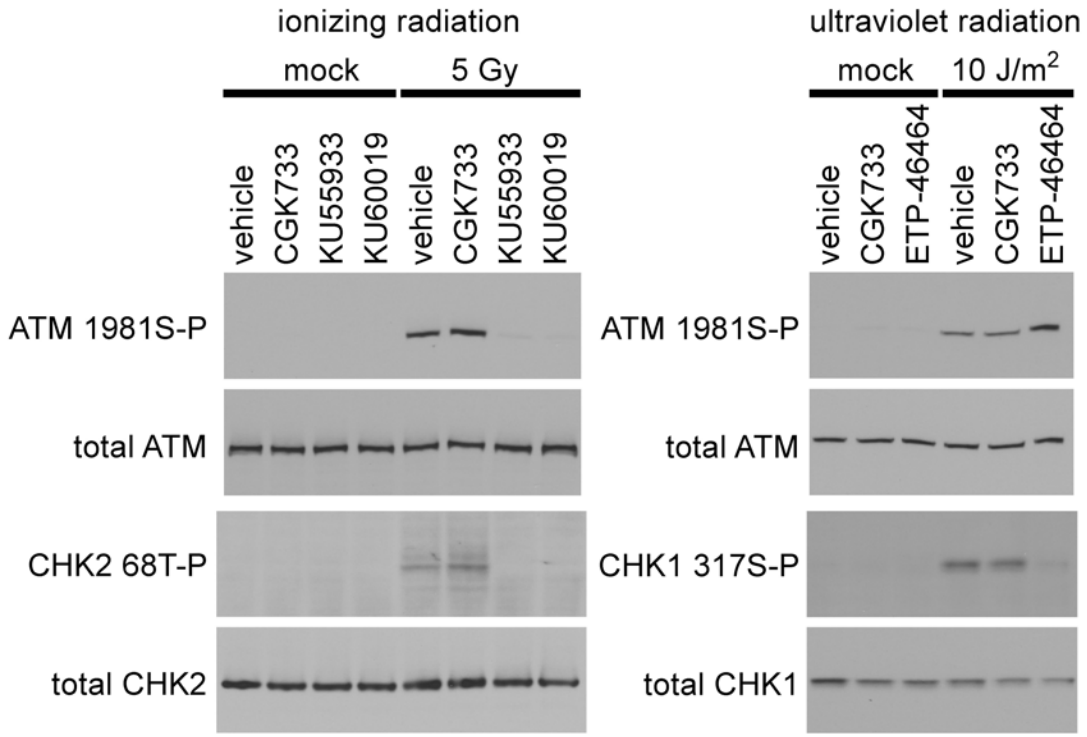

Figure 6. CGK733 does not inhibit ATM or ATR kinase activity in cells.

A. Immunoblots of IR-inducible ATM kinase-dependent phosphorylations on ATM serine 1981 and CHK2 threonine 68. H460 cells were treated with 10 μM CGK733, 10 μM KU55933 or 1 μM KU60019 from 30 min prior to exposure to 5 Gy γ-rays until harvest at 60 min following the insult. Lysates were resolved in 3-8% Tris-Acetate 1D SDS-PAGE gels and immunoblotted with anti-ATM 1981S-P, anti-ATM, anti-CHK2 68T-P and anti-CHK2.

B. Immunoblots of the phosphorylation of ATM on serine 1981 and ultraviolet radiation (UV)-induced phosphorylation on CHK1 serine 317. H460 human lung cancer cells were treated with either 10 μM CGK733 or 10 μM ETP-46464 from 30 min prior to exposure to 10 J/m^2 UV radiation until harvest at 6 h min following the insult. Lysates were resolved in 3-8% Tris-Acetate 1D SDS-PAGE gels and immunoblotted with anti-ATM 1981S-P, anti-ATM, anti-CHK1 317S-P and anti-CHK1.

2.5 CONCLUSIONS

We demonstrate that KU55933 and KU60019 can be used as "molecular switches" to selectively and transiently inhibit ATM kinase activity in cells. ATM kinase activity is inhibited in irradiated cells within 15 minutes of the addition of KU55933 or KU60019 and is restored within 15 minutes following the removal of KU55933 or KU60019 from cells. This distinctive attribute of KU55933 and KU60019 allows for studies designed to dissect the temporal requirement(s) for ATM kinase activity relative to the time of genotoxic exposure.

Importantly, we also show that CGK733 is *not* an ATM or ATR kinase inhibitor in cells. CGK733 does not inhibit ATM kinase signaling in H460 cells exposed to IR and CGK733 does not inhibit ATR signaling in H460 cells exposed to UV. We recognize that we did not use the same cell lines used in original CGK733 paper or in the subsequently published studies that have employed CGK733.[82,89,90] Thus, we acknowledge that, although unlikely, there is always the possibility that H460 may have a unique genetic background that prevents CGK733 from functioning as an ATM or ATR kinase inhibitor. Regardless, the demonstration that CGK733 does not inhibit ATM or ATR kinase activity in a cell line with intact ATM and ATR signaling warrants that proper controls be shown in future publications in which CGK733 is used to demonstrate that ATM or ATR kinase activities are actually inhibited.

3.0 CONSEQUENCES OF TRANSIENT ATM KINASE INHIBITION

3.1 INTRODUCTION

We previously showed that KU55933 can be used as a "molecular switch" to transiently inhibit ATM kinase activity in cells.[91] This attribute of KU55933 facilitates studies that temporally dissociate ATM kinase-dependent signaling and function(s). Here, we use KU55933 to isolate a temporal window, +15 minutes to +75 minutes following irradiation, during which ATM kinase activity is required for radioprotection. We also use KU55933 to dissociate an ATM kinase-dependent DNA repair mechanism from an ATM kinase-dependent cell cycle checkpoint mechanism. We show that ATM kinase inhibition from +15 minutes to +75 minutes following irradiation causes significant cellular phenotypes: cellular radiosensitivity, increased chromosome aberrations in late-S- and G_2-phases of the cell cycle and abrogation of sister chromatid exchange.

3.2 BACKGROUND

ATM encodes a protein kinase that is critical for the initiation of DNA damage responses in mammalian cells exposed to ionizing radiation (IR) and other agents that introduce double-strand breaks into DNA.[17,18,97] Cells derived from ataxia-telangiectasia (A-T) patients, who lack the ATM protein, exhibit defective cell cycle checkpoint responses, increased chromosome aberrations and increased cell death following IR, thus revealing the importance of ATM-dependent signaling in irradiated cells.[2]

ATM kinase activity is essential for the induction of DNA damage-induced cell cycle checkpoints. Within seconds of exposure to IR, ATM phosphorylates and activates downstream effector kinases, including checkpoint kinase 2 (CHK2), as well as numerous other substrates, and such modifications cause an arrest of the cell cycle at the G_1/S-phase and G_2/M-phase transitions.[24,29,33,92] DNA damage-induced cell cycle checkpoints were envisioned as a means to allow time for chromosome repair, thereby indirectly promoting chromosomal stability.[23] However, several lines of evidence suggest that the chromosomal instability of A-T cells is not entirely due to defective cell cycle checkpoints. For example, chromosome aberrations accumulate in irradiated A-T cells arrested in G_0 for up to 48 hours indicating this damage is not a consequence of defective cell cycle checkpoints.[38,40] Furthermore, when aphidicolin was used to block the G_1/S-phase transition in A-T cells, no decrease in cell death was observed following IR.[40] Since increased chromosome aberrations and cell death were evident in cells that were not

progressing through the cell cycle, these data are indicative of a DNA repair defect in A-T cells that is independent of cell cycle checkpoints.

ATM kinase activity has also been shown to have direct roles on DNA repair. DNA double-strand break (DSB) repair can occur through two mechanisms: homologous recombination (HR) repair and nonhomologous end joining (NHEJ).[42] HR is a high fidelity DSB repair mechanism that is generally restricted to the S- and G_2-phases of the cell cycle when a sister chromatid is available as a repair template.[43] ATM promotes the HR-mediated repair of DSBs in various systems, including in DT40 chicken cells in response to IR and in Chinese hamster cells in response to inhibition of poly ADP ribose polymerase (PARP).[98,99] Furthermore, ATM kinase activity has been reported to participate in DSB end resection, a key initiating step in HR.[48] Nevertheless, sister chromatid exchange (SCE), which is believed to be a cytological manifestation of HR at replication forks, is normal in A-T cells.[100-102] Therefore, the contribution of ATM to HR-mediated repair appears to be dispensible at replication forks.

NHEJ operates throughout the cell cycle but assumes most importance in G_1 when a sister chromatid is not available as a repair template.[44] The NHEJ machinery includes the DNA-dependent protein kinase (DNA-PK), a heterotrimer comprising a catalytic subunit and KU70 and KU80.[44] Additional components attributed to NHEJ machinery include the LIG IV/XRCC4 complex that has ligase activity, and also the Artemis endonuclease.[44] Previously, ATM kinase activity was implicated in NHEJ through its phosphorylation of Artemis.[45,46] ATM-dependent Artemis activity is required for the resolution of ~10% of DSBs by NHEJ in non-cycling G_0 cells with slow kinetics (i.e. repaired within several hours following IR).[45] Recently, ATM and Artemis have been reported to repair approximately 15% of IR-induced DNA double-strand breaks in G_2 cells through a HR repair mechanism also occurring with slow kinetics.[103]

Therefore, ATM and Artemis can function in a slow-repair process involving NHEJ or HR repair depending on the cell-cycle phase.[103] In these studies, the roles of ATM and Artemis in DNA double-strand breaks appear to represent the repair of DSBs located within or close to regions of heterochromatin.[103] Whereas, ATM-Artemis activity in heterochromatin involves DNA end-processing, ATM kinase also functions to relax heterochromatin by phosphorylating KAP1 (the corepressor for Krüppel-associated box zinc finger proteins).[104,105] Phosphorylated KAP1 spreads rapidly throughout chromatin and could thereby facilitate the entry of the DNA repair machinery.[104]

The precise nature of the lesion that is dependent on ATM function for resolution is not entirely known and the indispensable ATM-dependent mechanisms that ensure chromosome integrity are not fully understood. Here, we use KU55933 to isolate a temporal window during which ATM kinase activity is critically required for radioprotection and genome stability. We then identify the ATM kinase-dependent functions that mediate radioprotection and genome stability during this interval.

3.3 MATERIAL AND METHODS

3.3.1 Cell lines, irradiation and inhibitor treatment

The normal diploid fetal human lung fibroblast line IMR90 and non-small cell lung cancer cell line NCI-H460 were obtained from the American Type Culture Collection (ATCC). The A-T fibroblast cell line GM09607 was obtained from the Coriell Institute for Medical Research. H460 were cultured in RPMI supplemented with 10% FBS, and IMR90 and GM09607

were cultured in DMEM supplemented with 10% and 15% FBS, respectively. The Artemis-defective fibroblast line (CJ179-hTERT) was cultured in MEM supplemented with 15% FBS. KU55933 was reconstituted in DMSO and used at a final concentration of 10 μM. Cells were γ-irradiated in a Shepherd Mark I Model 68 [^{137}Cs] irradiator (J.L. Shepherd & Associates) at a dose rate of 77.0 R/min.

3.3.2 Clonogenic survival assay

One thousand cells were seeded in 60 mm petri dishes and treated with increasing doses of IR four hours post-plating. After 10 days, colonies were stained with 10% Giemsa/PBS solution. A colony was defined as a cluster of ≥50 cells, presumably having formed from a single cell. All experiments were performed in triplicate, and error is reported as the standard error of the mean.

3.3.3 siRNA transfections

H460 cells were transfected with either 40 nM siRNA targeted against ATM (5'-gcgccugauucgagauccutt-3') or a control siRNA targeted against luciferase using Lipofectamine 2000, according to the manufacturer's instructions (Invitrogen). Four days following transfection, cells were trypsinized, counted and plated for clonogenic survival assays. Cells were also collected at this time to generate lysates to validate loss of ATM protein expression by immunoblot.

3.3.4 Chromosome aberration analysis

T-25 flasks of IMR90 or H460 were exposed to increasing doses of irradiation 48 hours prior to being harvested with 50 nM calyculin A (Calbiochem, Gibbstown, NJ) for 30 minutes or 250 nM colcemid (Irvine Scientific, Santa Ana, CA) for two to four hours. The cells were harvested and dropped onto slides using conventional methods, and then solid-stained for eight minutes in 10% Giemsa. Chromosome aberrations included: chromosome breaks, chromatid gaps or breaks, quadriradials, triradials, giants, rings, minutes, dicentrics, fragments and dots. For the purposes of analysis, chromosome breaks, radials, giants, rings and dicentrics were assigned twice the weight of the other aberrations, as they involve two chromatid events. The total weighted aberrations (TWA) were determined per cell for each treatment. The standard error of the mean was used as the estimate of error in the sample.

3.3.5 G_2/M cell cycle checkpoint analysis

500,000 IMR90 fibroblasts were seeded in 60 mm dishes and exposed to 2 Gy irradiation 24 hours later. Fibroblasts were harvested at +75 minutes, +4 hours, +8 hours, and +12 hours following IR. For the time points at +4 hours, +8 hours, and +12 hours, the media containing KU55933 was removed at +75 minutes and replaced with pre-equilibrated media (media stored in a tissue culture flask overnight in an incubator set at 37° C and 5% CO_2) containing 100 ng/ml nocodazole to trap fibroblasts as they entered mitosis. Floating fibroblasts (obtained from media or 1x PBS wash) and trypsinized fibroblasts were collected and fixed overnight at -20°C in ice-cold 70% ethanol/1x PBS. Fixed fibroblasts were permeabilized on ice for eight minutes in

0.25% triton X-100/PBS. Permeabilized fibroblasts were blocked in 1% BSA/1x PBS for one hour, incubated with phospho-histone H3 (Ser10) Alexa Fluor® 647 conjugated antibody (Cell Signaling) for one hour and counterstained with propidium iodide (Roche). At least 50,000 fibroblasts per condition were analyzed by flow cytometry (Dako CyAn) and data were analyzed using Summit software (Dako). All experiments were performed in triplicate and the experiment was performed three times. Error bars were based on standard error of the mean.

3.3.6 Sister chromatid exchange (SCE) analysis

IMR90 or A-T fibroblasts (GM09607) were exposed to one cycle substitution (20 hours) with 10 μM BrdU prior to exposure to 2 Gy IR. Fibroblasts were allowed to recover for an additional 20 hours following treatment prior to harvesting in 250 nM colcemid (Irvine Scientific) for four hours. Harvested fibroblasts were dropped onto slides using conventional methods and metaphase spreads were differentially stained for SCE analysis. In brief, slides were incubated in Hoechst 33258 for 10 minutes, immersed in 55°C 2xSSC while exposed to a black light at a distance of 10 cm for 15 minutes. Exposed slides were then stained in 4% Giemsa for 10 minutes. Non-centromeric SCEs were scored for 50 fibroblasts. The standard error of the mean was used as the estimate of error in the sample. The experiments were performed two times.

3.4 RESULTS

3.4.1 ATM kinase activity is essential from +15 minutes to +75 minutes following irradiation for cell survival

We previously showed that the ATM kinase inhibitor KU55933 can be used as a "molecular switch," as ATM kinase activity is inhibited within 15 minutes of the addition of KU55933 to cells, and ATM kinase activity is restored within 15 minutes of the removal of KU55933 from cells.[19] We exploited this attribute of KU55933 to determine the critical window relative to the moment of IR during which ATM kinase activity is essential for radioprotection. Clonogenic survival assays were performed to determine the capacity of H460 cells to survive and replicate when ATM kinase activity was inhibited using 10 μM KU55933 for various intervals around an exposure to IR. The cellular radiosensitization seen when ATM kinase activity was inhibited for four hours (+15 minutes to +4 hours 15 minute) or one hour (+15 min to +75 min) accounted for 83% and 72%, respectively, of that seen when ATM kinase activity was inhibited for 17 hours (-45 minutes to +16 hours 15 minutes) following exposure to 5 Gy γ-rays (Figure 7).[19] The cellular radiosensitization seen when ATM kinase activity was inhibited for four hours (+15 minutes to +4 hours 15 minutes) or one hour (+15 minutes to +75 minutes) accounted for 70% and 33%, respectively, of that seen when ATM kinase activity was inhibited for 17 hours (-45 minutes to +16 hours 15 minutes) following exposure to 2.5 Gy γ-rays (Figure 7).[19] This shows that ATM kinase activity is required one hour following radiation for cell survival.

To address the possibility of an off-target effect of KU55933 on cellular radiosensitization, we compared the effect of KU55933 versus ATM protein disruption on cell

survival. The specificity of KU55993 for ATM is supported by its ability to inhibit ATM with an IC_{50} of 13 nM as opposed to DNA-PK (IC_{50} = 2.5 μM), mTOR (IC_{50} = 9.3 μM), PI-3K (IC_{50} = 16.6 μM), ATR (IC_{50} = > 100 μM) or PI-4K (IC_{50} = > 100 μM); moreover, 10 μM KU55933 does not radiosensitize A-T cells.[54] We confirmed that cellular radiosensitization of H460 cells seen with 10 μM KU55933 from +15 minutes to +75 minutes post-irradiation was identical to that seen when ATM protein was disrupted prior to the insult using siRNA (Figure 7).[19] The ATM protein disruption attained using siRNA resulted in an approximately 80% reduction in ATM protein and the cellular radiosensitization seen when ATM kinase activity was inhibited from +15 minutes to +75 minutes accounted for 72% of that seen when ATM kinase activity was inhibited for 17 hours following 5 Gy γ-rays (Figure 7).[19]

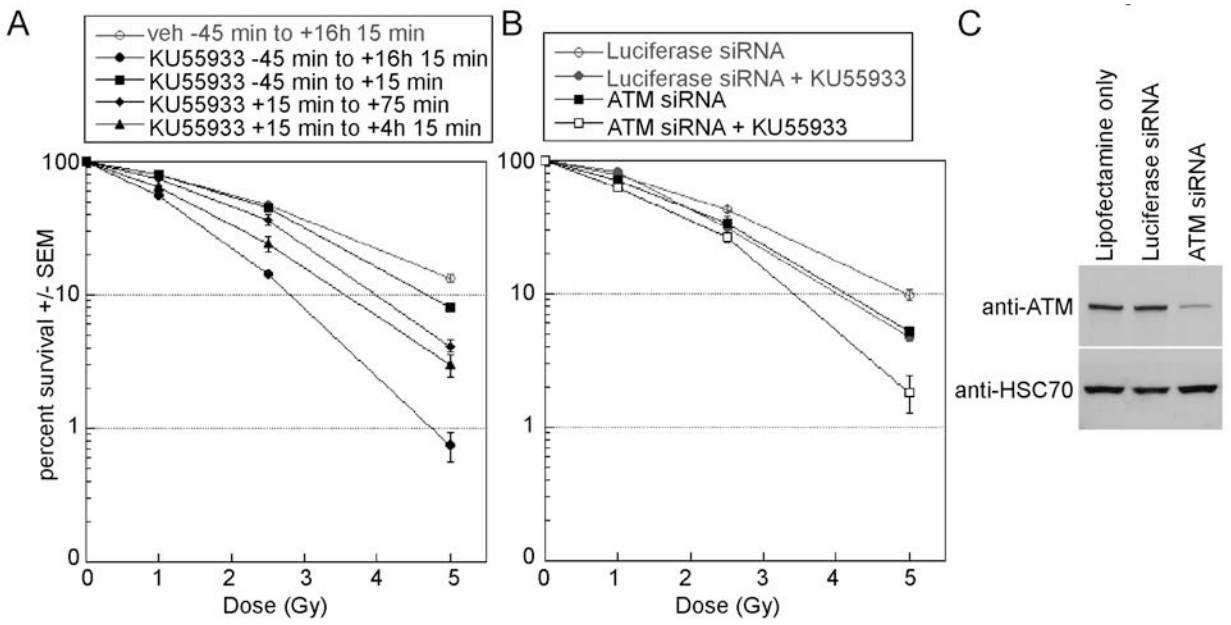

Figure 7. Sustained ATM kinase activity is essential for radioprotection.

A. Maximal radiosensitization is seen in H460 following 17 hours of 10 μM KU55933 treatment, from -45 min to +16 h 15min (irradiation at t=0). The cellular radiosensitization seen following four hours (+15 minutes to +255 minutes) and one hour (+15 minutes to +75 minutes) treatments with 10 μM KU55933 accounted for 83% and 72%, respectively, of that following 17 hours of 10 μM KU55933 at 5 Gy γ-rays. At 2.5 Gy γ-rays the cellular radiosensitization seen following four hours and one hour treatments with 10 μM KU55933 accounted for 70% and 33%, respectively, of that following 17 hours of treatment. **B.** The cellular radiosensitization seen in H460 cells when ATM kinase activity is inhibited using KU55933 from +15 min to +75 min is identical to that seen when ATM protein was disrupted using siRNA prior to the insult. H460 cells were mock-transfected or transfected with either siRNA targeted against ATM (5'-gcgccugauucgagauccutt-3') or a control siRNA targeted against luciferase. After four days, cells were concurrently plated for clonogenic survival assays and preparation of whole cell extracts. **C.** ATM protein levels are selectively reduced by 80% by the ATM siRNA. At the time of irradiation of the clonogenic survival assays, which had been set up concurrently, whole cell extracts were prepared and immunoblotted for validation of siRNA-mediated ATM protein disruption.

3.4.2 ATM kinase activity is essential from +15 minutes to +75 minutes following irradiation to suppress chromosomal instability.

Exponentially dividing IMR90 cells and H460 cells were treated with 10 μM KU55933 from +15 minutes to +75 minutes following exposure to 2 Gy γ-rays. Cells were harvested 48 hours later following an exposure to 250 nM colcemid, a microtubule inhibitor, or 50 nM calyculin A, which prematurely condenses chromatin allowing visualization of late-S-, G_2- and M-phase cells. In both H460 and IMR90 cells, there was ~1 break per cell, irrespective of KU55933 post-treatment or IR, with the exception of the cells exposed to both KU55933 and IR. The number of chromosome aberrations in H460 and IMR90 cells was increased approximately two-fold in late-S- and G_2-, but not M-phase, cells when ATM kinase was inhibited from +15 minutes to +75 minutes following exposure to 2 Gy IR (Fig. 8).[19] Approximately 83% of all aberrations are chromatid breaks in H460 cells and approximately 79% of all aberrations are chromatid breaks in IMR90 cells.[19]

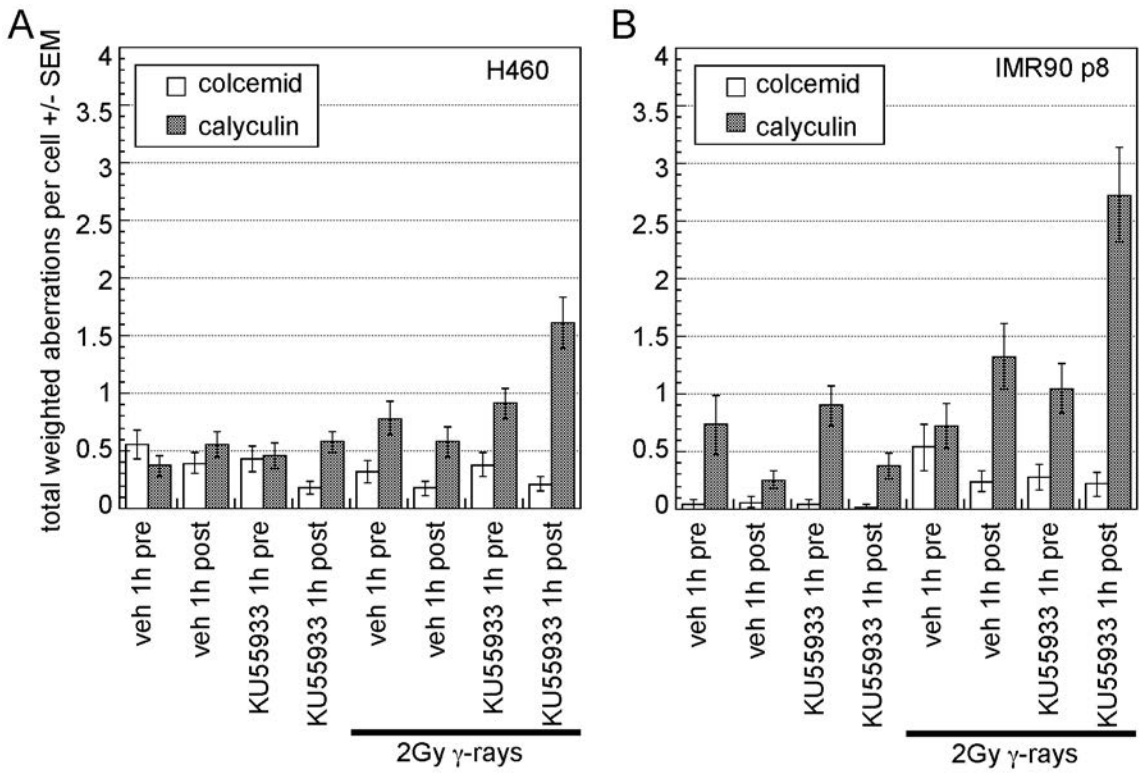

Figure 8. Transient ATM kinase inhibition from +15 minutes to +75 minutes following 2 Gy IR increases chromosomal aberrations.

The frequency of chromosome aberrations is increased 48 hours following irradiation in KU55933 treated late-S and G_2 cells. Cells were treated with 10 μM KU55933 from +15 minutes to +75 minutes following exposure to 2 Gy γ-rays. Cells were harvested 48 hours later following an exposure to 250 nM colcemid, a microtubule inhibitor, or 50 nM calyculin A, which prematurely condenses chromatin, allowing visualization of late-S- and G_2-phase cells. In order to compensate for differences in ploidy between cell lines, the total weighted aberrations per cell were compared. In both H460 (A) and IMR90 (B) cells, there was ~1 break per cell, irrespective of KU55933 post-treatment or irradiation, with the exception of the cells exposed to both KU55933 and irradiation. H460 and IMR90 cells exposed to both KU55933 and irradiation contained at least a two-fold increase in aberrations per cell.

3.4.3 15 minutes of ATM kinase activity following irradiation is sufficient to trigger the G_2/M cell cycle checkpoint and ATM kinase inhibition +15 minutes to +75 minutes following irradiation does not affect G_2/M cell cycle checkpoint recovery.

Because transient ATM kinase inhibition from +15 minutes to +75 minutes following exposure of cells to 2 Gy γ-rays is sufficient to cause the accumulation of persistent chromosome aberrations in late-S and G_2-, but not M-phase, cells, we hypothesized that the ATM kinase-dependent G_2/M cell cycle checkpoint may be induced within 15 minutes of exposure to 2 Gy γ-rays. In order to test this hypothesis, we utilized a flow cytometry-based G_2/M cell cycle checkpoint assay coupled with the microtubule inhibitor nocodazole to trap cells in mitosis.[106] We observed that induction of the G_2/M cell cycle checkpoint occurred rapidly in IMR90 fibroblasts treated with either KU55933 or vehicle from +15 min to +75 min following exposure to 2 Gy γ-rays, as indicated by the reduction of 4N cells positive for phosphorylated histone H3 at +75 minutes (Figure 9).[91] Furthermore, the recovery from the G_2/M arrest in IMR90 fibroblasts treated with KU55933 from +15 minutes to +75 minutes was comparable to that of vehicle controls at 4 hours, 8 hours and 12 hours following 2 Gy γ-rays (Figure 9).[91] Thus, 15 minutes of ATM activity is sufficient for the induction of the G_2/M cell cycle checkpoint following 2 Gy γ-rays and transient inhibition of the kinase activity of ATM from +15 minutes to +75 minutes post-IR does not affect recovery from this cell cycle checkpoint.

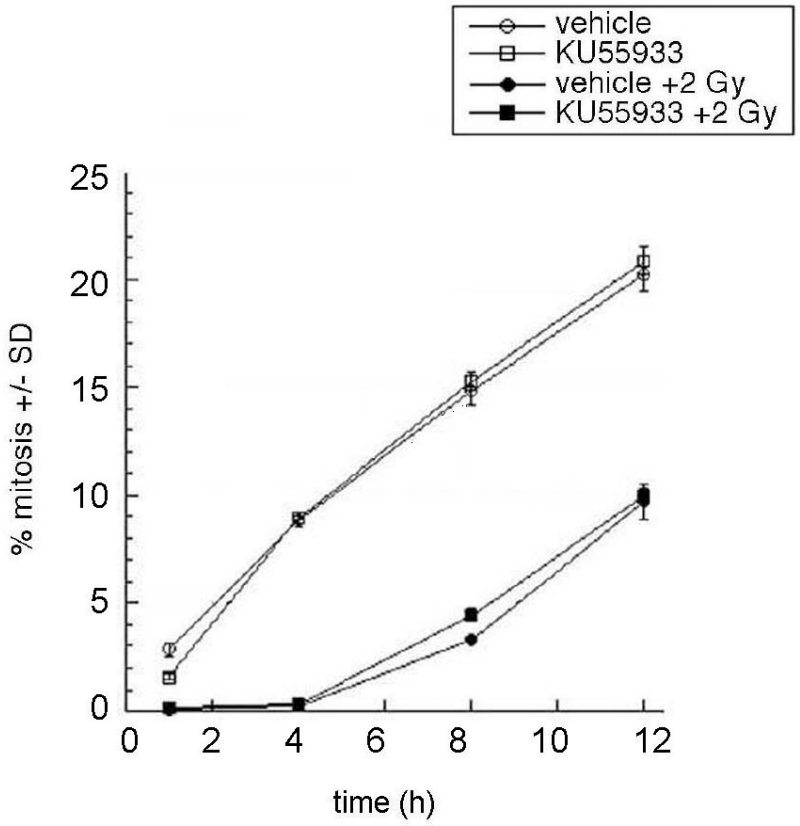

Figure 9. Transient ATM kinase inhibition +15 minutes to +75 minutes following 2 Gy IR does not affect G_2/M cell cycle checkpoint activation or recovery.

IMR90 fibroblasts were treated with KU55933 from +15 minutes to +75 minutes following 2 Gy IR, KU55933 was removed, and the microtubule inhibitor nocodazole was added in order to prevent cells from exiting mitosis. Fibroblasts were collected at +75 minutes, 4 hours, 8 hours, and 12 hours following IR for flow cytometric analysis of DNA content (% mitosis reflects 4N fibroblasts positive for phosphorylated histone H3 at +75 minutes). Recovery from the G_2/M checkpoint was not perturbed by addition of KU55933 from +15 to +75 min following 2 Gy IR. All conditions were performed in triplicate and the experiment was performed three times. Error bars were based on the standard error of the mean.

3.4.4 ATM kinase inhibition +15 minutes to +75 minutes following irradiation abrogates irradiation-induced sister chromatid exchange

Sister chromatid exchange (SCE) is believed to be a homologous recombination-mediated mechanism for the repair of stalled and collapsed DNA replication forks, which arise naturally during DNA replication or can occur if cells are irradiated in G_1 or S phase.[107] The molecular mechanisms of SCE and the role of ATM in SCE are not well understood. SCE is normal in A-T cells, indicating that ATM is not required for SCE.[100-102] Given that homologous recombination repair occurs in late-S- and G_2-phase, we hypothesized that the increase in chromosome aberrations that is seen with ATM kinase inhibition from +15 minutes to +75 minutes following irradiation can be attributed to defects in homologous recombination repair. To test this hypothesis, we compared the number of IR-induced SCEs in fibroblasts entering mitosis in the presence or absence of functional ATM.

We used four hours of treatment (from +8 hours to +12 hours post-irradiation) with colcemid, initiated 8 hours following IR, to trap cells in mitosis since recovery from the G_2/M arrest in IMR90 fibroblasts treated with KU55933 from +15 minutes to +75 minutes following IR was shown to be comparable to that of vehicle controls at four hours, eight hours, and 12 hours following IR (Figure 9).[91] We found that the IR-induced increase in SCE at 12 hours following IR was abrogated when cells were treated with KU55933 from +15 minutes to +75 minutes post-IR (Figure 10).[91] Importantly, SCE was not abrogated when ATM kinase activity was inhibited -45 minutes to +15 minutes following exposure to IR, indicating that IR-induced increase in SCE is not a consequence of mitotic recombination or a second round of DNA replication (Figure 10).[91]

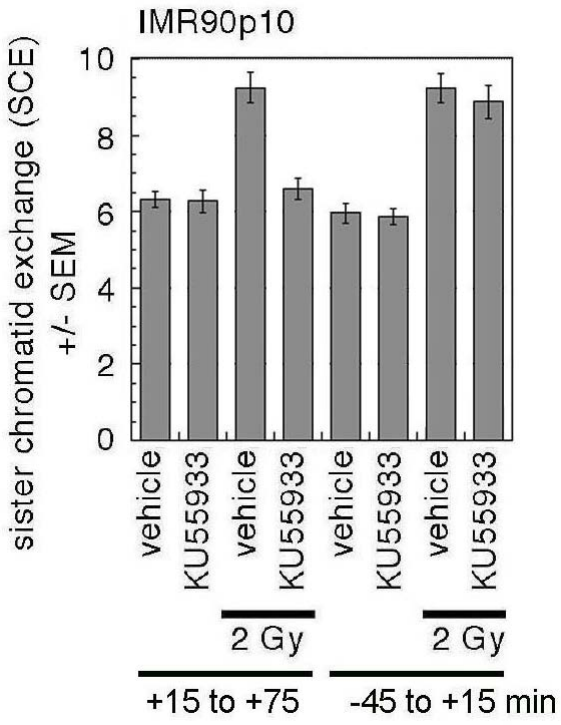

Figure 10. KU55933 abrogates IR-induced SCE in IMR90 cells.

Treatment with 10 μM KU55933 +15 minutes to +75 minutes following 2 Gy IR, but not -45 minutes to +15 minutes following 2 Gy IR, abrogates IR-induced SCE in IMR90 human primary lung fibroblasts.

To ensure that KU55933 does not have an "off-target" effect that disrupts SCE, we investigated the effect of KU55933 on SCE in irriadated GM09607 A-T fibroblasts, which lack ATM protein. We harvested the fibroblasts after a four hour treatment with colcemid (from +16 hours to +20 hours), which was initiated 16 hours following IR, to trap cells in mitosis and the number of SCEs per cell was counted in 50 cells. Each experiment was performed two times. In unirradiated A-T fibroblasts, we observed ~12 SCEs per cell both in fibroblasts treated with or without the ATM kinase inhibitor (Figure 11).[91] Inhibition of ATM activity also did not change the number of SCEs (~17) in A-T fibroblasts 20 hours following exposure to 2 Gy IR (Figure

11).[91] Thus, KU55933 does not appear to have an "off-target" effect that disrupt SCE in A-T fibroblasts. Because IR-induced SCE is intact in A-T fibroblasts, an ATM-independent mechanism of SCE clearly exists (Figure 11).[91,100-102] In addition, since KU55933 abrogates SCE in IMR90 fibroblasts, which have functional ATM protein, but not in A-T cells, which lack ATM protein, the cellular consequences of acute, transient inhibition of ATM kinase activity and chronic loss of ATM protein are distinct.[91]

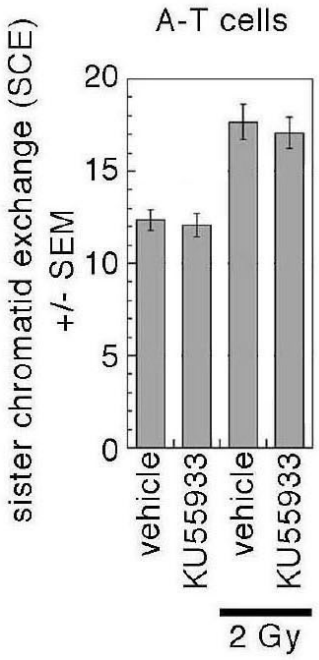

Figure 11. KU55933 does not abrogate SCE in A-T cells.

Treatment with 10 μM KU55933 from +15 minutes to +75 minutes following 2 Gy IR has no effect on IR-induced SCEs in GM09607 A-T fibroblasts.

3.5 CONCLUSIONS

Our finding that KU55933 can be used as a "molecular switch" to transiently inhibit ATM kinase activity in cells has facilitated unique analyses of ATM kinase-dependent signaling and function.[19] We show here that the cellular radiosensitization seen when ATM kinase activity is inhibited for only 1 hour (+15 minutes to +75 minutes) following irradiation, accounts for over 70% of the cellular radiosensitization seen when ATM kinase activity is inhibited for 17 hours (-45 minutes to +16 hours 15 minutes).[19] We also demonstrate that the number of chromosome aberrations in IMR90 and H460 cells, determined 48 hours following irradiation, is increased approximately two-fold in late-S- and G_2-, but not M-phase, when ATM kinase is inhibited from +15 minutes to +75 minutes following exposure to 2 Gy γ-rays.[19] The majority of these aberrations in H460 and in IMR90 cells are chromatid breaks, and it is important to highlight that the aberrations *persist* despite the fact that ATM kinase activity is restored at +75 minutes post-irradiation when KU55933 is removed from cells 47 hours prior to the preparation of the chromosome spreads.[19] These data indicate that chromosome damage accumulates very rapidly in the absence of ATM kinase activity +15 to +75 minutes post-irradiation and persists for days.[19]

Our finding that the number of chromosome aberrations in IMR90 and H460 cells is doubled in late-S- and G_2-, but not M-phase, suggested that the DNA damage that is formed as a consequence of transient ATM kinase inhibition induces an ATM kinase-dependent G_2/M cell cycle checkpoint. This would be consistent with the report that restoration of ATM kinase activity in mature lymphocytes that have transiently lost ATM function leads to loss of cells that have accumulated terminally deleted chromosomes, a finding that identifies a requirement for ATM in faithful end joining as well as checkpoint activation to prevent the persistence and

transmission of DNA DSBs.[108] We show here that 15 minutes of ATM kinase activity is sufficient to induce the G_2/M cell cycle checkpoint in response to IR and that neither the activation nor the recovery of this IR-induced cell cycle checkpoint is affected by ATM kinase inhibition from +15 minutes to +75 minutes (Fig. 9).[91] Using KU55933 to temporally dissect ATM kinase functions following irradiation, we have dissociated an ATM kinase-dependent DNA repair mechanism from an ATM kinase-dependent cell cycle checkpoint mechanism.[91]

We next hypothesized that the increase in chromosome aberrations that is seen in late-S- and G_2-phase with ATM kinase inhibition from +15 minutes to + 75 minutes following irradiation can be attributed to defects in homologous recombination repair given that homologous recombination repair of double-strand breaks occur in late-S- and G_2-phases of the cell cycle. To test this hypothesis, we compared the number of IR-induced SCEs in fibroblasts entering mitosis in the presence or absence of functional ATM and show that the increase in SCE in irradiated fibroblasts was abrogated when ATM kinase activity was transiently inhibited from +15 minutes to +75 minutes following exposure to IR (Fig. 10).[91] This result is surprising because DNA damage-induced SCE occurred in A-T fibroblasts (Fig. 11), suggesting that A-T fibroblasts have adapted to the loss of this function of ATM and can initiate SCE in response to DNA damage through an ATM-independent mechanism.[91] That is to say, the cellular consequences of acute ATM kinase inhibition and adaptation to loss of ATM protein are different in S-phase cells.[91,109]

Thus, we demonstrate that KU55933 can be used to temporally isolate and dissociate ATM kinase-dependent functions. Transient ATM kinase inhibition from +15 minutes to +75 minutes following IR has severe cellular consequences: radiosensitivity, increased chromosome

aberrations in late-S- and G_2-phases of the cell cycle and a defect in sister chromatid exchange.[19,91]

4.0 ATM KINASE ACTIVITY IN SPATIAL PROTEIN DYNAMICS

4.1 INTRODUCTION

DNA damage invokes the dynamic recruitment and assembly of proteins on damaged chromatin. ATM is a central kinase in the DNA damage response, but its effects on protein dynamics has not been well studied. Here, we use SILAC-based tandem mass spectrometry combined with a subcellular fractionation protocol to compare the proteomes of irradiated IMR90 cells treated with and without the selective ATM kinase inhibitor, KU55933, across four distinct subcellular fractions: cytoplasmic, soluble nuclear, chromatin and insoluble pellet. Analysis of the chromatin proteome shows that the retention of 53BP1 at damaged chromatin is decreased when cells are treated with KU55933. Using fluorescence recovery after photobleaching (FRAP), we show that the stability of GFP-53BP1 radiation-induced foci is decreased with KU55933. We also identify ANXA1 as a protein significantly enriched for protein-protein interactions with DNA damage response proteins. Following irradiation, in the presence of KU55933, ANXA1 levels are selectively decreased in the chromatin fraction, whereas cytoplasmic ANXA1 levels are unchanged with KU55933. These results provide a roadmap for understanding ATM kinase-dependent spatial protein dynamics in response to DNA damage.

4.2 BACKGROUND

The DNA damage response is a complex network of signal transduction pathways that activate processes such as DNA repair, cell cycle checkpoints, transcriptional regulation and chromatin reorganization in order to ensure cellular homeostasis and survival.[110-112] Key to the DNA damage response is ataxia telangiectasia-mutated (ATM), a 370 kilodalton serine/threonine protein kinase that is activated by agents that cause DNA double-strand breaks (DSBs).[113] Once activated, ATM phosphorylates substrates involved in DNA replication, DNA repair, cell cycle progression as well as other signal transduction pathways.[113] Loss of ATM protein due to mutations in the ATM gene results in ataxia telangiectasia (A-T), a human disease characterized by exquisite radiosensitivity and predisposition for cancer.[1,113] Global proteomic studies on ATM and the related kinase ATR have been aimed at identifying direct and indirect phosphorylation targets and have led to the identification of over 1,000 ATM and ATR substrate phosphorylation sites in cells.[20-22] However, the role of ATM kinase activity on the spatial dynamics of proteins in response to DNA damage has not been explored.

The DNA damage response is characterized by orchestrated spatial and temporal dynamics that are essential for an effective DNA repair.[114,115] Following exposure to genotoxic agents, proteins are rapidly mobilized and loaded onto damaged chromosomes, assembling protein complexes that mediate DNA repair.[114,115] Following irradiation, ATM phosphorylates histone H2AX, which is required to sustain the retention of repair proteins on H2AX-marked chromatin.[116,117] The concentration of these recruited proteins at chromatin amplifies ATM signaling and presumably increases the efficiency of DNA repair.[116,117] There is also precedent for ATM kinase regulation of protein dynamics across subcellular compartments. ATM kinase activity has previously been shown to regulate the localization of the deubiquitinase USP10.[118]

Following irradiation, USP10 translocates from the cytoplasm to the nucleus and stabilizes p53.[118] ATM kinase-dependent phosphorylation of USP10 at Thr42 and Ser337 regulates the translocation and stabilization of USP10.[118] Thus, ATM kinase-dependent relocalization of USP10 suppresses tumor growth by regulating the subcellular localization of p53.[118] USP10 deubiquitinates p53, reversing Mdm2-mediated p53 nuclear export and degradation.[118]

Multiple examples from human diseases show that defects in the recruitment and retention of DNA damage proteins on chromatin result in genome instability and cancer indicating that spatial protein dynamics have crucial functions in human health. Defects in the recruitment of BRCA1, the major human hereditary breast cancer susceptibility protein, result in breast cancer.[69,119] Defects in the loading of DNA interstrand crosslink repair proteins on chromatin cause the genome instability syndrome Fanconi Anemia.[69,119-121] Therefore, identifying proteins that are spatially regulated by ATM kinase activity could reveal additional functions for ATM in the DNA damage response which are clinically significant.

Here we use stable isotope labeling in cell culture (SILAC) quantitative mass spectrometry combined with a fractionation protocol to investigate the role of ATM kinase activity in DNA damage-induced spatial protein dynamics.[122]

4.3 METHODS

4.3.1 Cell culture

IMR90 and U2OS cells were cultured in DMEM supplemented with 10% fetal bovine serum and 100 units/mL penicillin/streptomycin. In the SILAC experiment, IMR90 cells were grown in DMEM supplemented with 10% fetal bovine serum dialyzed with a cutoff of 10 kDa (Pierce, Rockford, IL) and 100 units/mL penicillin/streptomycin. We cultured two separate populations of IMR90 cells in either "light" SILAC medium (supplemented with L-lysine and L-arginine with natural abundance isotopes) or in "heavy" SILAC medium (supplemented with $^{13}C_6$-lysine and $^{13}C_6{}^{15}N_4$-arginine) (Pierce, Rockford, IL) for at least 6 passages. Cells were tested for full incorporation of labeled isotopes after six passages.

4.3.2 Subcellular fractionation

IMR90 cells cultured in "light" and "heavy" SILAC medium were plated with equal cell numbers into three 60 mm petri dishes (6 total dishes). The next day, both cell populations were γ-irradiated with 2 Gy in a Shepherd Mark I Model 68 [^{137}Cs] irradiator (J.L. Shepherd & Associates, San Fernando, CA) at a dose rate of 78.3 R/min. At +15 minutes post-irradiation, KU55933 (KuDOS Pharmaceuticals) was added to the cells grown in "heavy" media so that the final concentration of KU55933 was 10 μM. The equivalent volume of DMSO (vehicle control) was added to the cells grown in "light" media.

At +75 minutes post-irradiation, the cells from both populations were washed twice with PBS, and cells from both "heavy" and "light" populations were fractionated as described

previously, with additional modifications.[123-125] 150 µL of Solution A [10 mM HEPES (pH 7.9), 10 mM KCl, 1.5 mM MgCl2, 0.34 sucrose, 10% glycerol, 0.1% triton X-100] was added to each 60 mm dish from the "heavy" and "light" populations, and the cells were scraped and collected into the same eppendorf tube (1:1 ratio) and incubated for five minutes on ice. Cells were centrifuged at 1,300 g on a Sorvall tabletop centrifuge, and the supernatant was collected as the cytoplasmic fraction.

The remaining pellet was washed once with Solution A, and resuspended in 400 µL of Buffer MN [Solution A with 1 mM $CaCl_2$] with four units of micrococcal nuclease (Worthington Biochemical Corporation, Lakewood, NJ) and the incubated in a 37°C waterbath for two minutes. 1mM EGTA was then added to the tube to stop the micrococcal nuclease reaction and the lysate was centrifuged at 1,300 g for seven minutes. The supernatant was collected and removed. The nuclear pellet was washed once in Solution A, then resuspended in 100 µL Solution B [3 mM EDTA, 0.2 mM EGTA], vortexed and allowed to incubate on ice for ten minutes. The tube was centrifuged at 10,000 g for seven minutes and the supernatant was collected as the soluble nuclear fraction. 100 µL of modified RIPA lysis buffer [20 mM HEPES, 137 mM NaCl, 10% glycerol, 1% triton X-100, 0.5% sodium deoxycholate, 0.1% SDS, 2 mM EDTA] was added to the pellet, the lysate was vortexed and incubated on ice for ten minutes. The tube was centrifuged at 1,000 g for ten minutes and the supernatant was collected as the chromatin fraction. 200 µL Laemmli buffer (Bio-Rad, Hercules, CA) was added directly to the remaining pellet for the insoluble fraction. Laemmli buffer was added to the cytoplasmic, soluble nuclear and chromatin fractions at a 1:1 volume ratio.

Phosphatase inhibitors (sodium orthovanadate, β-glycerophosphate, sodium pyrophosphate, sodium fluoride), SUMOylase inhibitor (N-ethylmaleimide), 1 mM DTT and a

complete mini EDTA-free protease inhibitor cocktail tablet (Roche Applied Science, Indianapolis, IN) were added to all fractionation buffers (Solution A, Buffer MN, Solution B, Modified RIPA) before use. The four fractions were resolved by 1D SDS-PAGE on a NuPAGE Novex 4-12% Bis-Tris precast gels (Invitrogen, Carlsbad, CA). The gel was stained with Coomassie blue to provide a general estimation of the protein lysate integrity. The gel lane from each fraction was sliced into ten equivalent sized bands (four fractions * ten slices=40 total bands) and proteins were digested in-gel overnight with sequencing grade trypsin (Promega, Madison, WI).

4.3.3 LC-MS/MS

The extracted tryptic peptides from each of the 40 gel bands were separately analyzed in duplicate by nanoflow reversed-phase (RP) LC coupled online by electrospray ionization with a hybrid linear ion trap-Orbitrap MS (ThermoFisher Scientific, San Jose, CA). Liquid chromatography was performed using a Dionex Ultimate 3000 nanoflow LC system (Dionex Corporation, Sunnyvale, CA). Separation of the sample was performed using a 75 μm inner diameter x 360 outer diameter x 45 cm-long fused silica capillary column (Polymicro Technologies, Phoenix, AZ) packed in house with 5 μm, 300 Å pore size Jupiter C-18 stationary phase (Phenomenex, Torrance, CA). After injection, the column was washed with 98% mobile phase A (0.1% formic acid in water) for 30 min and peptides were eluted by development of a linear gradient of 2% mobile phase B (0.1% formic acid in acetonitrile) to 42% mobile phase B in 140 min, then to 98% B in an additional 20 min, all at a constant flow rate of 250 nL/min. The MS was operated in a data-dependent MS/MS mode in which each full high resolution MS scan conducted in the Orbitrap was followed by seven MS/MS scans in the linear ion trap where the

seven most abundant peptide molecular ions dynamically determined from the MS scan were selected for tandem MS using a relative collision-induced dissociation (CID) energy of 30%. Dynamic exclusion was utilized to minimize redundant selection of peptides for CID.

4.3.4 Bioinformatics

Tandem mass spectra were searched for peptide identifications by running Inspect, against human IPI protein database (v3.75) with parent mass tolerance 2 Da and fragment mass tolerance 0:5.[126] At most one modification (K+6, R+10) was allowed. To distinguish between the false and correct peptide identifications, false discovery rate (FDR) approach using a standard target/decoy strategy was employed.[127] Each Inspect search result was individually filtered at 1% FDR. Quantification of protein abundance was be achieved by measuring the relative intensities of light and heavy peptides in the MS spectra, which were spaced by 6 daltons for peptides with Lys (K) or by 10 daltons for ones with Arg (R). Ratios were generated for each protein based on the corresponding peptide intensities of KU55933 to control (KU55933:vehicle) to determine the differential protein abundance in each fraction. Protein SILAC ratios will be determined by averaging all peptide SILAC ratios from all unique and common peptides identified per given protein.

4.3.5 Network analyses of the chromatin fraction

The Cytoscape NeMo algorithm was used to analyze the chromatin fraction to identify densely connected sub-component.[128] We used the ConsensusDB protein-protein interaction network, which includes ~100,000 known protein-protein interactions in human cells

downloaded from interaction databases such as BioGRID, IntAct, and HPRD.[129] Chromatin proteins from the screen were included in the analysis if the protein ratio fulfilled one of two criteria: absolute value(log_2ratio) > 0.58 or pval < 0.05. 29 sub-networks were identified and the final networks were generated from taking the union of the 29 subnetworks. The node colors was used to represent relative log_2ratio(KU55933/vehicle) protein abundance. Dark green nodes indicate a low log_2ratio(KU55933/vehicle), dark red nodes indicate a high log_2ratio(KU55933/vehicle), white nodes indicate proteins detected in the screen but were unchanged with KU55933 and grey nodes represent proteins which were not detected in the screen.

For the DNA damage response network enrichment analysis of the chromatin fraction, we determined what fraction of direct neighbors in a protein interaction network are DNA damage response (DDR) proteins. Chromatin proteins were included in the analyses if the protein ratio had a |log_2ratio(KU55933:control)| > 1.5 or with a p-value for differential expression below 0.05 We used the ConsensusPathDB protein-protein interaction network and a list of 434 proteins that function in the DDR for this analysis.[129] A p-value for DDR neighborhood enrichment was determined by an enrichment ratio: 1) # of neighbor genes involved in DDR/total # of neighbor genes and 2) # of DDR genes/total of # of genes in network. The hypergeometic distribution was used to generate a p-value for the significance of enrichment (distribution of ratio 1 versus distribution of ratio 2), which was corrected for multiple hypothesis testing using the Benjamini-Hochberg method.

4.3.6 Antibodies and plasmids

Antibodies used: mouse anti-ATM (Sigma), rabbit anti-phospho S1981 ATM (Epitomics), rabbit anti-p53 (Santa Cruz Biotech), mouse anti-GAPDH (Abcam), mouse anti-retinoblastoma (BD Biosciences), rabbit anti-histone H3 (Abcam), mouse anti-lamin A+C (Abcam) and mouse anti-53BP1 (Millipore). ms53BP1-GFP expression construct was a kind gift from Jiri Bartek. Lipofectamine 2000 (Invitrogen, Carlsbad, CA) was used for the transfection of plasmids into cells.

4.3.7 Live cell microscopy

GFP-mouse-53BP1 was transfected into U2OS cells using Lipofectamine 2000 (Invitrogen) and stable expression of GFP-ms53BP1 was selected using G418 (50 μg/mL). Cells were plated on 35 mm round glass bottom dishes (MatTek Corp.) and incubated overnight at 37°C with 5% CO_2. The next day, the dishes were irradiated with 2 Gy of ionizing radiation using a [^{137}Cs] source. 15 min post-irradiation, 10 μM KU55933 or the equivalent volume of DMSO (vehicle control) was added to the dishes and incubated at 37°C with 5% CO_2. At +60 min post-irradiation dishes were placed in an environmentally controlled closed chamber system (Tokai Hit) which was maintained at 37°C and 5% CO_2 during imaging. The chamber system was mounted on an inverted confocal microscope (Nikon A1, Nikon), controlled by NIS-Elements software.

At +75 minutes post-irradiation, time-lapse image acquisition was initiated on defined ionizing radiation-induced nuclear foci to obtain baseline intensities. Ionizing radiation-induced nuclear foci were then photobleached using a 488-laser set at 100% power, a scan speed of 1/8

frames per second, an exposure time of 53.57 seconds, allowing seven laser pulses to hit a defined region in a single nucleus. Time-lapse images were captured for 30 minutes following photobleaching (from +75 minutes to +105 minutes post-2 Gy IR), in 30 second intervals with the 488-laser set at 5% power, a scan size of 1024, a scan speed of ¼ frames per second, and a zoom of 1.499X. The excitation wavelength for GFP was the 488-laser and signal was collected through a CFI Plan Apo VC 60´ Oil objective, NA=1.40. Perfect focus system (PFS) was applied to automatically correct possible focus drift during the period of time-lapse imaging. Post-acquisition processing of image files was performed with NIS-Elements software. We performed a double normalization to correct for acquisition bleaching for each region of interest (ROI).[130] The mean pre-bleach whole cell intensity of a neighboring cell expressing GFP-53BP1 was divided by the mean whole cell intensity of the same neighboring cell at each time point in the post-bleach period, and this ratio was then multiplied to the FRAP curve at respective time points. To correct for background intensity, the mean intensity of a background ROI was subtracted from the neighboring cell ROIs and FRAP ROIs for each timepoint. Relative intensity (RI) was calculated by: $RI(t) = I(t)/I_{pb}$, where I_{pb} is the mean intensity of the ROI before photobleaching. Each data point was derived from the mean intensities of 5 different foci measurements from 5 different cells collected from 3 different experiments per condition. The error bars in the FRAP curve represent the standard error of the mean.

4.4 RESULTS

4.4.1 SILAC and LC-MS/MS

We grew two populations of IMR90 cells in either "light" media (DMEM supplemented with $^{12}C_6$-lysine and $^{12}C_6{}^{14}N_4$-arginine) or "heavy" media (DMEM supplemented with $^{13}C_6$-lysine and $^{13}C_6{}^{15}N_4$-arginine) to differentially label proteins with isotopes that can be distinguished using mass spectrometry (Figure 12).[122,131] Growth in heavy media had no effect on ATM kinase signaling in irradiated cells (Figure 12). KU55933 is a selective and reversible ATM kinase inhibitor that can be used to transiently inhibit ATM kinase activity in cells.[19,91] We have previously shown that 1 hour transient ATM kinase inhibition with KU55933, from +15 minutes to +75 minutes following 2 Gy of ionizing radiation, sensitizes cells, increases chromosome aberrations and abrogates sister chromatid exchange, demonstrating that sustained ATM kinase activity has critical functions one hour post-irradiation.[19,54,91] Thus, we incorporated the same temporal treatment window of KU55933 into the design of the SILAC workflow. At +15 minutes post-irradiation, cells grown in heavy media were treated with 10 μM KU55933, and cells grown in light media were treated with the equivalent volume of DMSO (vehicle control) for one hour at 37°C. At +75 minutes post-irradiation, both light and heavy cell populations were harvested, mixed at a 1:1 ratio, and fractionated using a protocol described previously with several modifications.[123-125] Four distinct subcellular fractions were generated as evidenced by the immunoblot detection of the cytoplasmic protein GAPDH, the soluble nuclear protein retinoblastoma, the chromatin-bound protein histone H3 and the nuclear matrix/nuclear membrane-associated protein Lamin A+C in fractionated lysates from unirradiated IMR90 cells (Fig. 12). All four fractions were separated by 1D SDS-PAGE and each gel lane was cut into ten

pieces, digested with trypsin, and analyzed by nanoflow reversed-phase (RP) LC coupled online by electrospray ionization with a hybrid linear ion trap-Orbitrap MS.

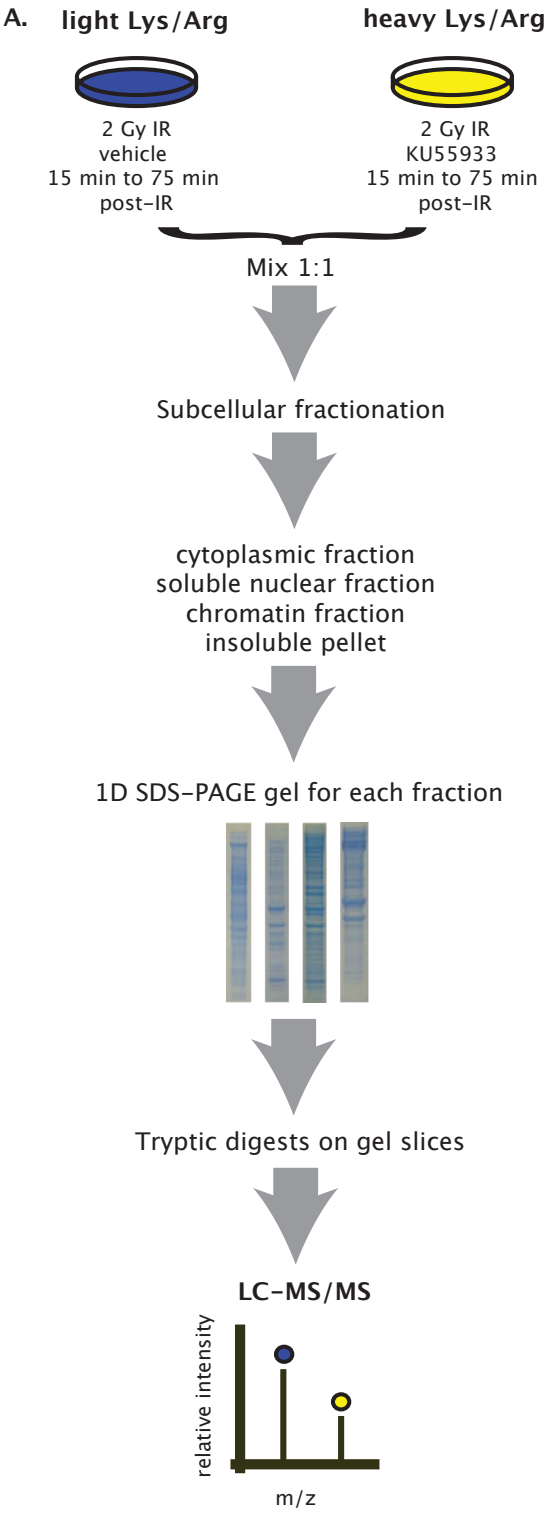
A.
light Lys/Arg
heavy Lys/Arg
2 Gy IR
vehicle
15 min to 75 min
post-IR
2 Gy IR
KU55933
15 min to 75 min
post-IR
Mix 1:1
Subcellular fractionation
cytoplasmic fraction
soluble nuclear fraction
chromatin fraction
insoluble pellet
1D SDS-PAGE gel for each fraction
Tryptic digests on gel slices
LC-MS/MS
relative intensity
m/z

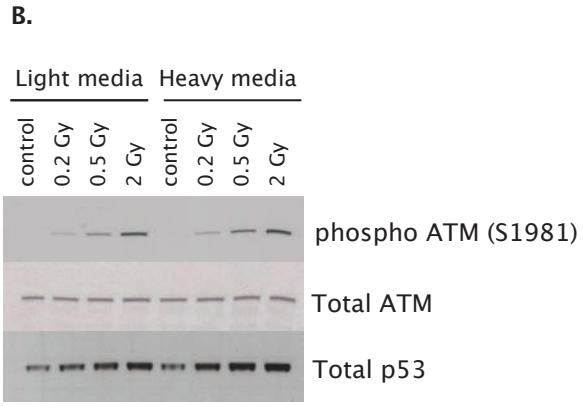
B.
Light media
Heavy media
control
0.2 Gy
0.5 Gy
2 Gy
control
0.2 Gy
0.5 Gy
2 Gy
phospho ATM (S1981)
Total ATM
Total p53

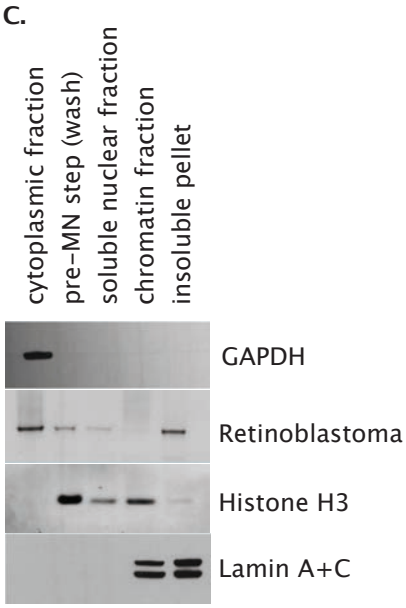
C.
cytoplasmic fraction
pre-MN step (wash)
soluble nuclear fraction
chromatin fraction
insoluble pellet
GAPDH
Retinoblastoma
Histone H3
Lamin A+C

Figure 12. SILAC workflow.

A. We used stable isotope labeling in cell culture (SILAC) with a subcellular fractionation and high-throughput identification of proteins by mass spectrometry to compare the proteomes of irradiated cells treated with an ATM kinase inhibitor (KU55933), with irradiated cells treated with DMSO (vehicle control). **B.** Growth in heavy media had no effect on ATM kinase signaling in irradiated cells. **C.** Four distinct subcellular fractions were generated as evidenced by the immunoblot detection of the cytoplasmic protein GAPDH, the soluble nuclear protein retinoblastoma, the chromatin-bound protein histone H3 and the nuclear matrix/nuclear membrane-associated protein Lamin A+C in fractionated lysates from unirradiated IMR90 cells.

A total of 18,271 pairs of distinct light and heavy peptides were quantified: 11,069 peptide pairs from the cytoplasmic fraction, 8,591 peptide pairs from the chromatin fraction, 4,607 pairs from the soluble nuclear fraction and 6,796 peptide pairs from the insoluble pellet fraction. Of the 18,271 peptide pairs, 16,360 were unique peptides and 1,911 were common peptides shared by more than 1 protein. Both unique and common peptide pairs were assigned to corresponding proteins. The light intensity, heavy intensity and ratio of heavy:light (KU55933:vehicle) intensities were averaged and normalized for each peptide in a given protein. The averaged ratios provided a measure of the relative abundance of the protein, such that a $\log_2$ratio <0 indicates a decrease, $\log_2$ratio >0 represents an increase, and a $\log_2$ratio =1 represents no change in protein abundance with KU55933 treatment. The total number of proteins identified was 4,196: 2,992 proteins in the cytoplasmic fraction, 1,470 proteins in the soluble nuclear fraction, 2,240 proteins in the chromatin fraction and 1,924 proteins in the insoluble nuclear fraction (Figure 13). The overlap in the shared number of proteins across the four fractions is depicted in Figure 14. To identify proteins that significantly change with KU55933 following irradiation, an MA plot was constructed for each fraction to visualize the differential expression with KU55933 treatment (Figure 15).

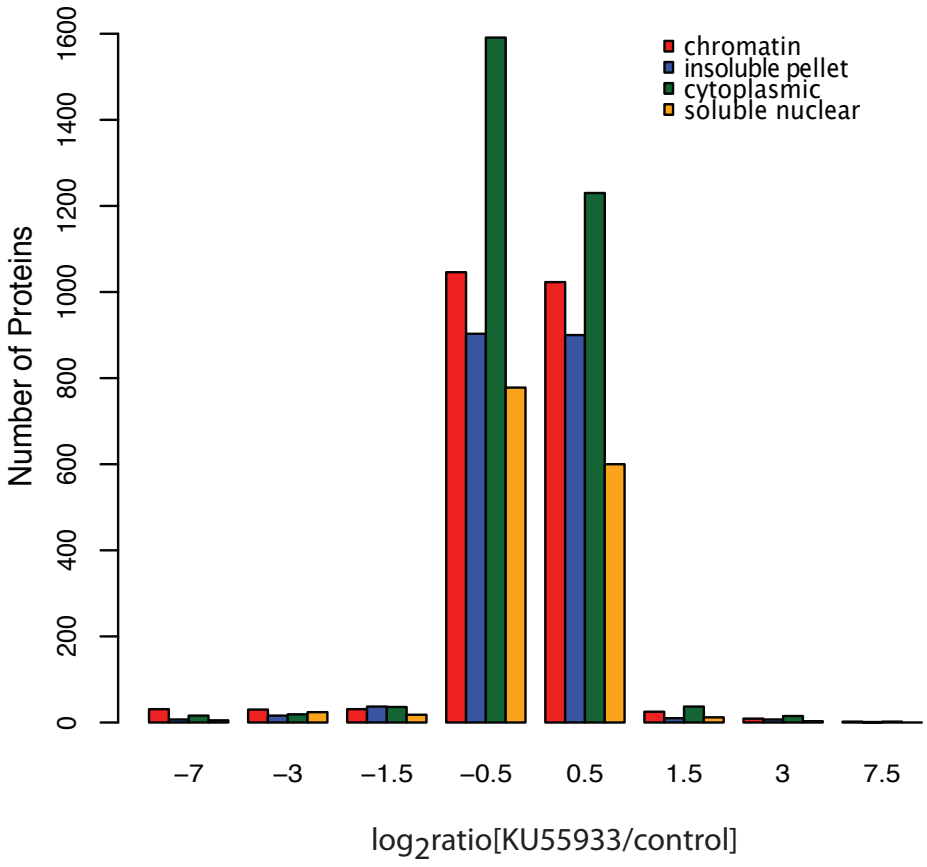

Figure 13. Distribution of proteins identified across fractions.

The light intensities, heavy intensities and the ratio of heavy:light (KU55933:vehicle) intensities were averaged and normalized for each peptide in a given protein. The averaged ratios provide a measure of the relative abundance of the protein, such that a $\log_2$ratio <0 indicates a decrease, $\log_2$ratio >0 represents an increase, and a $\log_2$ratio =1 represents no change in protein abundance with KU55933 treatment.

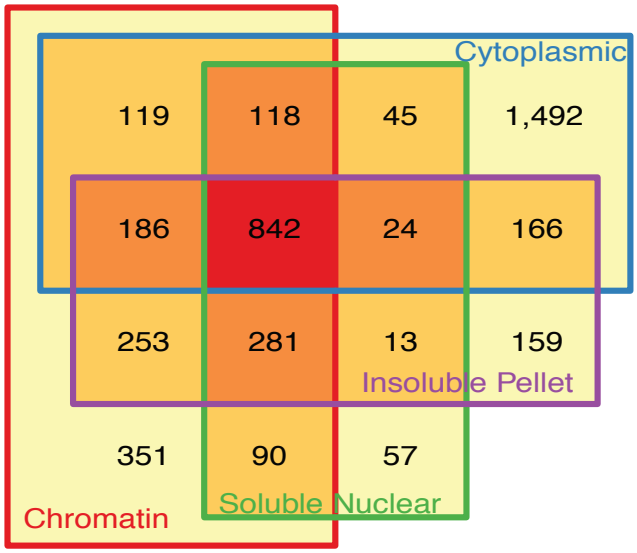

Figure 14. Overlapping proteins shared between fractions.

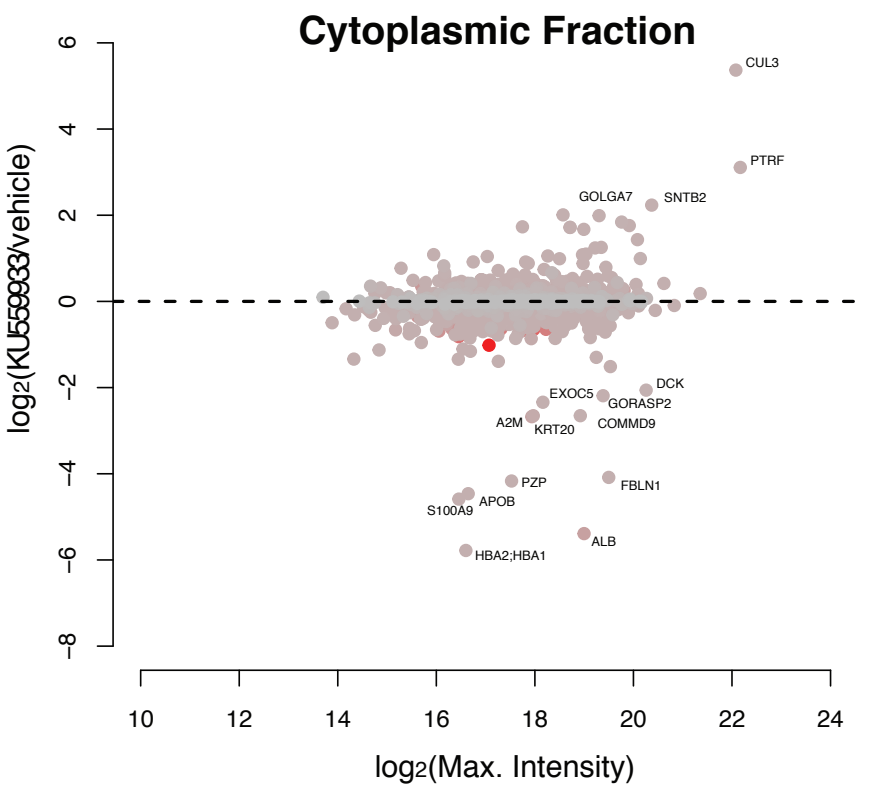
Cytoplasmic Fraction
log2(KU559933/vehicle)
log2(Max. Intensity)
CUL3
PTRF
GOLGA7
SNTB2
DCK
EXOC5
GORASP2
A2M
KRT20
COMMD9
PZP
FBLN1
S100A9
APOB
ALB
HBA2;HBA1

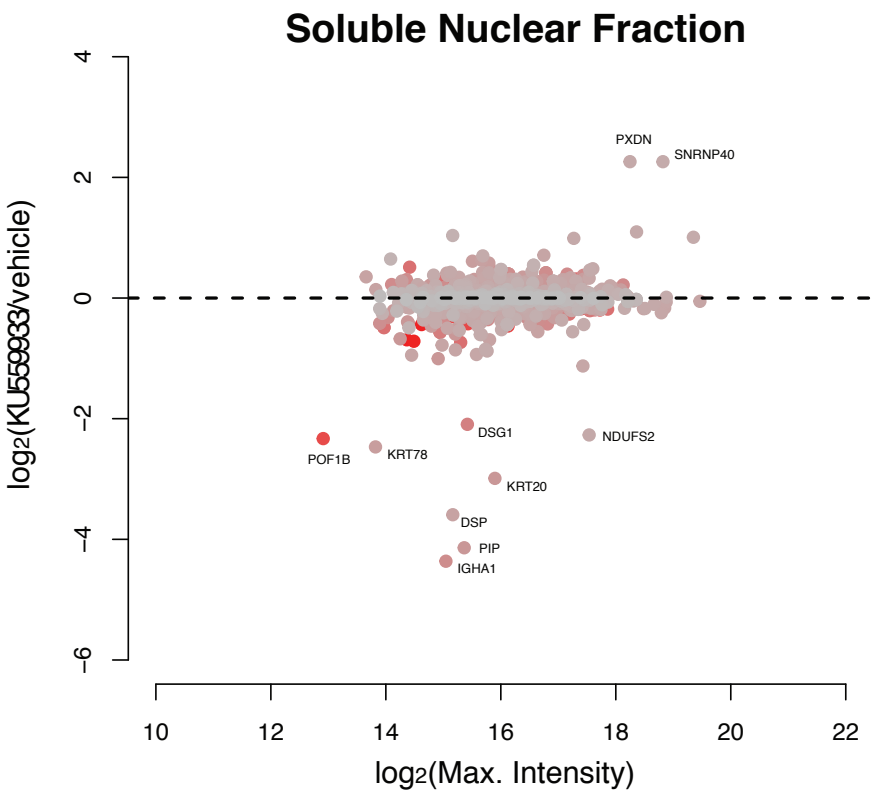
Soluble Nuclear Fraction
log2(KU559933/vehicle)
log2(Max. Intensity)
PXDN
SNRNP40
DSG1
NDUFS2
POF1B
KRT78
KRT20
DSP
PIP
IGHA1

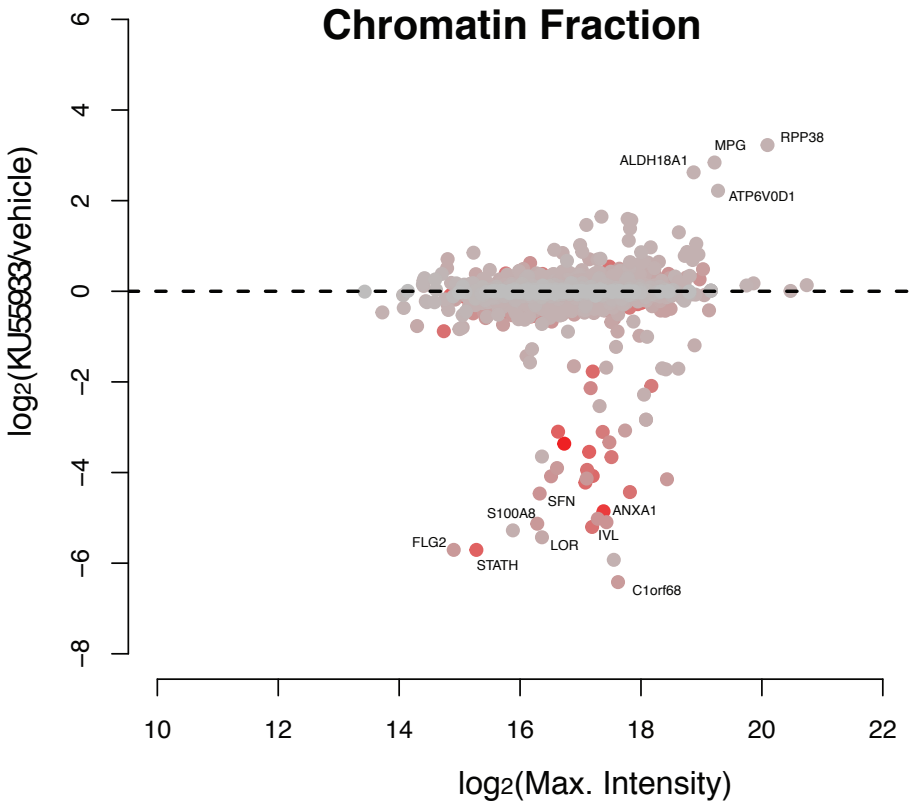
Chromatin Fraction
log2(KU55933/vehicle)
log2(Max. Intensity)
RPP38
MPG
ALDH18A1
ATP6V0D1
SFN
S100A8
ANXA1
IVL
FLG2
LOR
STATH
C1orf68

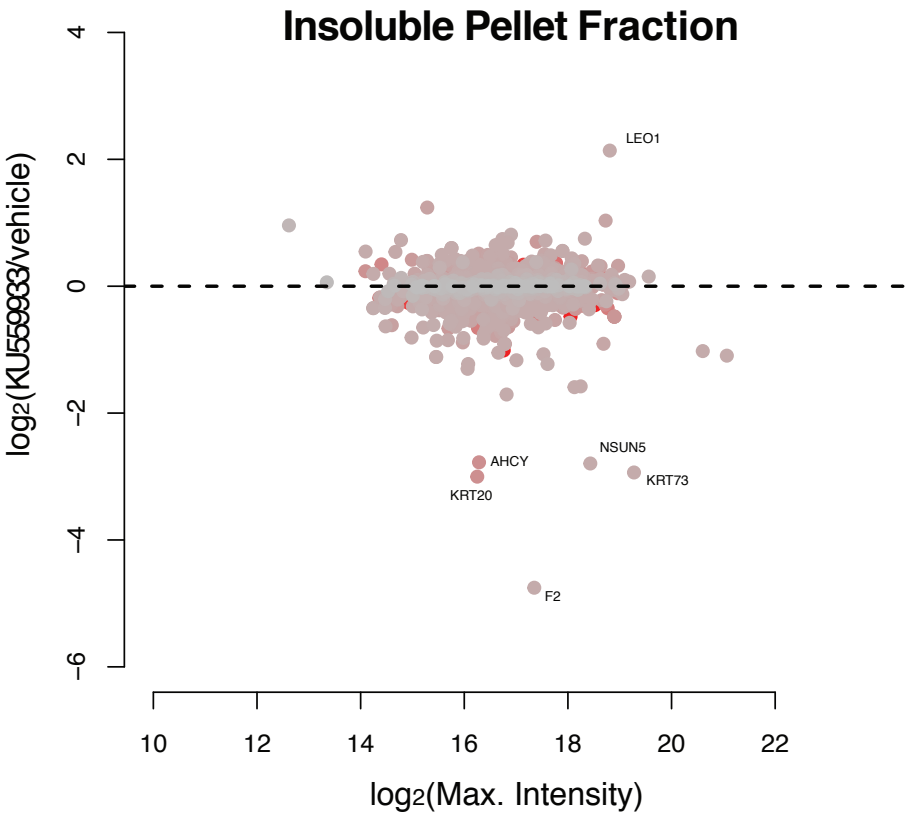
Insoluble Pellet Fraction
log2(KU55933/vehicle)
log2(Max. Intensity)
LEO1
NSUN5
AHCY
KRT73
KRT20
F2

Figure 15. MA plots of the cytoplasmic, soluble nuclear, chromatin and insoluble pellet fractions.

The y-axis represents the differential expression of the protein when irradiated cells are treated with KU55933 and the x-axis represents the relative abundance of the protein. A t-test was performed on the distribution of light peptide intensities and heavy peptide intensities for each protein to generate a p-value for the differential expression of each protein. The pink-to-red color gradient used for the data points is a representation of the p-value generated from the t-test, with red indicating a smaller p-value or greater confidence in the $\log_2$ratio determined for the protein and grey coloring denoting that significance was not achieved. Proteins were not plotted if p-values could not be generated (i.e. only a single pair of intensity values were determined for a protein) or if either the light or heavy intensities for a peptide pair were zero. Out of the four fractions, the chromatin fraction showed the greatest number of proteins that changed with KU55933, as represented on the MA plot by the cluster of data points at the extreme ends of the y-axis

4.4.2 Network analyses of the chromatin fraction

Increased chromosome aberrations and decreased sister chromatid exchange, a cytological manifestation of homologous recombination repair of DNA double-strand breaks, are two phenotypes that we observe in irradiated IMR90 cells that are treated with KU55933 +15 minutes to +75 minutes following irradiation.[19,91,107] Thus, we directed our focus onto the chromatin fraction to identify proteins whose retention at damaged chromatin changes with KU55933. Using Network Module identification (NeMo) in Cytoscape, we interrogated the chromatin fraction to isolate densely connected molecular interaction networks, which often represent protein complexes and or biological processes.[128] We identified seven subnetworks enriched for Gene Ontology functional categories such as transmembrane receptor tyrosine kinase signaling, ligase activity, nuclear pore, ribonuclearprotein complex, chromatin remodeling, vesicles and cytosketal (Figure 16). [132]

Transmembrane receptor protein tyrosine kinase signaling pathway

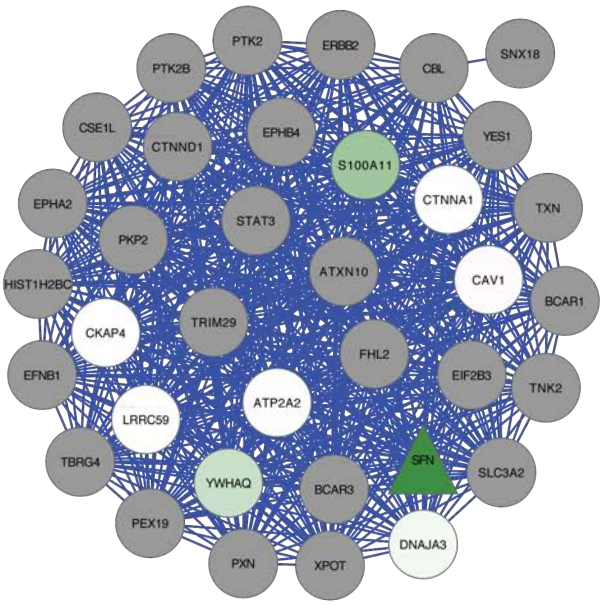

Ligase activity, forming carbon-carbon bonds

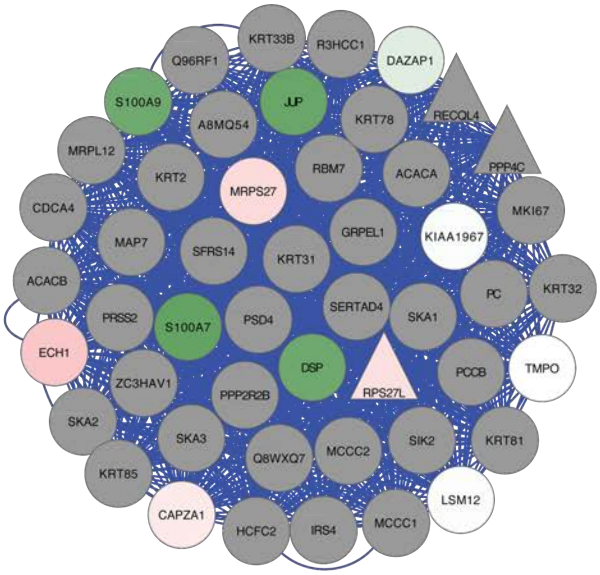

Nuclear Pore

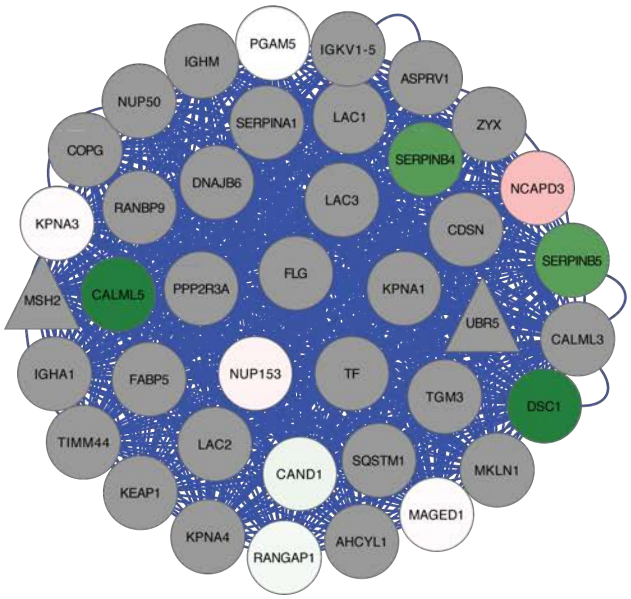

Ribonucleoprotein complex

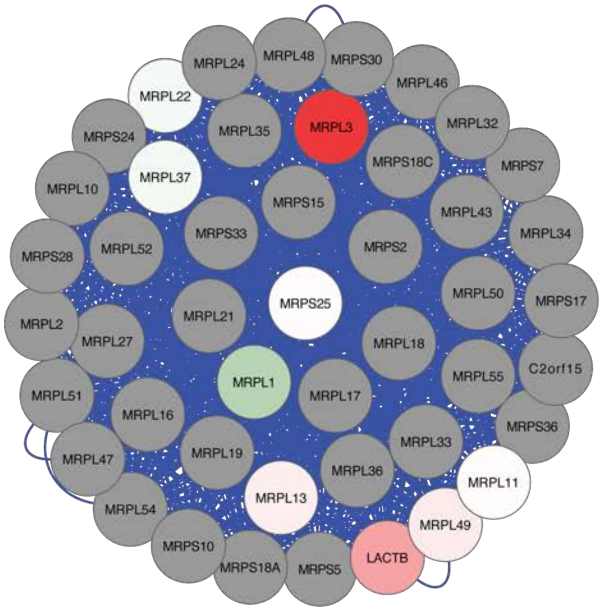

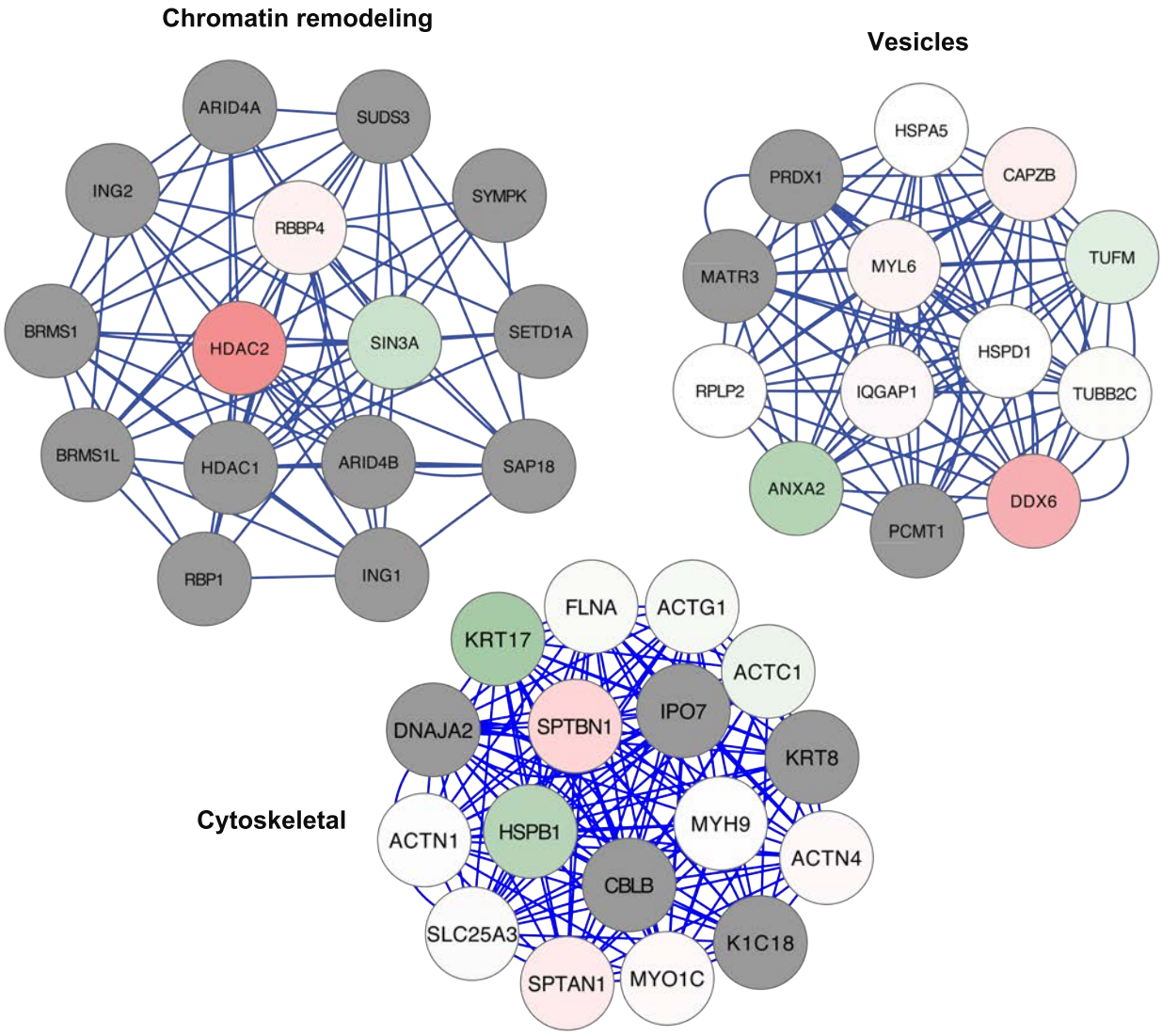

Figure 16. Functional subnetworks identified in the chromatin fraction.

The NeMo algorithm and the ConsensusPathDB protein-protein interaction network was used to identify densely connected sub-components in the chromatin fraction. Triangle nodes designate known DNA damage response proteins and circle nodes designate non-DNA damage response proteins. Dark green nodes indicates a low $\log_2$ratio (KU55933:control) of protein abundance, while dark red indicates a high $\log_2$ratio (KU55933:control) of protein abundance. Grey nodes indicate proteins that were not measured in the screen. White nodes indicate proteins that were detected in the screen but unchanged with KU55933.

4.4.2.1 The 53BP1 DNA damage response network

We further studied the chromatin fraction to look for protein that changed significantly with KU55933 that were also enriched for direct interactions with DNA repair proteins. Based on these analyses, 53BP1 (TP53BP1) was both differentially present in the chromatin and most significantly enriched for direct DNA damage protein neighbors, with a p-value of enrichment of $2*10^{-21}$ (Figure 17). The enrichment ratio for 53BP1 was 16.4 and 52.3% of its direct neighbors were DNA damage proteins. The retention of 53BP1 in the chromatin fraction decreased by 30% with KU55933 ($\log_2$ratio= -0.3) and the p-value of this differential expression was 0.0007. Using Cytoscape, we visualized the 53BP1 DNA damage-subnetwork (Figure 18).[133] In Figure 19, we include a representative tandem mass spectrum of a 53BP1 peptide (^{1631}SNVSSPATPTASSSSSTTPTR^{1651}) which showed approximately 50% lower abundance in the KU55933-treated cells.

Gene ID	Significance of Neighborhood Enrichment (p-value)	Enrichment Ratio for DDR Genes in in Neighborhood	% of Neighbors in DDR	Raw p-value for differential expression	Log_2 ratio of protein expression
AHNAK	0.055	10.5	33.3	0.0003	0.2
TP53BP1	**2.16E -21**	**16.4**	**52.3**	**0.0007**	**-0.3**
ANXA1	0.097	2.5	7.9	0.0020	-4.9
WDR18	0.136	4.8	15.4	NA	-2.2
PSMA4	0.004	3.4	10.7	NA	-1.6

Figure 17. DNA damage neighborhood enrichment analysis of the chromatin fraction.

For each protein, we determined what fraction of its direct neighbors in a protein interaction network are DNA damage response (DDR) proteins. Chromatin proteins were included in the analyses if the protein ratio had a $|\log_2 ratio(KU55933:control)| > 1.5$ or a p-value for differential expression below 0.05. We used the ConsensusPathDB protein-protein interaction network and a list of 434 proteins known to function in the DNA damage response for this analysis. A p-value for DNA damage neighborhood enrichment was determined by comparing two enrichment ratios: 1) # of neighbor genes involved in DDR/total # of neighbor genes and 2) # of DDR genes/total of # of genes in network. The hypergeometric distribution was used to generate a p-value for the significance of enrichment (distribution of ratio 1 versus distribution of ratio 2), which was corrected for multiple hypothesis testing using the Benjamini-Hochberg method. 53BP1 (TP53BP1) was determined to be the protein most significantly enriched for direct DNA damage protein neighbors, with a p-value of enrichment of $2*10^{-21}$.

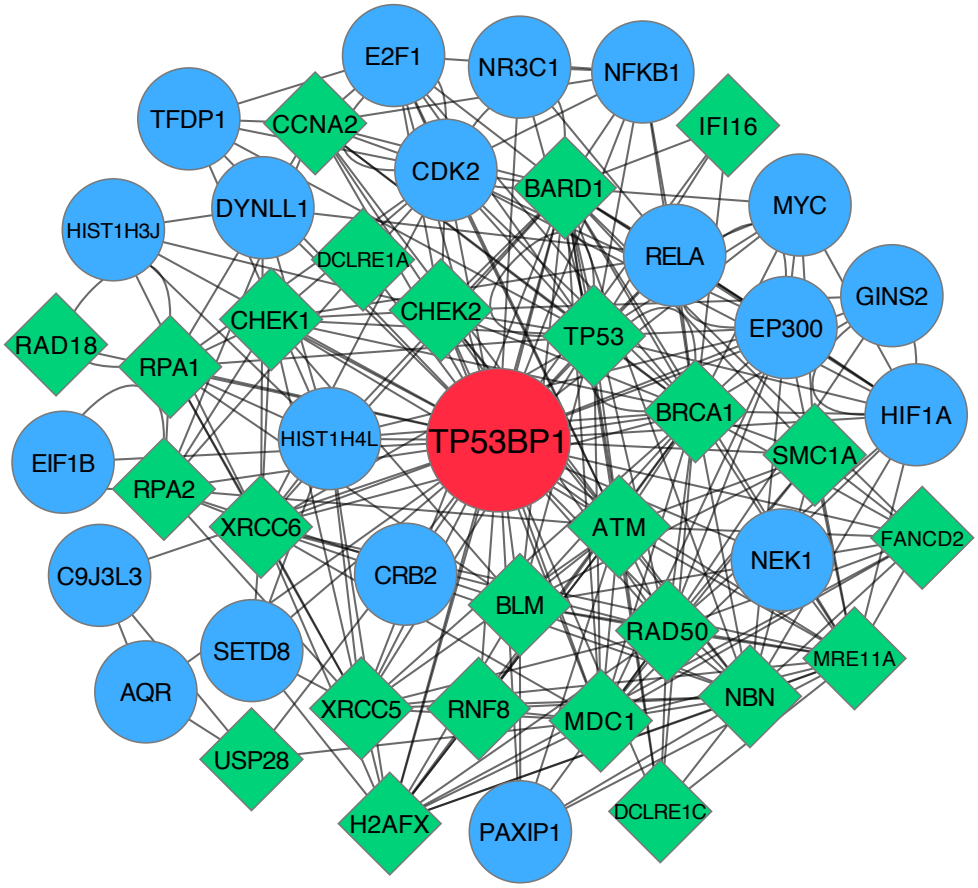

Figure 18. The 53BP1 DNA damage response neighborhood.

Cytoscape was used to visualize the 53BP1 DNA damage response network, which consists of 46 nodes and 268 edges or protein-protein interactions. The green diamond-shaped nodes denote DNA damage response proteins and the blue circular nodes denote non-DNA damage response proteins.

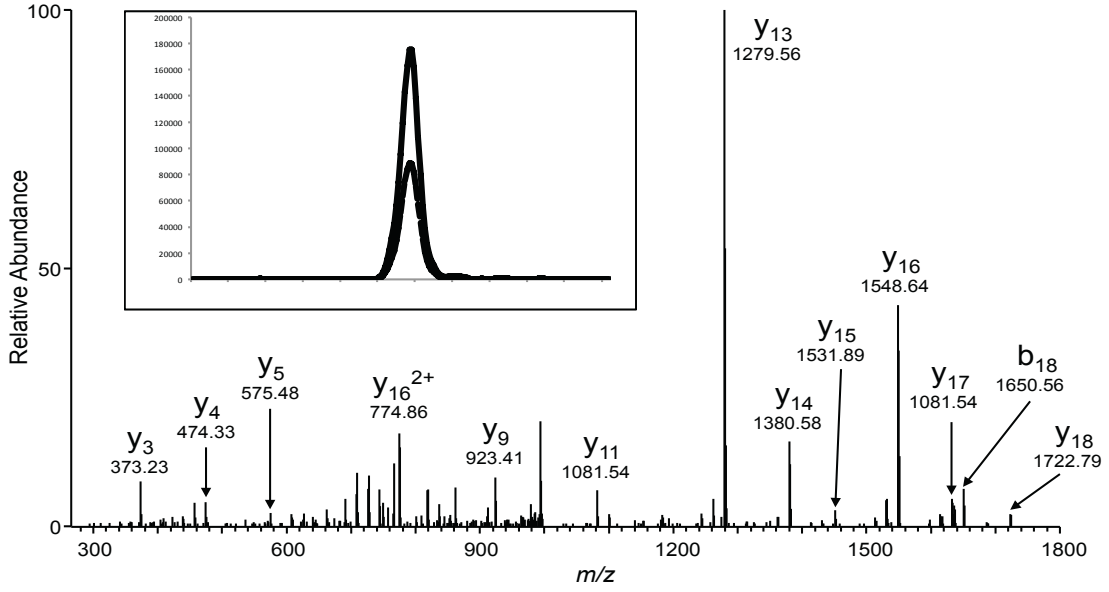

Figure 19. Representative tandem mass spectrum of 53BP1.

The 53BP1 peptide (^{1631}SNVSSPATPTASSSSSTTPTR^{1651}) shows approximately 50% lower abundance in the KU55933-treated cells (inset).

4.4.2.2 The ANXA1 DNA damage response network

The anti-inflammatory protein ANXA1 is also significantly enriched for protein-protein interactions with DNA damage proteins. The retention of ANXA1 in the chromatin fraction decreased with KU55933 by a $\log_2$ratio= -4.9, and the p-value of this differential expression was 0.002. Figure 20 depicts the ANXA1 DNA damage-subnetwork, which consists of 146 nodes and 4,428 edges. In a plot of all the proteins identified in both the cytoplasmic and chromatin fractions, ANXA1 protein levels in irradiated cell does not change with KU55933, but are selectively decreased in the chromatin (Figure 21). Figure 22 shows the overlay of mass

chromatograms from the light (untreated; solid-line) and heavy (treated; dashed-line) isotopomeric peptide pair (^{189}SEDFGVNEDLADSDAR^{204}) identified from annexin A1.

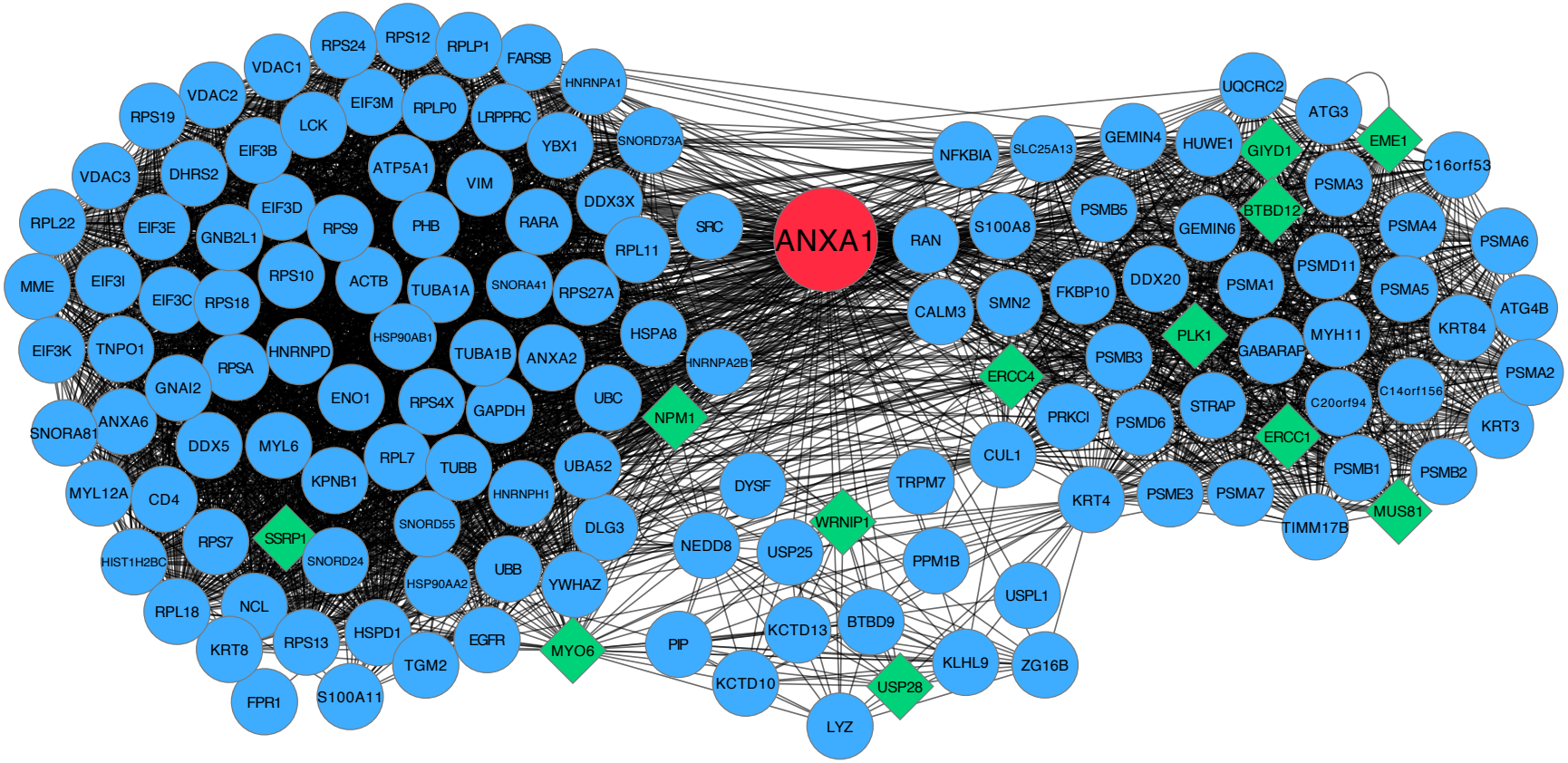

Figure 20. The ANXA1 DNA damage response neighborhood.

Cytoscape was used to visualize the ANXA1 DNA damage response network, which consists of 146 nodes and 4,428 edges or protein-protein interactions. The green diamond-shaped nodes denote DNA damage response proteins and the blue circular nodes denote non-DNA damage response proteins.

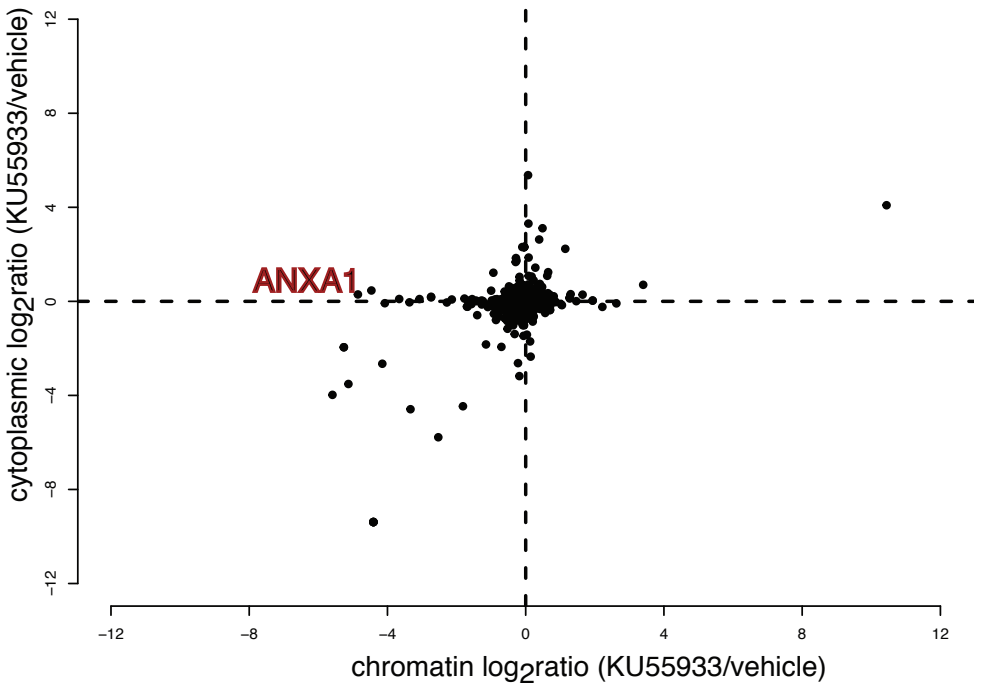

Figure 21. Pair-wise comparison of cytoplasmic versus chromatin fractions.

ANXA1 protein abundance does not change in the cytoplasm of irradiated cells when treated with KU55933, but changes significantly in the chromatin fraction.

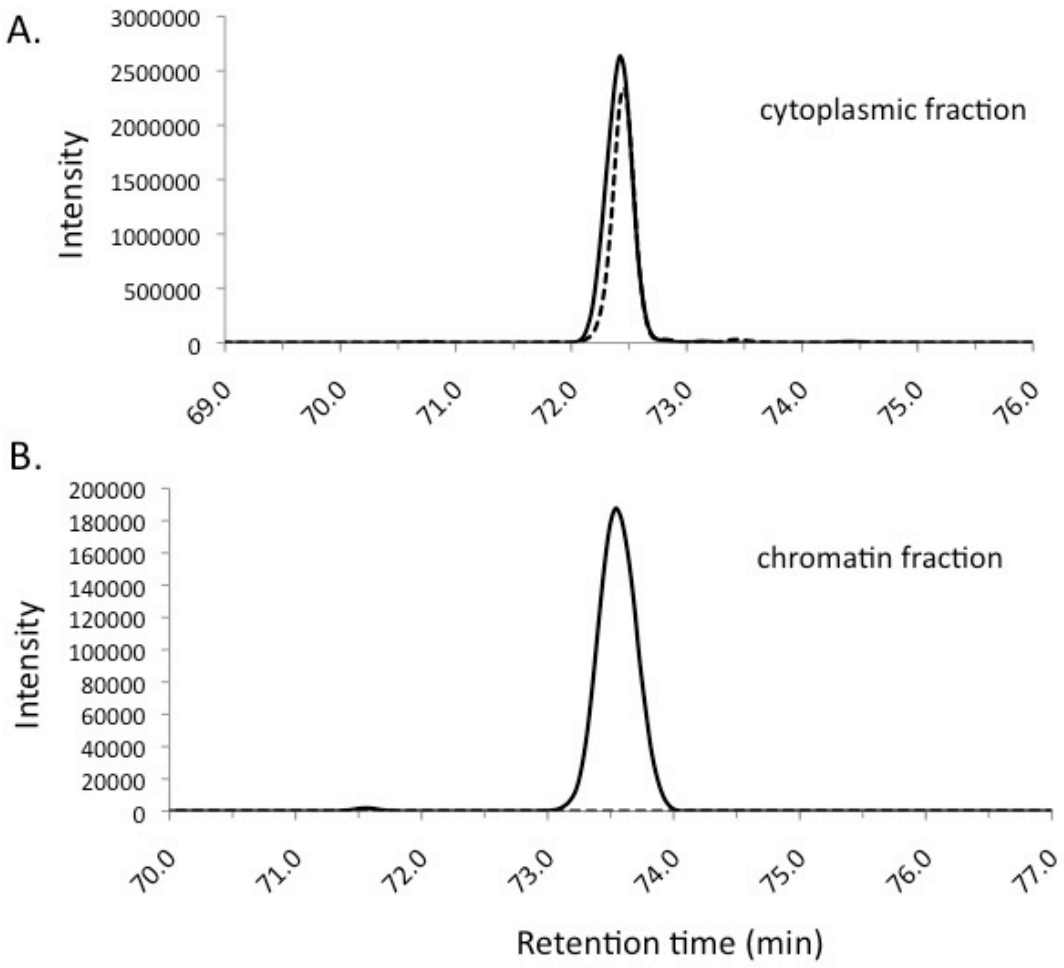

Figure 22. Overlay of ANXA1 mass chromatograms from the cytosplamic and chromatin fractions.

The light (vehicle; solid-line) and heavy (KU55933; dashed-line) isotopomeric peptide pair (^{189}SEDFGVNEDLADSDAR^{204}) identified from ANXA1 demonstrates an approximate equivalent abundance in the untreated and treated cells in the cytoplasmic fraction (A) and the lack of a detectable heavy peptide (KU55933; dashed line) in the chromatin fraction (B).

4.4.3 53BP1 chromatin dynamics

DNA damage proteins have been shown to localize to the sites of DSB within seconds to minutes following ionizing radiation (IR) exposure, resulting in the formation of microscopically detectable nuclear domains referred to as ionizing radiation-induced foci (IRIF). 53BP1 is one of the earliest proteins recruited to IRIF, accumulating at DNA damage sites two to three minutes after damage induction.[134-136] 53BP1 is highly mobile in the nucleus of non-irradiated cells, however upon binding to IRIF, the mobility of 53BP1 is greatly reduced.[137,138] 53BP1 has known functions in non-homologous end-joining (NHEJ) of DNA double-strand breaks and in transducing ATM-dependent cell-cycle checkpoints.[135,139-143] Recruitment of 53BP1 to DNA double-strand breaks is ATM-independent, but 53BP1 at DNA breaks requires γ-H2AX.[136,143] In cells lacking 53BP1, phosphorylation of ATM substrates is reduced, suggesting that 53BP1 functions upstream of ATM.[135,141] 53BP1 is also a substrate of ATM, with phosphorylation sites at serines 6, 25, 29 and 784, although these phosphorylation sites are dispensible for 53BP1 localization to IRIF.[143]

In our experiments, KU55933 is added to the cells +15 minutes post-irradiation, which is sufficient time for the rapid recruitment of 53BP1 to DNA damage sites.[134-136] We have previously shown that transient ATM kinase inhibition with KU55933 from +15 min to +75 min post-irradiation does not affect the number of 53BP1 or γ-H2AX foci when measured at +75 minutes, +6 hours and +12 hours post-irradiation in cells fixed with paraformaldehyde[91] We repeated the fractionation protocol in irradiated IMR90 cells in order to validate by immunoblot that 53BP1 chromatin retention is reduced with KU55933 (Figure 23). Thus, the LC-MS/MS and

immunoblots of chromatin fraction lysates indicate that 53BP1 is reduced in the chromatin fraction in irradiated cells treated with KU55933.

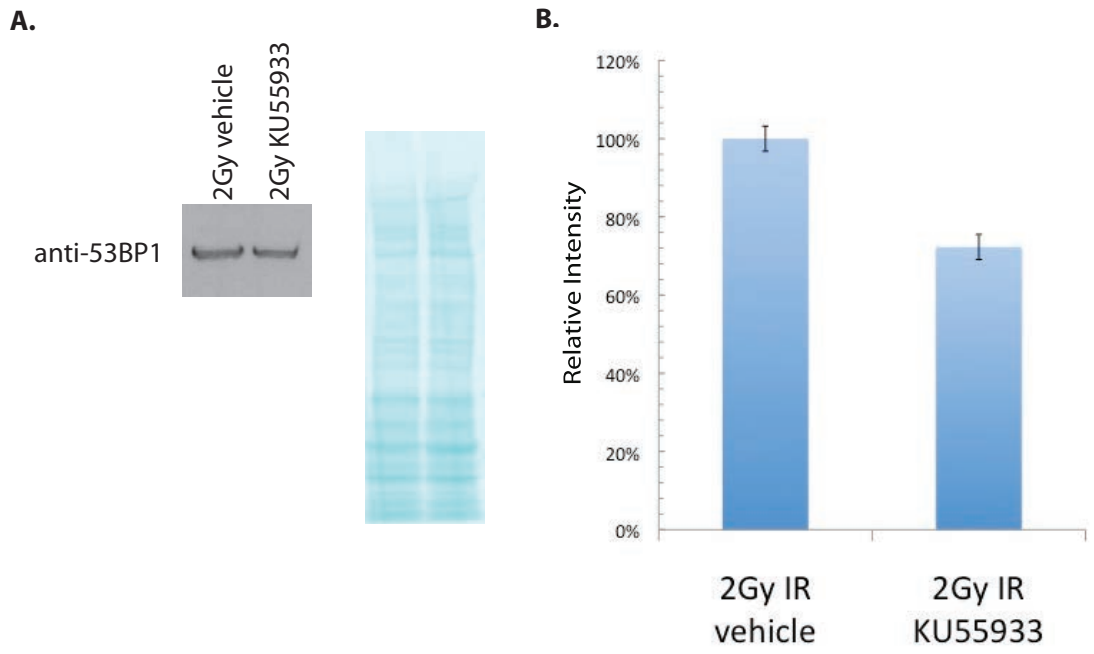

Figure 23. Immunoblot validation of 53BP1 differential expression in chromatin with KU55933.

A. Fractionation chromatin lysates from irradiated IMR90 cells show that 53BP1 chromatin retention is reduced with KU55933. An image of the nitrocellulose membrane stained with fast green is included to demonstrate equal loading of the chromatin fraction lysates. B. ImageJ quantification of immunoblots show 28% reduction in 53BP1 n the chromatin fraction in irradiated cells when treated with KU55933. The experiment was performed three separate times, and the error bars reflect the standard deviation.

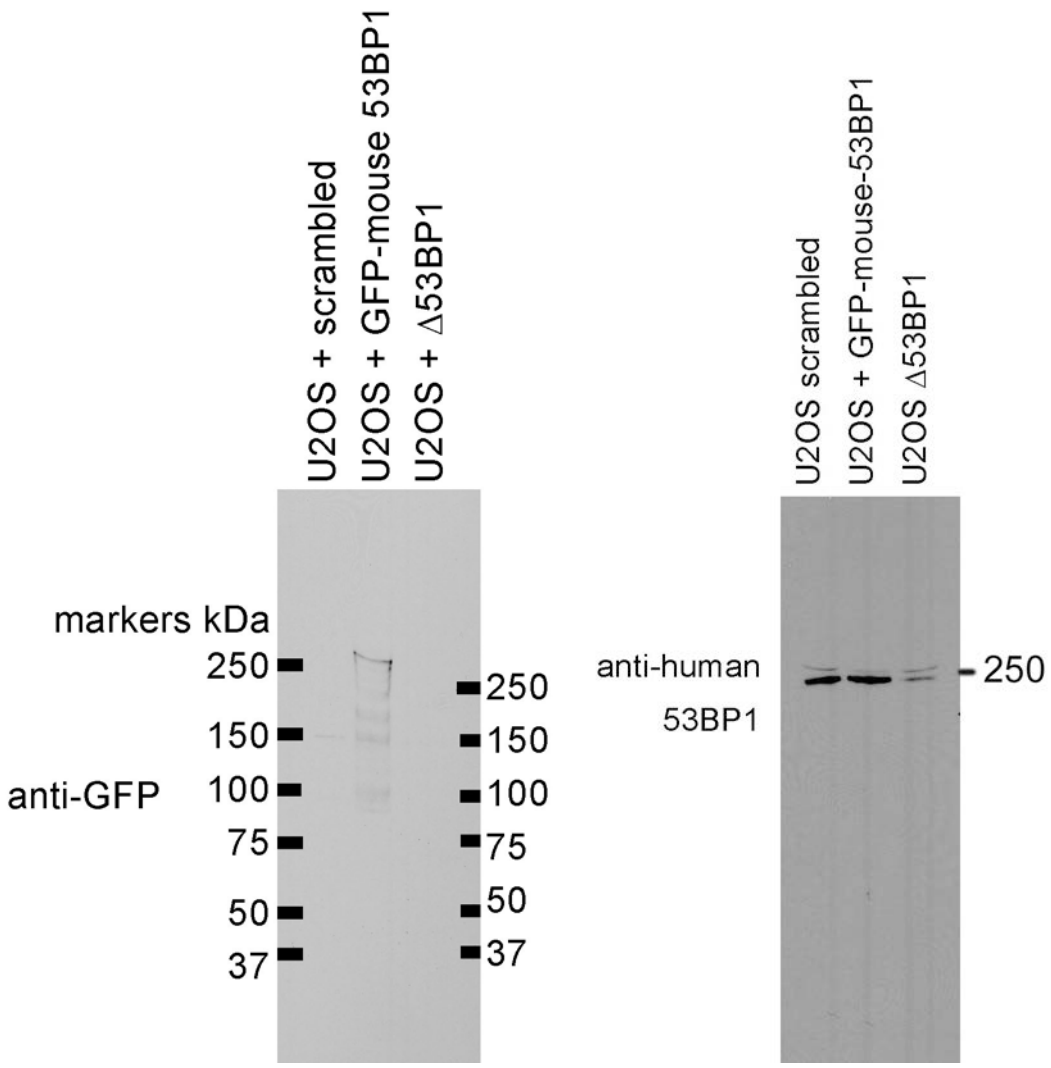

Figure 24. U2OS cells transfected with the msGFP-53BP1 construct expresses intact ms53BP1.

Immunoblots show that GFP-ms53BP1 transfected into U2OS cells (left immunoblot) migrates to a similar molecular weight as endogenous human 53BP1 on 1D SDS-PAGE (right immunoblot).

We hypothesized that KU55933 increases the mobility of 53BP1 at IRIF, such that 53BP1 protein complexes are destabilized at IRIF. To test this, we performed fluorescence recovery after photobleaching (FRAP) experiments to analyze the dynamics of IRIF-associated

GFP-53BP1. U2OS cells transfected with GFP-ms53BP1 were irradiated with 2 Gy and treated with either DMSO (vehicle control) or KU55933 for +15 minutes to +75 minutes post irradiation.[144] We performed immunoblots to show that the GFP-ms53BP1 construct is intact (Figure 24). We see that the extent of fluorescence recovery of GFP-m53BP1 in irradiated cells treated with vehicle control was approximately 90%, whereas the extent of fluorescence recovery in irradiated cells treated with KU55933 was approximately 70% (Figure 25). We interpret this data to mean that immediately after photobleaching, GFP-53BP1 rapidly diffuses throughout the photobleached area. The rapid diffusion of GFP-53BP1 occurs similarly in the vehicle- and the KU55933-treated cells as indicated by the similar slopes of the vehicle and KU55933 FRAP curves, immediately after photobleaching. These early interactions represent transient interactions of GFP-53BP1 at IRIF. The decrease in the rate of recovery of GFP-53BP1 in irradiated cells treated with KU55933 likely represents the decrease in the *strength* of GFP-53BP1 binding at IRIF, such that over time the off-rate of GFP-53BP1 at binding sites located at IRIF is increased with KU55933.

A.

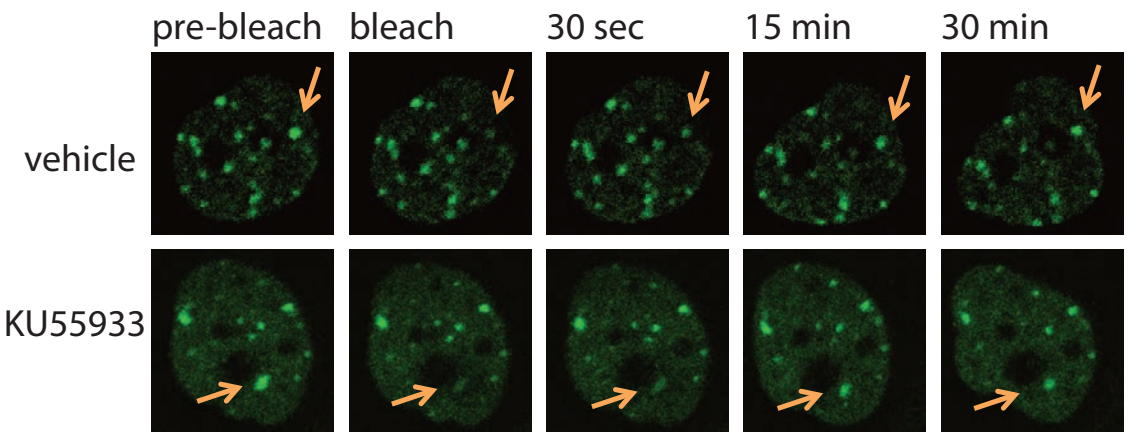
pre-bleach
bleach
30 sec
15 min
30 min
vehicle
KU55933

B.

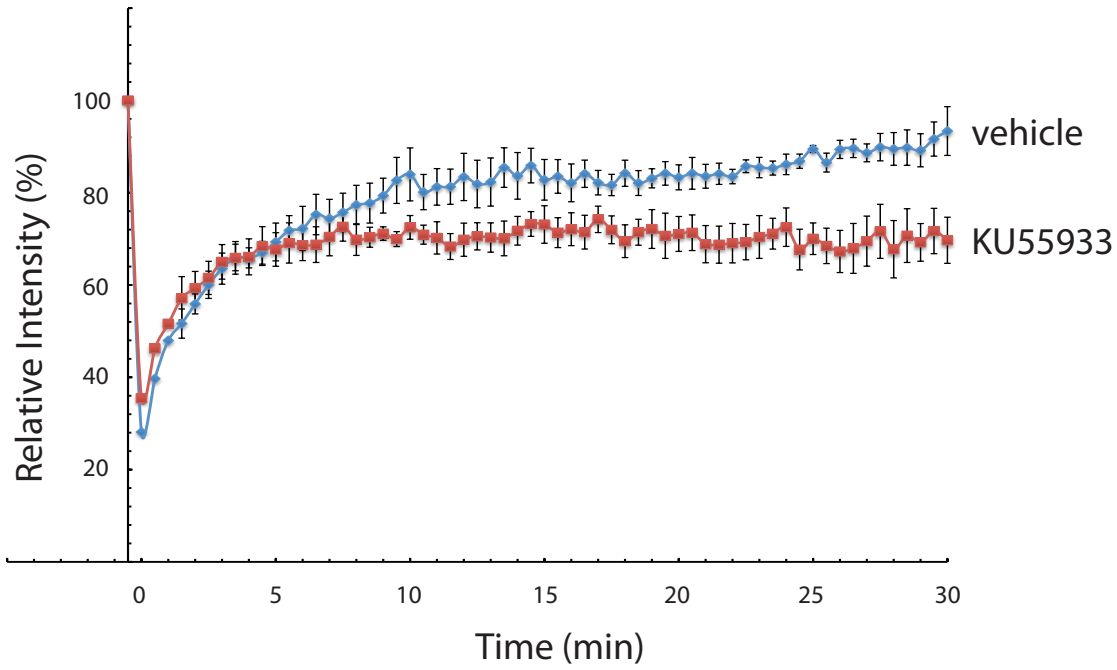
Relative Intensity (%)
100
80
60
40
20
0
5
10
15
20
25
30
Time (min)
vehicle
KU55933

Figure 25. FRAP analysis of GFP-53BP1.

A. Representative timecourse of images of GFP-m53BP1 in irradiated U2OS cells expressing GFP-53BP1 and treated with 10 μM KU55933 or vehicle control from +15 to +75 minutes following 2 Gy IR. The photobleached regions are designated by the arrows. **B.** FRAP analysis of GFP-m53BP1. At +75 min post-irradiation, a 488 pulse laser was used at 100% power, which allowed photobleaching of GFP-ms53BP1 IRIF without inducing DNA damage. From +75 minutes to +105 minutes post-irradiation (30 minute duration), the fluorescence recovery of the GFP-ms53BP1 foci was measured every 30 seconds. Next, we used FRAP to analyze the IRIF-associated GFP-m53BP1 in irradiated cells treated with or without KU55933. U2OS cells stably expressing GFP-m53BP1 were exposed to 2 Gy of γ-rays from a [^{137}Cesium] source and incubated for 15 minutes at 37 degrees prior to adding 10 μM KU55933 or DMSO (vehicle control) for 1 hour (+15 minutes to +75 minutes post-irradiation). At +75 minutes post-irradiation, we used a 488 pulse laser at a power that did not induce DNA damage to photobleach IRIF. The relative fluorescence intensity curve was plotted using the mean of five IRIF, each in a different nucleus from five different cells derived from three different experiments. Error bars reflect standard error of the mean.

4.5 CONCLUSION

The spatial dynamics of proteins in response to DNA damage is critical to genome stability.[69,119-121] Here, we developed a novel high throughput proteomics approach to identify protein dynamics that are regulated by ATM kinase activity following irradiation. Although studies exploring the ATM kinase-dependent phosphoproteome following DNA damage have been performed, studies on global ATM kinase-dependent spatial proteome dynamics following DNA damage have not been reported.[20-22] Knowledge of the subcellular distribution of proteins within cells and how the spatial distribution changes in response to DNA damage is generally lacking. Recently, Boisvert et. al. used SILAC-based mass spectrometry to analyze a whole cell extract created by recombining differentially labeled cytoplasmic, nuclear, and nucleolar fractions derived from cells in which proteins have been mass-labeled with three different heavy isotope labels.[145,146] This approach, termed "spatial proteomics," provides an innovative method of quantitatively mapping the proteomes of the subcellular compartments and capturing the dynamic protein movement that occurs between subcellular compartments, particularly following treatment with etoposide.[145] Here, we provide an alternative method to that of Boisvert et. al. that allows the investigation of additional subcellular compartments to the cytoplasmic, nuclear, and nucleolar fractions, such as the chromatin fraction, which is particularly relevant for studies on the DNA damage response.

In a comparison between the cytoplasmic and chromatin fractions, we found that the anti-inflammatory protein ANXA1 exhibits a dramatic decrease in protein abundance in the chromatin fraction when ATM kinase activity was inhibited, whereas loss of sustained ATM kinase activity did not affect the levels of ANXA1 in the cytoplasmic fraction. Interestingly, a

previous study demonstrated that ANXA1 translocates from the cytoplasm to the nucleus following heat-induced DNA damage.[147] It is tempting to speculate that ANXA1 translocation may also occur in response to radiation-induced DNA damage and that radiation-induced translocation or chromatin stabilization of ANXA1 may be regulated by ATM kinase activity. In our studies, ANXA1 did not change in the cytoplasmic fraction of irradiated cells with KU55933, but ANXA1 levels decreased significantly with KU55933 in the chromatin fraction. It is possible that there is a small amount of ANXA1 that moves to the nucleus following irradiation in an ATM kinase-dependent manner, but the corresponding reduction from the cytoplasmic pool cannot be detected because of the significantly greater levels of ANXA1 in the cytoplasm fraction versus in the chromatin fraction. If this is determined to be the case, then ANXA1 localization may be a useful biomarker for radiation exposure. Further studies are needed to determine the functions of ANXA1 at chromatin in response to genotoxic stress.

In an analysis of the chromatin proteome, we discovered reduced 53BP1 retention in the chromatin fraction when ATM kinase inhibited is inhibited from +15 minutes to +75 minutes post-irradiation. 53BP1 is a nuclear protein that undergoes a dynamic interaction with chromatin in undamaged cells. Following DNA damage, the interaction of 53BP1 with chromatin increases due to its immobilization at and around DNA double-strand breaks.[137,138] We studied the protein dynamics of GFP-53BP1 using live cell microscopy imaging and FRAP analysis and show that the fluorescence recovery of GFP-53BP1 at photobleached ionizing radiation-induced foci (IRIF) is decreased in cells treated with KU55933 +15 minutes to +75 minutes post-2 Gy IR (70% recovery) compared to irradiated cells treated with the vehicle control (90% recovery). These data indicate that the exchange of 53BP1 at IRIF is impaired when ATM kinase activity is inhibited. Immunoblots of fractionated lysates show that 53BP1 levels in the chromatin fraction

of irradiated cells are also decreased with KU55933, which argues against photobleached GFP-53BP1 being trapped at chromatin as explanation for the decrease in fluorescence recovery of GFP-53BP1 foci. Rather, it appears that ATM kinase inhibition disrupts the dynamic interaction of 53BP1 with chromatin such that 53BP1 binding or retention at chromatin is impaired. Thus, sustained ATM kinase activity functions to stabilize 53BP1 protein complexes at chromatin.

The assembly and retention of 53BP1 at doublestrand breaks requires direct interaction between the Tudor domain of 53BP1 and dimethylated lysine 79 of histone H3.[148] While H3-dmK79 is not a DNA damage-dependent modification, it has been suggested that chromosome relaxation proximal to doublestrand breaks can indirectly increase recognition and binding of 53BP1 to chromatin at these residues.[148] The retention of 53BP1 at chromatin also requires the ATM kinase-dependent phosphorylation of histone H2AX on serine 139.[140,149] In contrast to H3-dmK79, γ-H2AX is induced by DNA damage.[150] It is possible that sustained ATM kinase signaling following DNA damage is required to allow 53BP1 access to H3-dmK79 through structural changes to the chromatin and/or that sustained ATM kinase signaling is required to maintain the phosphorylation of histone H2AX on serine 139 to retain 53BP1 at chromatin. We do not think that phosphorylation of histone H2AX on serine 139 accounts for our observations, however, because KU55933 reduces the chromatin retention of 53BP1 even in unirradiated fractionated lysates (unpublished observations). However, further studies are needed to determine how 53BP1 stability at chromatin is regulated by ATM kinase activity.

Understanding the role of ATM kinase signaling on the stability of 53BP1 repair complexes has clinical significance. Mutations that result in defects in homologous recombination repair of doublestrand breaks can predispose cells to tumorigenesis, as seen in BRCA1 mutant cells.[151] Recently, loss of 53BP1 was shown to decrease chromosome aberrations

and reverse the proliferation defect of BRCA1 mutant cells.[152,153] 53BP1 loss reverses cisplatin sensitivity induced by Brca1 inactivation and was shown to restore ATM kinase-dependent homologous recombination repair.[152,153] 53BP1 deletion promotes homologous recombination repair of doublestrand breaks by permitting the processing of broken DNA ends into recombinogenic single-stranded DNA.[153] Since DNA end processing has been shown to be dependent on ATM kinase activity, it has been suggested that ATM kinase inhibitors may be used in combination with a PARP inhibitor to further sensitize BRCA1 mutant cells that have acquired resistance to cisplatin.[153] Our data shows that ATM kinase inhibition following irradiation disrupts the localization of 53BP1 at chromatin suggesting that in addition to inhibiting DNA end processing in BRCA null/53BP1 null cells, kinase-inhibited ATM may also reduce 53BP1 at chromatin. It would be interesting to see if kinase-dead mutations in ATM are found as a mechanism of resistance in BRCA1 mutant cancer cells.

5.0 DISCUSSION

ATM kinase inhibitors have proven to be instrumental in studies of ATM kinase-dependent functions. We showed that KU55933 and KU60019 can be used as "molecular switches" to selectively and transiently inhibit ATM kinase activity in cells, and that the immediate and reversible nature of KU55933- and KU60019-mediated inhibition enables studies that temporally isolate ATM kinase functions.[19,91] We demonstrate the use of KU55933 in dissociating an ATM kinase-dependent DNA repair mechanism from an ATM kinase-dependent cell cycle checkpoint mechanism.[91] Significantly, we found ATM kinase inhibition from +15 minutes to +75 minutes following ionizing radiation (IR) results in severe phenotypes: KU55933 radiosensitizes cells, increases chromosome aberrations and abrogates sister chromatid exchange (Figure 26).[19,91,109] Surprisingly, we found that with regards to sister chromatid exchange, kinase-inhibited ATM functions differently from loss of ATM protein.[91]

To determine the global protein dynamic changes that depend on ATM kinase activity +15 minutes to +75 minutes post-IR, we performed a SILAC-based mass spectrometry proteomics screen. Through our protein-protein interaction network analyses, we found that 53BP1 and ANXA1 are enriched for interactions with DNA damage proteins and that the protein dynamics of 53BP1 is altered with transient ATM kinase inhibition. This study demonstrates the

use of an integrative proteomics and systems biology approach in predicting ATM kinase-dependent spatial protein dynamics that are critical for genome stability.

Figure 26. Transient kinase inhibition of ATM has long-term consequences, even after restoration of ATM kinase activity (removal of inhibitor).

Treatment with KU55933 (ATMi) from +15 minutes to +75 minutes following ionizing radiation (IR) results in severe cellular phenotypes. At 12 hours post-IR, we observed a decrease in sister chromatid exchange (SCE), a cytological manifestation of homologous recombination repair of DNA double-strand breaks at the replication fork. At 48 hours post-IR, there is an increase in chromosome aberrations. Cell proliferation and survival are decreased at ~10 days, as measured by clonogenic assay.

An intriguing question that arose from these studies is how does kinase-inhibited ATM function differently from loss of ATM protein? The finding that DNA damage-induced SCE was maintained in A-T cells that express no ATM protein and that the ATM kinase inhibitors had no effect on DNA damage-induced SCE in A-T cells, indicates that the disruption of DNA damage-induced SCE in cells expressing ATM is not a consequence of an "off-target" effect of either KU55933 or KU60019.[91] These data revealed for the first time that the consequences of inhibition of ATM kinase activity and adaptation to ATM protein disruption are distinct.[91,109] We had considered that ATM's known functions in cell cycle checkpoints might contribute to the observed defect in SCE but were unable to detect any defect in either the activation or the recovery of the G_2/M checkpoint when ATM kinase was transiently inhibited.[91] This was the most significant checkpoint to our analyses of SCE that was performed in mitotic cells trapped from 8-12 hours following insult. Any delay in G_2/M checkpoint recovery following transient ATM kinase inhibition might have prevented cells containing SCEs entering mitosis leading to an apparent lack of SCE.

We hypothesize that localization of ATM is likely key to this mechanism. Since SCE represents the repair of damaged DNA replication forks, we favor a model in which "kinase-inhibited ATM" presents a physical impediment to SCE at DNA double-strand breaks (DSBs) at damaged replication forks.[107] We speculate that kinase-inhibited ATM can localize to DSBs at damaged replication forks. In fact, several mutant ATM proteins that lacked kinase activity against downstream substrates formed IR-induced foci in A-T cells, suggesting that ATM recruitment to DNA damaged-induced foci is independent of ATM kinase activity.[154] However, we propose that once ATM kinase is recruited to DSBs at damaged replication forks, local ATM kinase activity is required both to phosphorylate substrates that mediate DSB repair and to allow

mobilization of ATM itself such that DSB repair can physically proceed (Figure 27).[109] Kinase-inhibited ATM may disrupt large-scale MRE11 complex conformational changes, impairing homologous recombination repair of DSBs.

Such a mechanism, in which kinase-inhibited ATM would physically block the repair of replication associated DNA damage by physically impeding homologous recombination repair (HR), is analogous to the recent finding that 53BP1 inhibits HR in Brca1-deficient cells by blocking DSB end resection.[153] DNA breaks in Brca1-deficient cells are aberrantly joined into complex chromosome aberrations by a process dependent on the nonhomologous end-joining (NHEJ) factors 53BP1 and DNA Ligase 4.[153] Loss of 53BP1 in Brca1-mutant cells promotes ATM kinase-dependent processing of DSBs to produce recombinogenic single-stranded DNA competent for error-free repair by HR.[153] In contrast, Lig4 deficiency does not rescue the HR defect in Brca1 mutant cells but prevents the joining of chromatid breaks into chromosome rearrangements.[153] These results indicate that HR and NHEJ compete to process DSBs that arise during replication. Bunting et al. proposed that a critical function for BRCA1, and perhaps other factors that commit breaks to HR, might be to remove end-joining proteins such as 53BP1 from replication associated breaks.[153] In other words, the key mechanism by which 53BP1 regulates the choice of HR versus NHEJ could be via inhibition of DSB resection by the physical presence of 53BP1 itself. Thus, it is possible that phosphorylations on 53BP1 and BRCA1, both known substrates of ATM, are also required for ATM mobilization at DSBs.

In accordance with this model, we hypothesize that ATM kinase activity is associated with the removal of ATM protein itself and/or NHEJ proteins from replication-associated breaks. For instance, ATM kinase-dependent MRE11/CtIP-mediated DSB resection and/or MRE11-mediated nucleosome displacement might facilitate the generation of nucleosome-free ssDNA

regions that would be incompatible with continued 53BP1 chromatin binding but accessible for recruitment of HR proteins.[155-159] Thus, ATM kinase activity may commit replication associated DNA damage to HR repair through the displacement of NHEJ factors. It is possible that kinase inhibition of ATM protein localized at sites of replication-associated DSBs prevents the displacement of ATM protein itself from these sites, leaving behind rather large physical impediments to repair. Furthermore, the fact that SCE is not recovered when the ATM kinase inhibitor is removed and ATM kinase activity restored in cells suggests that there are temporal restrictions to this process (possibly due to loss of substrate availability upon the restoration of ATM kinase activity), which when disrupted results in irreversible consequences.[19,91] Live cell imaging studies comparing the normal GFP-tagged ATM protein dynamics and that of kinase-inhibited GFP-tagged ATM (treated with KU55933 +15 minutes to +75 minutes post-IR) and kinase-inhibited GFP-tagged ATM (-15 minutes to +75 minutes post-IR) will help determine if this hypothesis is correct. We would predict that in cells treated with KU55933 +15 minutes to +75 minutes post-IR, the fluorescence recovery after photobleaching of GFP-tagged ATM is impaired, indicating that ATM is retained longer at doublestrand breaks when ATM kinase activity is inhibited +15 minutes to +75 minutes post-IR.

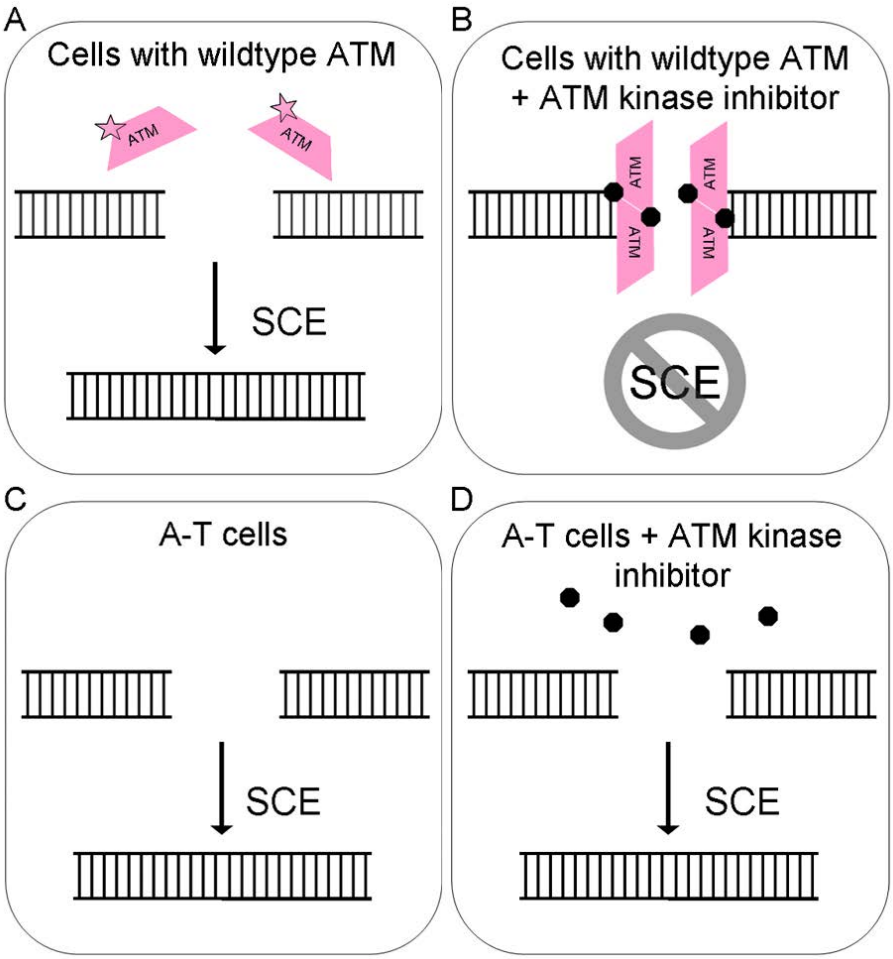

Figure 27. Inhibition of ATM kinase activity does not phenocopy A-T cells: model for ATM localization.

In cells with functional ATM protein, DNA double-strand breaks at the replication fork can be repaired via sister chromatid exchange (SCE) (A). When ATM kinase activity is inhibited, SCE is disrupted, possibly via a mechanism that immobilizes ATM itself at the break, resulting in a physical and irreversible block to DNA double-strand break repair (B). A-T cells, which lack detectable ATM protein, are competent for SCE (C). SCE in A-T cells is not disrupted by ATM kinase inhibitors, indicating that the ATM kinase-dependent decrease in SCE in cells with normal ATM is not due to an off-target effect of the inhibitors (D).

We used a SILAC-based mass spectrometry screen to identify ATM kinase-dependent spatial protein dynamics that occur in irradiated cells when cells were treated with KU55933 +15 minutes to +75 minutes post-IR. We found that ATM kinase inhibition results in decreased 53BP1 retention at chromatin, suggesting that kinase-inhibited ATM may destabilize 53BP1 protein complexes at sites of DNA repair. This has important clinical implications since 53BP1 was shown to decrease chromosome aberrations and reverse the proliferation defect of BRCA1 mutant cells.[152,153] This suggest that ATM kinase inhibition post-irradiation can be used to mimic the loss of 53BP1 in cells with mutant BRCA1. The SILAC screen also implicated ANXA1 in DNA repair, which may function as a biomarker for radiation damage, demonstrating the power of proteomics and systems biology in identifying novel candidate biomarkers for cancer therapy. Future studies on ANXA1 and it role on genomic stability following DNA damage are needed. For instance, does ANXA1 actually have a function in DNA repair? Determining the effects of ANXA1 depletion on radiosensitization, chromosome aberrations and sister chromatid exchange would be incredibly informative, as well as understanding the biological significance of ANXA1 translocation from the cytoplasm to the nucleus and the significance of its retention at chromatin.

Also, what is the relationship between ATM kinase activity and ANXA1? Determining the nature of this interaction may have important clinical implications. ANXA1 is involved in the constitutive nuclear factor-κB (NF-κB) activation seen in solid tumors, and suppression of ANXA1 in highly metastatic breast cancer cells prevents migration and metastasis.[160] ANXA1 can bind to and interact with components of the NF-κB pathway, IKKγ or NEMO, in immunoprecipitation studies, and silencing of ANXA1 prevents the interaction of NEMO and RIP1 suggesting that ANXA1 is critical for the activation of NF-κB.[160] Importantly, ATM activates the NF-κB pathway, which regulates genes involved in the inhibition of apoptosis and

promotion of cell survival in response to DNA damage.[161-164] ATM-induced NF-κB signaling is implicated in enabling cancer cells to survive genotoxic therapy.[165] ATM has been shown to mediate cell fate via the NF-κB pathway by mediating the interaction of NEMO, RIP1, FADD, and caspase-8, leading to caspase activation.[166] Therefore, it is possible that ANXA1 functions in the ATM-dependent activation of NF-κB signaling and that ANXA1 can be targeted to modulate cell fate following genotoxic therapy.

The ATM and ANXA1 interaction discovered through the SILAC screen may have also revealed a plausible explanation for the ATM kinase-dependent abrogation of sister chromatid exchange (SCE). It is possible that ATM kinase inhibition +15 minutes to +75 minutes post-IR destabilizes the SLX4-SLX1 protein complex, which is required for the cleavage of Holliday junctions, preventing the formation of crossover products of homologous recombination repair.[167,168] In the SILAC screen we discovered that KU55933 results in a dramatic decrease in chromatin-bound ANXA1 in irradiated cells. The DNA repair neighborhood network analyses performed on the chromatin fraction revealed that ANXA1 is significantly enriched for DNA repair proteins. The strongest interaction revealed by these analyses was that ANXA1 binds directly to the DNA repair protein SLX1 (GIYD1). SLX1, which forms a complex with SLX4, functions as a structure specific endonuclease, which recognizes and cleaves DNA structures that are formed as intermediates in homologous recombination repair of DNA double-strand breaks (DSBs).[110,167,168] In addition to SLX1, SLX4 forms multi-protein complexes with two other structure-specific endonucleases (ERCC4-ERCC1 and MUS81-EME1), the mismatch repair complex MSH2-MSH3, components of the telomere shelterin complex TRF2-RAP1, C20orf94 and PLK1.[168] Depletion of SLX4 reduces the efficiency of repair of I-SceI-induced DSBs by 25% in human cells, demonstrating that SLX4 functions in homologous recombination repair.[168]

Pertinent to the molecular mechanism of SCE, the SLX1-SLX4 module promotes cleavage of double Holliday Junctions (HJ). HJs are four-stranded structures involving two homologous DNA duplexes that must be resolved into linear duplexes, which are produced during the homologous recombination repair of DNA double-strand breaks.[43,169]

The cleavage of Holliday junctions is a necessary step in the formation of SCE. The common steps of homologous recombination repair of a DNA double-strand break are processing of a DNA double-strand break to give single-strand DNA (ssDNA), formation of a filament on the ssDNA ends, strand invasion into a homologous sequence to form a D-loop and DNA polymerase extension.[43] Homologous recombination repair can be further subdivided into three sub-pathways: gene conversion, single-strand annealing, and break-induced replication.[43,170] If both ends of the DSB are present, then the damage is repaired by gene conversion using one of three mechanisms: DNA double-strand break repair involving Holliday junction resolvase-dependent processing of the junction, double Holliday junction dissolution involving Bloom helicase-dependent branch migration and topoisomerase-dependent decatenation of the junction, or synthesis-dependent strand annealing, which does not involve dHJ structures (Figure 28).[43,170] Two types of repair products result, depending on the mechanism employed: crossovers, in which DNA strands are exchanged relative to the initial chromosome organization, and noncrossovers, where no DNA strand exchange occurs.[43,170] DNA double-strand break repair generates both crossover or noncrossover products, while SDSA and HJ dissolution generate noncrossover products (Figure 28).[43,170] SCE is a process whereby two sister chromatids break and rejoin with one another, physically exchanging regions of the parental strands in the duplicated chromosomes, thus, SCE is a manifestation of a crossover event.[107]

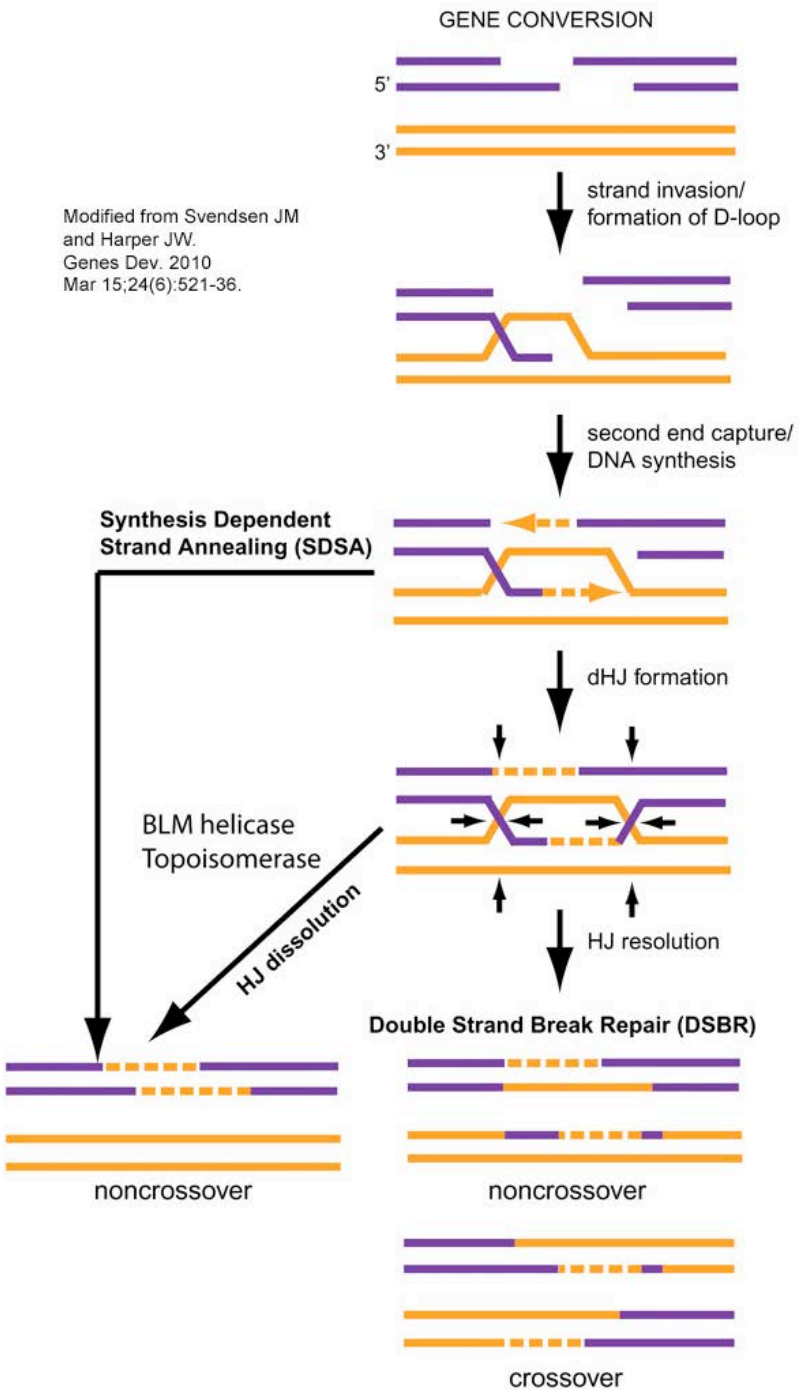

Figure 28. Sub-pathways of homologous recombination repair of DSBs that result in crossovers.

Double-strand break repair can generate either crossover or noncrossover products, while Synthesis Dependent Strand Annealing and HJ dissolution generate only noncrossover products.

Recently, the SLX4-SLX1 complex was reported to promote SCE. In Bloom's syndrome cells, which are defective for Holliday junction dissolution and harbor abnormally high SCEs, the depletion of SLX4 was shown to reduce the frequency of SCEs, indicating that the SLX4-SLX4 module promotes SCE formation.[171] It is possible that the loss of ANXA1 retention in the chromatin fraction identified in the SILAC screen serves as a biomarker for the loss of the SLX-SLX4 protein complex at the chromatin, since ANXA1 binds directly to SLX1. I hypothesize that ATM kinase inhibition destabilizes SLX1-SLX4 complexes at the chromatin, preventing the formation of homologous recombination repair crossover products and this results in the abrogation of SCE. It would be interesting to see if the chromatin retention of SLX1 and SLX4 are decreased in irradiated cells treated with KU55933 +15 minutes to +75 minutes post-IR. Furthermore, FRAP studies on GFP-SLX1 and GFP-SLX4 would reveal whether protein dynamics of the SLX4-SLX1 complex is disrupted in irradiated cells with KU55933. GFP-tagged SLX4 protein has already been found to colocalize with γH2AX, in U2OS and HT1080 cells, in response to DNA damage demonstrating that SLX4-SLX4 is recruited to DNA damage-induced foci.[168]

Interestingly, SLX4 was also identified as a target of the ATM/ATR protein kinase in irradiated human cells.[21] SLX4 is also phosphorylated by the yeast orthologs of ATM and ATR, Tel1 and Mec1.[172] Thus, SLX4 may be the ATM kinase substrate phosphorylation that is essential for promoting IR-induced SCE. Future studies on the effect of SLX4 phosphorylation mutants on radiosensitivity, chromosome aberrations and IR-induced SCEs in cells treated with KU55933 would help determine the function(s) of the ATM phosphorylation sites on SLX4.

The status of the chromatin environment is another consideration that may contribute to the effect of ATM kinase inhibition on SCE. ATM kinase activity is required to phosphorylate KAP-1 resulting in the relaxation of heterochromatin.[173] In G_2 cells, ATM and Artemis are reported to function in homologous recombination repair of DNA double-strand breaks at heterochromatin.[103] Perhaps the loss of ATM kinase signaling +15 minutes to +75 minutes post-IR abrogates SCE specifically at heterochromatin. It would be interesting to determine the effect of ATM kinase inhibition +15 minutes to +75 minutes post-IR on SCE in Artemis-depleted and KAP-1-depleted cells and to determine if ATM promotes SCE specifically at sites of heterochromatin.

This has been an exciting time to study ATM. With development and availability of ATM kinase inhibitors, I have been able to study ATM kinase activity in a way that was never previously possible. As the bioavailability of the compounds improve, we may finally be able to determine the efficacy of ATM kinase inhibitors in humans as anti-cancer agents. ATM kinase inhibitors are promising as strategies for cancer therapy. Many cancer cells acquire a defect in a DNA repair pathway early during tumor development, which can promote additional mutations that are necessary for most normal cells to become transformed. As a result, the multiplicity of DNA repair pathways that function in normal cells is often not available in cancer cells, and thus cells are crippled when these residual repair pathways are inhibited. Inhibitors of ATM kinase activity could be effective in eliminating cancer cells that express functional ATM protein and also have compromised DNA repair pathways. These cells are expected to have higher basal levels of replicative stress and are likely sensitive to ATM kinase inhibitors, since they are expected to be more reliant on ATM kinase-mediated SCE for DNA repair.

Several studies have already documented numerous synthetic lethal interactions with inhibition of ATM kinase activity.[69-72] Future studies are needed to further elucidate the mechanisms underlying these synthetic lethal interactions. Furthermore, genome-wide siRNA screens to identify synthetic lethal interactions with ATM kinase inhibition in human cells would provide an incredible resource for guiding the rationale use of ATM kinase inhibitors as anti-cancer agents. It will be interesting to see what new synthetic lethal relationships with ATM kinase inhibitors are uncovered in the future, and how they change the way we envisage the use of these compounds.

The studies described in this thesis demonstrate the utility of ATM kinase inhibitors in determining temporal and spatial functions of ATM. We demonstrate that timing is absolutely critical. Loss of ATM kinase activity +15 minutes to +75 minutes post-IR results in 70% of the maximal radiosensitization seen with ATM kinase inhibition 17 hours post-IR inhibition, and is significantly more radiosensitizing than a -15 minutes to +45 minutes post-IR inhibition window.[19] This alone suggests that *when* ATM kinase inhibitors are administered in the clinic relative to radiation treatment can affect the efficacy of ATM kinase inhibitors. The spatial dynamics of proteins are also important. How the movement and localization of proteins are affected by loss of ATM kinase activity is clinically significant. Several of the protein movements identified in the SILAC screen could be powerful functional biomarkers of genome instability. The rationale and novel design of our screen provides a model for future studies aimed at identifying functional biomarkers of radiosensitivity and genome instability.

BIBLIOGRAPHY

1. Boder E, Sedgwick RP. Ataxia-telangiectasia; a familial syndrome of progressive cerebellar ataxia, oculocutaneous telangiectasia and frequent pulmonary infection. Pediatrics 1958;21:526-54.

2. McKinnon PJ. ATM and ataxia telangiectasia. EMBO Rep 2004;5:772-6.

3. Palau F, Espinos C. Autosomal recessive cerebellar ataxias. Orphanet J Rare Dis 2006;1:47.

4. Micol R, Ben Slama L, Suarez F, et al. Morbidity and mortality from ataxia-telangiectasia are associated with ATM genotype. J Allergy Clin Immunol 2011.

5. Derheimer FA, Kastan MB. Multiple roles of ATM in monitoring and maintaining DNA integrity. FEBS Lett 2010;584:3675-81.

6. Gilad S, Khosravi R, Shkedy D, et al. Predominance of null mutations in ataxia-telangiectasia. Hum Mol Genet 1996;5:433-9.

7. Lakin ND, Weber P, Stankovic T, Rottinghaus ST, Taylor AM, Jackson SP. Analysis of the ATM protein in wild-type and ataxia telangiectasia cells. Oncogene 1996;13:2707-16.

8. Gotoff SP, Amirmokri E, Liebner EJ. Ataxia telangiectasia. Neoplasia, untoward response to x-irradiation, and tuberous sclerosis. Am J Dis Child 1967;114:617-25.

9. Lovejoy CA, Cortez D. Common mechanisms of PIKK regulation. DNA Repair (Amst) 2009;8:1004-8.

10. Bosotti R, Isacchi A, Sonnhammer EL. FAT: a novel domain in PIK-related kinases. Trends Biochem Sci 2000;25:225-7.

11. Perry J, Kleckner N. The ATRs, ATMs, and TORs are giant HEAT repeat proteins. Cell 2003;112:151-5.

12. Lavin MF. ATM and the Mre11 complex combine to recognize and signal DNA double-strand breaks. Oncogene 2007;26:7749-58.

13. Smith GC, Jackson SP. The DNA-dependent protein kinase. Genes Dev 1999;13:916-34.

14. Cimprich KA, Cortez D. ATR: an essential regulator of genome integrity. Nat Rev Mol Cell Biol 2008;9:616-27.

15. Falck J, Coates J, Jackson SP. Conserved modes of recruitment of ATM, ATR and DNA-PKcs to sites of DNA damage. Nature 2005;434:605-11.

16. Bakkenist CJ, Kastan MB. DNA damage activates ATM through intermolecular autophosphorylation and dimer dissociation. Nature 2003;421:499-506.

17. Banin S, Moyal L, Shieh S, et al. Enhanced phosphorylation of p53 by ATM in response to DNA damage. Science 1998;281:1674-7.

18. Canman CE, Lim DS, Cimprich KA, et al. Activation of the ATM kinase by ionizing radiation and phosphorylation of p53. Science 1998;281:1677-9.

19. White JS, Choi S, Bakkenist CJ. Irreversible chromosome damage accumulates rapidly in the absence of ATM kinase activity. Cell Cycle 2008;7:1277-84.

20. Bensimon A, Schmidt A, Ziv Y, et al. ATM-dependent and -independent dynamics of the nuclear phosphoproteome after DNA damage. Sci Signal 2010;3:rs3.

21. Matsuoka S, Ballif BA, Smogorzewska A, et al. ATM and ATR substrate analysis reveals extensive protein networks responsive to DNA damage. Science 2007;316:1160-6.

22. Olsen JV, Vermeulen M, Santamaria A, et al. Quantitative phosphoproteomics reveals widespread full phosphorylation site occupancy during mitosis. Sci Signal 2010;3:ra3.

23. Weinert TA, Hartwell LH. The RAD9 gene controls the cell cycle response to DNA damage in Saccharomyces cerevisiae. Science 1988;241:317-22.

24. Painter RB, Young BR. Radiosensitivity in ataxia-telangiectasia: a new explanation. Proc Natl Acad Sci U S A 1980;77:7315-7.

25. Xu B, O'Donnell AH, Kim ST, Kastan MB. Phosphorylation of serine 1387 in Brca1 is specifically required for the Atm-mediated S-phase checkpoint after ionizing irradiation. Cancer Res 2002;62:4588-91.

26. Taniguchi T, Garcia-Higuera I, Xu B, et al. Convergence of the fanconi anemia and ataxia telangiectasia signaling pathways. Cell 2002;109:459-72.

27. Lim DS, Kim ST, Xu B, et al. ATM phosphorylates p95/nbs1 in an S-phase checkpoint pathway. Nature 2000;404:613-7.

28. Santra MK, Wajapeyee N, Green MR. F-box protein FBXO31 mediates cyclin D1 degradation to induce G1 arrest after DNA damage. Nature 2009;459:722-5.

29. Kastan MB, Zhan Q, el-Deiry WS, et al. A mammalian cell cycle checkpoint pathway utilizing p53 and GADD45 is defective in ataxia-telangiectasia. Cell 1992;71:587-97.

30. Harper JW, Adami GR, Wei N, Keyomarsi K, Elledge SJ. The p21 Cdk-interacting protein Cip1 is a potent inhibitor of G1 cyclin-dependent kinases. Cell 1993;75:805-16.

31. Bao S, Tibbetts RS, Brumbaugh KM, et al. ATR/ATM-mediated phosphorylation of human Rad17 is required for genotoxic stress responses. Nature 2001;411:969-74.

32. Xu B, Kim ST, Lim DS, Kastan MB. Two molecularly distinct G(2)/M checkpoints are induced by ionizing irradiation. Mol Cell Biol 2002;22:1049-59.

33. Zampetti-Bosseler F, Scott D. Cell death, chromosome damage and mitotic delay in normal human, ataxia telangiectasia and retinoblastoma fibroblasts after x-irradiation. Int J Radiat Biol Relat Stud Phys Chem Med 1981;39:547-58.

34. Terzoudi GI, Manola KN, Pantelias GE, Iliakis G. Checkpoint abrogation in G2 compromises repair of chromosomal breaks in ataxia telangiectasia cells. Cancer Res 2005;65:11292-6.

35. Suganuma M, Kawabe T, Hori H, Funabiki T, Okamoto T. Sensitization of cancer cells to DNA damage-induced cell death by specific cell cycle G2 checkpoint abrogation. Cancer Res 1999;59:5887-91.

36. Levine AJ. p53, the cellular gatekeeper for growth and division. Cell 1997;88:323-31.

37. Sarkaria JN, Eshleman JS. ATM as a target for novel radiosensitizers. Semin Radiat Oncol 2001;11:316-27.

38. Little JB, Nagasawa H. Effect of confluent holding on potentially lethal damage repair, cell cycle progression, and chromosomal aberrations in human normal and ataxia-telangiectasia fibroblasts. Radiat Res 1985;101:81-93.

39. Smith PJ, Paterson MC. Effect of aphidicolin on de novo DNA synthesis, DNA repair and cytotoxicity in gamma-irradiated human fibroblasts. Implications for the enhanced radiosensitivity in ataxia telangiectasia. Biochim Biophys Acta 1983;739:17-26.

40. Cornforth MN, Bedford JS. On the nature of a defect in cells from individuals with ataxia-telangiectasia. Science 1985;227:1589-91.

41. Jones LA, Scott D, Cowan R, Roberts SA. Abnormal radiosensitivity of lymphocytes from breast cancer patients with excessive normal tissue damage after radiotherapy: chromosome aberrations after low dose-rate irradiation. Int J Radiat Biol 1995;67:519-28.

42. Wyman C, Kanaar R. DNA double-strand break repair: all's well that ends well. Annu Rev Genet 2006;40:363-83.

43. San Filippo J, Sung P, Klein H. Mechanism of eukaryotic homologous recombination. Annu Rev Biochem 2008;77:229-57.

44. Downs JA, Jackson SP. A means to a DNA end: the many roles of Ku. Nat Rev Mol Cell Biol 2004;5:367-78.

45. Riballo E, Kuhne M, Rief N, et al. A pathway of double-strand break rejoining dependent upon ATM, Artemis, and proteins locating to gamma-H2AX foci. Mol Cell 2004;16:715-24.

46. Poinsignon C, de Chasseval R, Soubeyrand S, et al. Phosphorylation of Artemis following irradiation-induced DNA damage. Eur J Immunol 2004;34:3146-55.

47. Goodarzi AA, Yu Y, Riballo E, et al. DNA-PK autophosphorylation facilitates Artemis endonuclease activity. Embo J 2006;25:3880-9.

48. Huertas P, Cortes-Ledesma F, Sartori AA, Aguilera A, Jackson SP. CDK targets Sae2 to control DNA-end resection and homologous recombination. Nature 2008;455:689-92.

49. Sartori AA, Lukas C, Coates J, et al. Human CtIP promotes DNA end resection. Nature 2007;450:509-14.

50. Lengsfeld BM, Rattray AJ, Bhaskara V, Ghirlando R, Paull TT. Sae2 is an endonuclease that processes hairpin DNA cooperatively with the Mre11/Rad50/Xrs2 complex. Mol Cell 2007;28:638-51.

51. Coquerelle TM, Weibezahn KF, Lucke-Huhle C. Rejoining of double strand breaks in normal human and ataxia-telangiectasia fibroblasts after exposure to 60Co gamma-rays, 241Am alpha-particles or bleomycin. Int J Radiat Biol Relat Stud Phys Chem Med 1987;51:209-18.

52. Foray N, Priestley A, Alsbeih G, et al. Hypersensitivity of ataxia telangiectasia fibroblasts to ionizing radiation is associated with a repair deficiency of DNA double-strand breaks. Int J Radiat Biol 1997;72:271-83.

53. Lavin MF, Shiloh Y. The genetic defect in ataxia-telangiectasia. Annu Rev Immunol 1997;15:177-202.

54. Hickson I, Zhao Y, Richardson CJ, et al. Identification and characterization of a novel and specific inhibitor of the ataxia-telangiectasia mutated kinase ATM. Cancer Res 2004;64:9152-9.

55. Rainey MD, Charlton ME, Stanton RV, Kastan MB. Transient inhibition of ATM kinase is sufficient to enhance cellular sensitivity to ionizing radiation. Cancer Res 2008;68:7466-74.

56. Golding SE, Rosenberg E, Valerie N, et al. Improved ATM kinase inhibitor KU-60019 radiosensitizes glioma cells, compromises insulin, AKT and ERK prosurvival signaling, and inhibits migration and invasion. Mol Cancer Ther 2009;8:2894-902.

57. Friend SH, Oliff A. Emerging uses for genomic information in drug discovery. N Engl J Med 1998;338:125-6.

58. Kaelin WG, Jr. Choosing anticancer drug targets in the postgenomic era. J Clin Invest 1999;104:1503-6.

59. Hartwell LH, Szankasi P, Roberts CJ, Murray AW, Friend SH. Integrating genetic approaches into the discovery of anticancer drugs. Science 1997;278:1064-8.

60. Chan DA, Giaccia AJ. Harnessing synthetic lethal interactions in anticancer drug discovery. Nat Rev Drug Discov 2011;10:351-64.

61. Harris CC, Hollstein M. Clinical implications of the p53 tumor-suppressor gene. N Engl J Med 1993;329:1318-27.

62. Liu TC, Hwang TH, Bell JC, Kirn DH. Translation of targeted oncolytic virotherapeutics from the lab into the clinic, and back again: a high-value iterative loop. Mol Ther 2008;16:1006-8.

63. Olivier M, Petitjean A, Marcel V, et al. Recent advances in p53 research: an interdisciplinary perspective. Cancer Gene Ther 2009;16:1-12.

64. Gien LT, Mackay HJ. The Emerging Role of PARP Inhibitors in the Treatment of Epithelial Ovarian Cancer. J Oncol 2010;2010:151750.

65. Fong PC, Boss DS, Yap TA, et al. Inhibition of poly(ADP-ribose) polymerase in tumors from BRCA mutation carriers. N Engl J Med 2009;361:123-34.

66. Schultz N, Lopez E, Saleh-Gohari N, Helleday T. Poly(ADP-ribose) polymerase (PARP-1) has a controlling role in homologous recombination. Nucleic Acids Res 2003;31:4959-64.

67. Bryant HE, Schultz N, Thomas HD, et al. Specific killing of BRCA2-deficient tumours with inhibitors of poly(ADP-ribose) polymerase. Nature 2005;434:913-7.

68. Farmer H, McCabe N, Lord CJ, et al. Targeting the DNA repair defect in BRCA mutant cells as a therapeutic strategy. Nature 2005;434:917-21.

69. Kennedy RD, Chen CC, Stuckert P, et al. Fanconi anemia pathway-deficient tumor cells are hypersensitive to inhibition of ataxia telangiectasia mutated. J Clin Invest 2007;117:1440-9.

70. Marsit CJ, Liu M, Nelson HH, Posner M, Suzuki M, Kelsey KT. Inactivation of the Fanconi anemia/BRCA pathway in lung and oral cancers: implications for treatment and survival. Oncogene 2004;23:1000-4.

71. van der Heijden MS, Brody JR, Gallmeier E, et al. Functional defects in the fanconi anemia pathway in pancreatic cancer cells. Am J Pathol 2004;165:651-7.

72. Jiang H, Reinhardt HC, Bartkova J, et al. The combined status of ATM and p53 link tumor development with therapeutic response. Genes Dev 2009;23:1895-909.

73. Reinhardt HC, Aslanian AS, Lees JA, Yaffe MB. p53-deficient cells rely on ATM- and ATR-mediated checkpoint signaling through the p38MAPK/MK2 pathway for survival after DNA damage. Cancer Cell 2007;11:175-89.

74. Vogelstein B, Lane D, Levine AJ. Surfing the p53 network. Nature 2000;408:307-10.

75. Sarkaria JN, Busby EC, Tibbetts RS, et al. Inhibition of ATM and ATR kinase activities by the radiosensitizing agent, caffeine. Cancer Res 1999;59:4375-82.

76. Sarkaria JN, Tibbetts RS, Busby EC, Kennedy AP, Hill DE, Abraham RT. Inhibition of phosphoinositide 3-kinase related kinases by the radiosensitizing agent wortmannin. Cancer Res 1998;58:4375-82.

77. Vlahos CJ, Matter WF, Hui KY, Brown RF. A specific inhibitor of phosphatidylinositol 3-kinase, 2-(4-morpholinyl)-8-phenyl-4H-1-benzopyran-4-one (LY294002). J Biol Chem 1994;269:5241-8.

78. Ui M, Okada T, Hazeki K, Hazeki O. Wortmannin as a unique probe for an intracellular signalling protein, phosphoinositide 3-kinase. Trends Biochem Sci 1995;20:303-7.

79. Izzard RA, Jackson SP, Smith GC. Competitive and noncompetitive inhibition of the DNA-dependent protein kinase. Cancer Res 1999;59:2581-6.

80. Zhou BB, Chaturvedi P, Spring K, et al. Caffeine abolishes the mammalian G(2)/M DNA damage checkpoint by inhibiting ataxia-telangiectasia-mutated kinase activity. J Biol Chem 2000;275:10342-8.

81. Block WD, Merkle D, Meek K, Lees-Miller SP. Selective inhibition of the DNA-dependent protein kinase (DNA-PK) by the radiosensitizing agent caffeine. Nucleic Acids Res 2004;32:1967-72.

82. Won J, Kim M, Kim N, et al. Small molecule-based reversible reprogramming of cellular lifespan. Nat Chem Biol 2006;2:369-74.

83. Normile D. Scientific misconduct. Science retracts discredited paper; bitter patent dispute continues. Science 2009;324:450-1.

84. Won J, Kim M, Kim N, et al. Retraction: small molecule-based reversible reprogramming of cellular lifespan. Nat Chem Biol 2008;4:431.

85. Walker EH, Pacold ME, Perisic O, et al. Structural determinants of phosphoinositide 3-kinase inhibition by wortmannin, LY294002, quercetin, myricetin, and staurosporine. Mol Cell 2000;6:909-19.

86. van Steensel B, Smogorzewska A, de Lange T. TRF2 protects human telomeres from end-to-end fusions. Cell 1998;92:401-13.

87. Takai H, Smogorzewska A, de Lange T. DNA damage foci at dysfunctional telomeres. Curr Biol 2003;13:1549-56.

88. Won J, Kim M, Yi YW, Kim YH, Jung N, Kim TK. A magnetic nanoprobe technology for detecting molecular interactions in live cells. Science 2005;309:121-5.

89. Cruet-Hennequart S, Glynn MT, Murillo LS, Coyne S, Carty MP. Enhanced DNA-PK-mediated RPA2 hyperphosphorylation in DNA polymerase eta-deficient human cells treated with cisplatin and oxaliplatin. DNA Repair (Amst) 2008;7:582-96.

90. Shrivastav M, Miller CA, De Haro LP, et al. DNA-PKcs and ATM co-regulate DNA double-strand break repair. DNA Repair (Amst) 2009;8:920-9.

91. White JS, Choi S, Bakkenist CJ. Transient ATM kinase inhibition disrupts DNA damage-induced sister chromatid exchange. Sci Signal 2010;3:ra44.

92. Matsuoka S, Huang M, Elledge SJ. Linkage of ATM to cell cycle regulation by the Chk2 protein kinase. Science 1998;282:1893-7.

93. Zhao H, Piwnica-Worms H. ATR-mediated checkpoint pathways regulate phosphorylation and activation of human Chk1. Mol Cell Biol 2001;21:4129-39.

94. Charrier JD, Durrant SJ, Golec JM, et al. Discovery of potent and selective inhibitors of ataxia telangiectasia mutated and Rad3 related (ATR) protein kinase as potential anticancer agents. J Med Chem 2011;54:2320-30.

95. Toledo LI, Murga M, Zur R, et al. A cell-based screen identifies ATR inhibitors with synthetic lethal properties for cancer-associated mutations. Nat Struct Mol Biol 2011;18:721-7.

96. Reaper PM, Griffiths MR, Long JM, et al. Selective killing of ATM- or p53-deficient cancer cells through inhibition of ATR. Nat Chem Biol 2011;7:428-30.

97. Savitsky K, Bar-Shira A, Gilad S, et al. A single ataxia telangiectasia gene with a product similar to PI-3 kinase. Science 1995;268:1749-53.

98. Morrison C, Sonoda E, Takao N, Shinohara A, Yamamoto K, Takeda S. The controlling role of ATM in homologous recombinational repair of DNA damage. Embo J 2000;19:463-71.

99. Bryant HE, Helleday T. Inhibition of poly (ADP-ribose) polymerase activates ATM which is required for subsequent homologous recombination repair. Nucleic Acids Res 2006;34:1685-91.

100. Galloway SM, Evans HJ. Sister chromatid exchange in human chromosomes from normal individuals and patients with ataxia telangiectasia. Cytogenet Cell Genet 1975;15:17-29.

101. Bartram CR, Koske-Westphal T, Passarge E. Chromatid exchanges in ataxia telangiectasia, Bloom syndrome, Werner syndrome, and xeroderma pigmentosum. Ann Hum Genet 1976;40:79-86.

102. Galloway SM. Ataxia telangiectasia: the effects of chemical mutagens and x-rays on sister chromatid exchanges in blood lymphocytes. Mutat Res 1977;45:343-9.

103. Beucher A, Birraux J, Tchouandong L, et al. ATM and Artemis promote homologous recombination of radiation-induced DNA double-strand breaks in G2. Embo J 2009;28:3413-27.

104. Ziv Y, Bielopolski D, Galanty Y, et al. Chromatin relaxation in response to DNA double-strand breaks is modulated by a novel ATM- and KAP-1 dependent pathway. Nat Cell Biol 2006;8:870-6.

105. White DE, Negorev D, Peng H, Ivanov AV, Maul GG, Rauscher FJ, 3rd. KAP1, a novel substrate for PIKK family members, colocalizes with numerous damage response factors at DNA lesions. Cancer Res 2006;66:11594-9.

106. Xu B, Kastan MB. Analyzing cell cycle checkpoints after ionizing radiation. Methods Mol Biol 2004;281:283-92.

107. Wilson DM, 3rd, Thompson LH. Molecular mechanisms of sister-chromatid exchange. Mutat Res 2007;616:11-23.

108. Callen E, Jankovic M, Difilippantonio S, et al. ATM prevents the persistence and propagation of chromosome breaks in lymphocytes. Cell 2007;130:63-75.

109. Choi S, Gamper AM, White JS, Bakkenist CJ. Inhibition of ATM kinase activity does not phenocopy ATM protein disruption: implications for the clinical utility of ATM kinase inhibitors. Cell Cycle 2010;9:4052-7.

110. Ciccia A, Elledge SJ. The DNA damage response: making it safe to play with knives. Mol Cell 2010;40:179-204.

111. Harper JW, Elledge SJ. The DNA damage response: ten years after. Mol Cell 2007;28:739-45.

112. Jackson SP, Bartek J. The DNA-damage response in human biology and disease. Nature 2009;461:1071-8.

113. Lavin MF. Ataxia-telangiectasia: from a rare disorder to a paradigm for cell signalling and cancer. Nat Rev Mol Cell Biol 2008;9:759-69.

114. Lisby M, Barlow JH, Burgess RC, Rothstein R. Choreography of the DNA damage response: spatiotemporal relationships among checkpoint and repair proteins. Cell 2004;118:699-713.

115. Lukas C, Falck J, Bartkova J, Bartek J, Lukas J. Distinct spatiotemporal dynamics of mammalian checkpoint regulators induced by DNA damage. Nat Cell Biol 2003;5:255-60.

116. Fernandez-Capetillo O, Celeste A, Nussenzweig A. Focusing on foci: H2AX and the recruitment of DNA-damage response factors. Cell Cycle 2003;2:426-7.

117. Paull TT, Rogakou EP, Yamazaki V, Kirchgessner CU, Gellert M, Bonner WM. A critical role for histone H2AX in recruitment of repair factors to nuclear foci after DNA damage. Curr Biol 2000;10:886-95.

118. Yuan J, Luo K, Zhang L, Cheville JC, Lou Z. USP10 regulates p53 localization and stability by deubiquitinating p53. Cell 2010;140:384-96.

119. Cohn MA, D'Andrea AD. Chromatin recruitment of DNA repair proteins: lessons from the fanconi anemia and double-strand break repair pathways. Mol Cell 2008;32:306-12.

120. Levitus M, Waisfisz Q, Godthelp BC, et al. The DNA helicase BRIP1 is defective in Fanconi anemia complementation group J. Nat Genet 2005;37:934-5.

121. Levran O, Attwooll C, Henry RT, et al. The BRCA1-interacting helicase BRIP1 is deficient in Fanconi anemia. Nat Genet 2005;37:931-3.

122. Mann M. Functional and quantitative proteomics using SILAC. Nat Rev Mol Cell Biol 2006;7:952-8.

123. Mendez J, Stillman B. Chromatin association of human origin recognition complex, cdc6, and minichromosome maintenance proteins during the cell cycle: assembly of prereplication complexes in late mitosis. Mol Cell Biol 2000;20:8602-12.

124. Smits VA, Reaper PM, Jackson SP. Rapid PIKK-dependent release of Chk1 from chromatin promotes the DNA-damage checkpoint response. Curr Biol 2006;16:150-9.

125. Zou L, Cortez D, Elledge SJ. Regulation of ATR substrate selection by Rad17-dependent loading of Rad9 complexes onto chromatin. Genes Dev 2002;16:198-208.

126. Tanner S, Shu H, Frank A, et al. InsPecT: identification of posttranslationally modified peptides from tandem mass spectra. Anal Chem 2005;77:4626-39.

127. Elias JE, Gygi SP. Target-decoy search strategy for increased confidence in large-scale protein identifications by mass spectrometry. Nat Methods 2007;4:207-14.

128. Rivera CG, Vakil R, Bader JS. NeMo: Network Module identification in Cytoscape. BMC Bioinformatics 2010;11 Suppl 1:S61.

129. Kamburov A, Wierling C, Lehrach H, Herwig R. ConsensusPathDB--a database for integrating human functional interaction networks. Nucleic Acids Res 2009;37:D623-8.

130. Phair RD, Gorski SA, Misteli T. Measurement of dynamic protein binding to chromatin in vivo, using photobleaching microscopy. Methods Enzymol 2004;375:393-414.

131. Ong SE, Mann M. Stable isotope labeling by amino acids in cell culture for quantitative proteomics. Methods Mol Biol 2007;359:37-52.

132. Dennis G, Jr., Sherman BT, Hosack DA, et al. DAVID: Database for Annotation, Visualization, and Integrated Discovery. Genome Biol 2003;4:P3.

133. Shannon P, Markiel A, Ozier O, et al. Cytoscape: a software environment for integrated models of biomolecular interaction networks. Genome Res 2003;13:2498-504.

134. Anderson L, Henderson C, Adachi Y. Phosphorylation and rapid relocalization of 53BP1 to nuclear foci upon DNA damage. Mol Cell Biol 2001;21:1719-29.

135. DiTullio RA, Jr., Mochan TA, Venere M, et al. 53BP1 functions in an ATM-dependent checkpoint pathway that is constitutively activated in human cancer. Nat Cell Biol 2002;4:998-1002.

136. Schultz LB, Chehab NH, Malikzay A, Halazonetis TD. p53 binding protein 1 (53BP1) is an early participant in the cellular response to DNA double-strand breaks. J Cell Biol 2000;151:1381-90.

137. Bekker-Jensen S, Lukas C, Melander F, Bartek J, Lukas J. Dynamic assembly and sustained retention of 53BP1 at the sites of DNA damage are controlled by Mdc1/NFBD1. J Cell Biol 2005;170:201-11.

138. Pryde F, Khalili S, Robertson K, et al. 53BP1 exchanges slowly at the sites of DNA damage and appears to require RNA for its association with chromatin. J Cell Sci 2005;118:2043-55.

139. Difilippantonio S, Gapud E, Wong N, et al. 53BP1 facilitates long-range DNA end-joining during V(D)J recombination. Nature 2008;456:529-33.

140. Fernandez-Capetillo O, Chen HT, Celeste A, et al. DNA damage-induced G2-M checkpoint activation by histone H2AX and 53BP1. Nat Cell Biol 2002;4:993-7.

141. Lee JH, Goodarzi AA, Jeggo PA, Paull TT. 53BP1 promotes ATM activity through direct interactions with the MRN complex. Embo J 2010;29:574-85.

142. Wang B, Matsuoka S, Carpenter PB, Elledge SJ. 53BP1, a mediator of the DNA damage checkpoint. Science 2002;298:1435-8.

143. Ward IM, Minn K, Jorda KG, Chen J. Accumulation of checkpoint protein 53BP1 at DNA breaks involves its binding to phosphorylated histone H2AX. J Biol Chem 2003;278:19579-82.

144. Axelrod D, Koppel DE, Schlessinger J, Elson E, Webb WW. Mobility measurement by analysis of fluorescence photobleaching recovery kinetics. Biophys J 1976;16:1055-69.

145. Boisvert FM, Lam YW, Lamont D, Lamond AI. A quantitative proteomics analysis of subcellular proteome localization and changes induced by DNA damage. Mol Cell Proteomics 2010;9:457-70.

146. Boisvert FM, Lamond AI. p53-Dependent subcellular proteome localization following DNA damage. Proteomics 2010.

147. Nair S, Hande MP, Lim LH. Annexin-1 protects MCF7 breast cancer cells against heat-induced growth arrest and DNA damage. Cancer Lett 2010;294:111-7.

148. Huyen Y, Zgheib O, Ditullio RA, Jr., et al. Methylated lysine 79 of histone H3 targets 53BP1 to DNA double-strand breaks. Nature 2004;432:406-11.

149. Celeste A, Fernandez-Capetillo O, Kruhlak MJ, et al. Histone H2AX phosphorylation is dispensable for the initial recognition of DNA breaks. Nat Cell Biol 2003;5:675-9.

150. Rogakou EP, Boon C, Redon C, Bonner WM. Megabase chromatin domains involved in DNA double-strand breaks in vivo. J Cell Biol 1999;146:905-16.

151. Moynahan ME, Jasin M. Mitotic homologous recombination maintains genomic stability and suppresses tumorigenesis. Nat Rev Mol Cell Biol 2010;11:196-207.

152. Bouwman P, Aly A, Escandell JM, et al. 53BP1 loss rescues BRCA1 deficiency and is associated with triple-negative and BRCA-mutated breast cancers. Nat Struct Mol Biol 2010;17:688-95.

153. Bunting SF, Callen E, Wong N, et al. 53BP1 inhibits homologous recombination in Brca1-deficient cells by blocking resection of DNA breaks. Cell 2010;141:243-54.

154. Barone G, Groom A, Reiman A, Srinivasan V, Byrd PJ, Taylor AM. Modeling ATM mutant proteins from missense changes confirms retained kinase activity. Hum Mutat 2009;30:1222-30.

155. Cuadrado M, Martinez-Pastor B, Murga M, et al. ATM regulates ATR chromatin loading in response to DNA double-strand breaks. J Exp Med 2006;203:297-303.

156. Dodson GE, Tibbetts RS. DNA replication stress-induced phosphorylation of cyclic AMP response element-binding protein mediated by ATM. J Biol Chem 2006;281:1692-7.

157. Jazayeri A, Falck J, Lukas C, et al. ATM- and cell cycle-dependent regulation of ATR in response to DNA double-strand breaks. Nat Cell Biol 2006;8:37-45.

158. Myers JS, Cortez D. Rapid activation of ATR by ionizing radiation requires ATM and Mre11. J Biol Chem 2006;281:9346-50.

159. Tsukuda T, Fleming AB, Nickoloff JA, Osley MA. Chromatin remodelling at a DNA double-strand break site in Saccharomyces cerevisiae. Nature 2005;438:379-83.

160. Bist P, Leow SC, Phua QH, et al. Annexin-1 interacts with NEMO and RIP1 to constitutively activate IKK complex and NF-kappaB: implication in breast cancer metastasis. Oncogene 2011;30:3174-85.

161. Criswell T, Leskov K, Miyamoto S, Luo G, Boothman DA. Transcription factors activated in mammalian cells after clinically relevant doses of ionizing radiation. Oncogene 2003;22:5813-27.

162. Huang TT, Wuerzberger-Davis SM, Wu ZH, Miyamoto S. Sequential modification of NEMO/IKKgamma by SUMO-1 and ubiquitin mediates NF-kappaB activation by genotoxic stress. Cell 2003;115:565-76.

163. Li N, Banin S, Ouyang H, et al. ATM is required for IkappaB kinase (IKKk) activation in response to DNA double strand breaks. J Biol Chem 2001;276:8898-903.

164. Piret B, Schoonbroodt S, Piette J. The ATM protein is required for sustained activation of NF-kappaB following DNA damage. Oncogene 1999;18:2261-71.

165. Janssens S, Tschopp J. Signals from within: the DNA-damage-induced NF-kappaB response. Cell Death Differ 2006;13:773-84.

166. Biton S, Ashkenazi A. NEMO and RIP1 control cell fate in response to extensive DNA damage via TNF-alpha feedforward signaling. Cell 2011;145:92-103.

167. Fekairi S, Scaglione S, Chahwan C, et al. Human SLX4 is a Holliday junction resolvase subunit that binds multiple DNA repair/recombination endonucleases. Cell 2009;138:78-89.

168. Svendsen JM, Smogorzewska A, Sowa ME, et al. Mammalian BTBD12/SLX4 assembles a Holliday junction resolvase and is required for DNA repair. Cell 2009;138:63-77.

169. Holliday R. A mechanism for gene conversion in fungi. Genet Res 2007;89:285-307.

170. Svendsen JM, Harper JW. GEN1/Yen1 and the SLX4 complex: Solutions to the problem of Holliday junction resolution. Genes Dev 2010;24:521-36.

171. Wechsler T, Newman S, West SC. Aberrant chromosome morphology in human cells defective for Holliday junction resolution. Nature 2011;471:642-6.

172. Flott S, Alabert C, Toh GW, et al. Phosphorylation of Slx4 by Mec1 and Tel1 regulates the single-strand annealing mode of DNA repair in budding yeast. Mol Cell Biol 2007;27:6433-45.

173. Goodarzi AA, Noon AT, Deckbar D, et al. ATM signaling facilitates repair of DNA double-strand breaks associated with heterochromatin. Mol Cell 2008;31:167-77.